Computational Study of Critical Flow Discharge
in Supercritical Water Cooled Reactors

Computational Study of Critical Flow Discharge in Supercritical Water Cooled Reactors

By

Madhuri Chatharaju, B.Tech.

A Thesis

Submitted to the School of Graduate Studies

in Partial Fulfillment of the Requirements

for the Degree

Master of Applied Science

McMaster University

MASTER OF APPLIED SCIENCE (2011)   McMaster University

(Engineering Physics)   Hamilton, Ontario, Canada

TITLE: Computational Study of Critical Flow Discharge in
                          Supercritical Water Cooled Reactors

AUTHOR: Madhuri Chatharaju, B.Tech. (KITS-Warangal, India)

SUPERVISOR: Dr. D.R. Novog

NUMBER OF PAGES: xiii, 114

Abstract

Supercritical Water-cooled Reactor (SCWR) is a Generation-IV nuclear reactor design that operates on a direct energy conversion cycle above the thermodynamic critical point of water (374^0C and 22.1 MPa), and offers higher thermal efficiency and considerable design simplification. As an essential step in the design of SCWR safety systems, the accident behaviour of the reactor is evaluated to ensure that the safety systems can achieve safe shutdown for all the design basis accidents. Unfortunately, the computational tools and computer codes that are currently employed for safety analysis have little application in the supercritical region, and faces significant challenges in simulating the transitions from subcritical to supercritical conditions.

This thesis examines the predictive capabilities of Computational Fluid Dynamics (CFD) code STAR-CCM+ by evaluating critical flow (or choked flow) due to accidental release of coolant from supercritical fluid systems. The biggest challenge of this research is that the current version of STAR-CCM+ does not support supercritical simulations because the steam tables included in the package are only limited to the subcritical subset of the thermodynamic fluid properties.

The research was carried out in two stages. In the first stage, the CFD code STAR-CCM+ was customized to simulate supercritical conditions by, (i) Generating updated steam tables to include subcritical and supercritical fluid properties and using more pressure and temperature points in the pseudo critical region (22 – 25 MPa, 645 - 660 K) to handle the rapid changes in the fluid properties, and (ii) Implementing a multi-dimensional steam table interpolation scheme to access the fluid property data at any thermodynamic state during the simulation. In the second stage, the customized CFD code was extensively evaluated by simulating several accidental release scenarios from supercritical conditions using rounded-edge and sharp-edge nozzles and the model results were validated with experimental data. To overcome the solution stability (or convergence) issues encountered during the supercritical simulations, a fine tuning

procedure was proposed that guaranteed convergence for all the case studies considered in this thesis.

The simulation results revealed that the CFD model produced results that were in good agreement with experimental data and only about 10% prediction error was noticed for most cases considered in the thesis. Considering the sensitivity of the CFD model for upstream temperatures and pressures, these results appear to be quite reasonable. From the computational experience gained in this research , we believe that the CFD code STAR-CCM+ is a very useful tool to perform thermal hydraulic simulations for supercritical systems. However, an appropriate customization and extensive validation of the code is required before it can be exclusively used for safety analysis.

Acknowledgements

I thank my supervisor Dr. D.R. Novog for his continuous support, patience and invaluable guidance during the period of my study. Without his help, it would not have been possible to finish the thesis.

Thanks to my friends at McMaster who were very helpful during the initial phases of my research. I appreciate Ima, Paul, Hummel, Fang and Pouya for assisting me in different phases of my research.

I would like to dedicate this thesis to my husband (Ravi Pula) for his cooperation, encouragement, guidance and love. A single word 'Thanks' is not enough for what he has done. He means everything to me in my life.

Special thanks to my parents (Ravinder Chatharaju & Sujatha Kuna) and younger brother (Vinay Chatharaju) for their eternal love. I can never forget their motivation and moral support in hard times during my Master's degree. Love them a lot.

Table of Contents

List of Figures

List of Tables

1.   Introduction

The nuclear reactor systems have been evolving for the past six decades as shown in Figure 1, which clearly highlights the past, present and future nuclear reactor technologies. As one can see, Generation I reactors were the early prototype power reactors, while Generation II reactors were the first commercial reactors built around world, which comprised of light water reactors such as the Pressurized Water Reactors (PWRs), Boiling Water Reactors (BWR) and heavy water reactor such as CANada Deuterium Uranium reactor (CANDU).
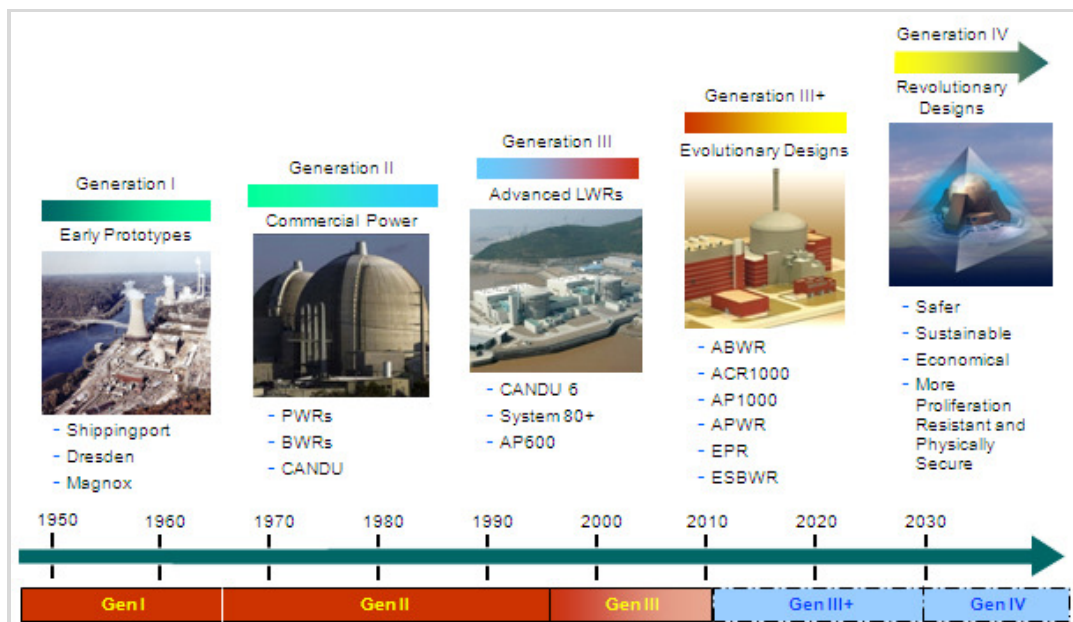
Figure 1: Evolution of Nuclear Reactor Systems (GIF, 2011)

Further advancements to the Generation II reactor designs resulted in Generation III and Generation III+ systems. Many of the Generation III designs are currently in operation, where as Generation III+ designs are the systems for upcoming new constructions. With an aim to achieve enhanced safety and cost effective power generation, Generation IV International Forum (GIF) has proposed six new Generation IV designs for future reactor systems, which are expected to come into operation only

after 2030. At present, the research on Generation IV systems is focused on materials and chemistry, core design, thermal hydraulics and feasibility studies (DOE, 2003, Torgerson et al., 2006, Bae et al., 2009, Sakurai et al., 2009 and Shan & Leung, 2009).

A fundamental challenge in the Generation IV program, in particular for the designs utilizing water above its thermodynamic critical state (known as supercritical water reactors), is that the tools and computer codes needed in the design stages have had little application in the supercritical region, and in particular in simulating the transitions from subcritical to supercritical conditions as well as transitions through the pseudo critical temperature.

1.1   Background

Supercritical Water-cooled Reactor (SCWR) system (DOE, 2003), as shown in Figure 2, is one of the six major Generation IV designs and the topic of interest for the current research work. SCWR is a high temperature - high pressure water cooled reactor designed to operate on a direct energy conversion cycle above the thermodynamic critical point of water (374^0C and 22.1 MPa). It is a promising technology mainly because of its high thermal efficiency (about 45% vs. about 33% efficiency for current Light water reactors) and considerable design simplification.
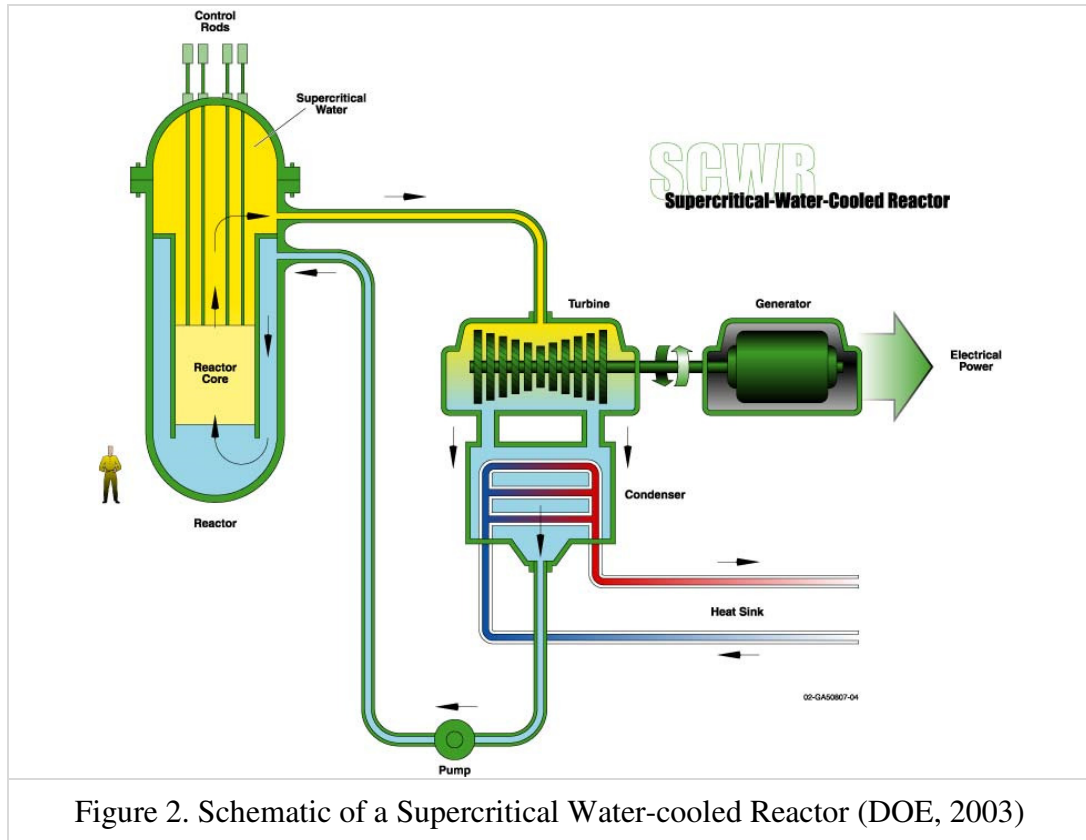
Figure 2. Schematic of a Supercritical Water-cooled Reactor (DOE, 2003)

With the operating conditions above the critical pressure, coolant boiling does not occur. As a result, the coolant remains in single-phase throughout the system during normal operating conditions. Because of this and the direct once through energy conversion cycle, the need for equipment such as recirculation and jet pumps, pressurizer, steam generators, steam separators and dryers used in the current Light Water Reactors are eliminated. The reference SCWR system is designed for 1700 MWe, typically with an operating pressure of about 25 MPa and core inlet and outlet temperatures of about 280 ^{0}C and 550 ^{0}C. The coolant density for these systems decreases from about 760 kg/m^3 at the core inlet to about 90 kg/m^3 at the core outlet, thus exhibiting complex fluid behavior in the coolant system.

A key activity in the pre-conceptual design stage is to evaluate the potential accident behaviour of the SCWR to ensure that the safety systems envisioned can achieve safe shutdown for all design basis accidents and meet pre-defined acceptance criteria on

maximum sheath and fuel temperatures. These accidents include Loss of Offsite Power (LOOP), Loss of Flow (LOF), Reactivity Induced Accidents (RIA) and Loss of Coolant Accidents (LOCA). The main focus of this thesis is on Loss of Coolant Accidents and the evaluation of thermal hydraulic phenomena during such accidental releases to assist in the design of safety systems. Specifically, this thesis examines the predictive capabilities of Computational Fluid Dynamics (CFD) for simulating the critical flow discharge from a supercritical fluid system.

Accidental coolant releases from the SCWR typically result in rapid depressurization (or blowdown) of the coolant circuit, where the coolant releases from high pressure into a lower pressure environment. At the break location, the fluid discharge velocity increases with increasing pressure differential and reaches a maximum value, and beyond some limiting differential pressure the flow is no longer affected by the downstream pressure outside the break. This limitation on the fluid velocity is called choking condition and fluid flow under such condition is called critical flow (or choked flow).

Critical flow is defined as the maximum discharge flow rate through small diameter breaks which is no longer affected by the downstream conditions. For a single-phase coolant release, the maximum velocity is limited by the speed of sound (i.e., critical flow is equal to sonic velocity being achieved within the nozzle or discharge region). For liquid discharge, the depressurization may involve some flashing of the liquid into vapour, creating a two-phase discharge fluid. The critical flow in this case may be much more difficult to model and often relies on either empirical or semi-empirical formulations.

In general, critical flow dominates the progress of the transient, coolant inventory in the core, and, thus, the temperatures of the fuel elements. It is therefore, important to study the critical flow characteristics at supercritical conditions in order to analyze the consequences from a LOCA and support the design and operation of the SCWR and its safety systems.

A limited number of experiments have been conducted to evaluate critical flow of water at supercritical conditions (Chen et al., 2009, Mignot et al., 2007 and Lee et al., 1983). The experiments were conducted under adiabatic conditions due to the complexity in interpreting heat transfer and fluid flow in the supercritical regime. The results have shown that traditional critical flow models in thermal hydraulic codes such as RELAP are incapable of accurately predicting the super-critical behaviour. These experiments, however are useful to build new empirical correlations and also validate computational codes.

On the other hand, computational tools are also available to perform these evaluations, which can model the steady-state, transients and design basis accidents. LOCA simulations in particular present a unique challenge since the pressure and temperatures can change rapidly when coupled to significant property sensitivities in the supercritical region with temperature and pressure. The significant variation in the thermo-physical properties of water near the pseudo-critical temperature are shown in Figure 3. This large variation typically results in an unusual flow and heat transfer behaviour and makes the computational evaluation very challenging. A reliable knowledge of thermal-hydraulic behavior can provide us an insight on the magnitude of accident consequences and enables us to define appropriate safety margins proactively for inherently safer nuclear designs.
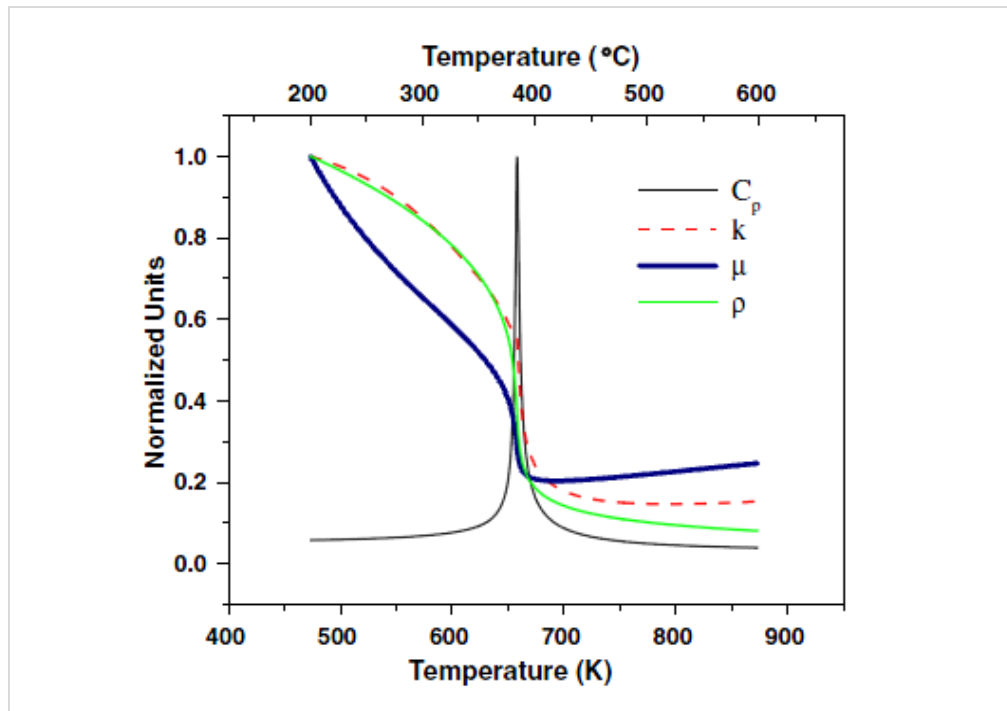
Figure 3. Thermo-physical properties of water at 25 MPa (Licht et al., 2008)

One-dimensional (1-D) computational codes are most commonly used in the nuclear industry to perform thermal hydraulic simulations for safety analysis and design of reactor systems. RELAP is a well known computational code that embeds a non-homogeneous, non-equilibrium two-fluid model consisting of six fundamental equations and relevant closure correlations to address single and two-phase fluid flow behavior. Although, these codes are widely used in the nuclear industry, the major drawback with these codes is their inability to address the three-dimensional effects of fluid flow (e.g., swirling flows, separated flows, flows in complex geometries etc.), which add significant value to the safety analysis.

The three-dimensional (3-D) computational codes such as Computational Fluid Dynamics (CFD) codes can address these details appropriately. CFD codes typically incorporate the solution of the conservation equations of mass, momentum and energy, and other allied equations in three-dimensions to describe the thermal hydraulic behavior.

There has been a wide body of literature on the application of CFD to single-phase flows, and recently more work has been published on two-phase flow CFD. An attractive feature of CFD for SCWR flows is that the fluid in our case stays in single-phase and hence there is significant work, in for example the applicability of turbulence models and closure relationships, which can be used.

The current work is an attempt to investigate the ability of Computational Fluid Dynamics (CFD) codes to evaluate critical flow under supercritical conditions. A detailed description of the thesis objectives are elaborated in the following section.

1.2   Thesis Objectives

The primary objective of this work is to investigate the ability of the commercial CFD code (STARCCM+) to perform thermal hydraulic simulations, in particular critical flow evaluation, under supercritical conditions of water and identify the challenges posed by the code to accomplish such analysis.

CFD codes have been tested earlier (Menter, 2002 and Smith, 2010) to perform similar simulations but only under sub-critical conditions. To test its validity for supercritical evaluations, it is necessary to design case studies, perform simulations and compare the results with available experimental data. At present, there is limited experimental data to describe the critical flow phenomena at supercritical conditions. Recently, Chen and co-authors (Chen et al., 2009) at the China Institute of Atomic Energy conducted critical flow experiments over a wide range of supercritical conditions using two different nozzle designs, so that the effect of nozzle shapes (entrance effects) on the flow patterns can also be investigated. To our knowledge, we found these experiments best suitable to test our CFD model and verify its validity for supercritical conditions. Therefore, the CFD models in this research were based on their nozzle designs and the simulation experiments were conducted using the initial stagnation conditions employed in their experiments, so that the simulation results can be directly validated with the experimental data.

While accomplishing the primary objective, the main goals of this work have been laid out as:

- To develop a CFD model that can be used to study the flow patterns and choking phenomena during a postulated Loss of Coolant Accident (LOCA) in Supercritical reactor systems.

- To validate the thermal model results with experimental data (Cheng et al., 2009) in order to gain confidence on the predictions and further use it for safety and design analysis.

- To investigate the sensitivity of the CFD model for different mesh sizes and turbulence models.

- To identify the challenges posed by CFD codes and the advantages it offers over 1-D computational codes.

It is important to understand that a well validated CFD model could be used to investigate the thermal-hydraulic phenomena in supercritical systems during normal operation and accidents, system performance under a variety of conditions to enhance the knowledge on safety and performance assessment. Also, it should be noted that an attractive feature of this validation is that the supercritical fluid discharges to the environment as superheated steam, and hence two-phase conditions are precluded, this avoids the complexity of having to utilize a two-fluid CFD approach.

1.3 Scope of Work

It has been postulated by Mignot et al. (2007), that depending upon the initial conditions of water during supercritical experiments, three regions of behaviour can be identified as shown in Figure 4. In Region 1, the fluid remains in a single phase during the blow down event, going from a supercritical condition to subcritical, superheated gas. In the second and third regions, a second phase appears when the fluid approaches the two phase region with condensation in Region 2 and vaporization in Region 3. The fluid

could be in any of these regions during a transient blow down event occurring due to LOCA in supercritical systems.
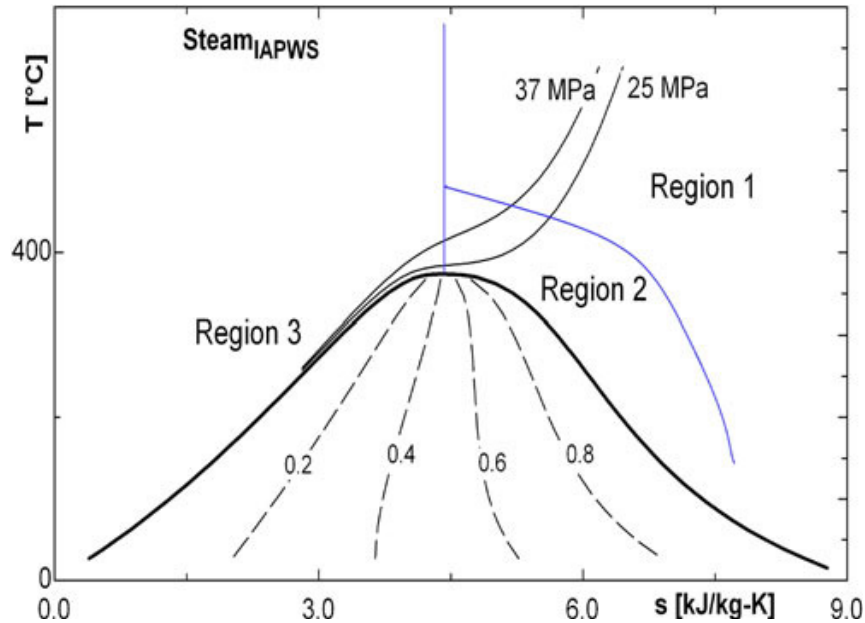
Figure 4. Temperature Entropy diagram with three regions at supercritical conditions (Mignot et al., 2007, Corrardini, 2009)

A single-phase computational code can model the conditions in Region 1, Region 2 and Region 3 pretty well, where as a two-phase code is required to model the conditions near and inside the two-phase region. Two-phase CFD modeling (Nakatsuka et al., 2009 and Smith, 2010) is still in the development phase and therefore its applicability for transitions from supercritical conditions to two-phase flow has not been reported.

Single-phase computational fluid dynamics modeling is very well understood, but its application for supercritical conditions is limited; and thus far has been limited to in-house developed CFD codes (Gallaway et al., 2008). Since, the primary objective of this research is to investigate the validity of commercial CFD code for supercritical simulations, the current work is focused on single-phase evaluation. Therefore, only single-phase modeling is considered in this research.

The major challenge for using commercial CFD codes for supercritical conditions is due to fluid property relationships, which is mainly attributed to the unavailability of supercritical water property database, and the availability of wide-applicable turbulence models in this region. In many cases, the codes would simply quit and generate a error message related to water property, when attempted to solve a supercritical problem. This is understandable because the current CFD codes embed only a portion of the IAPWS-IF97 (International Association for the Properties of Water and Steam) water property database that is valid only for subcritical conditions. The testing of turbulence models in these codes for SCWR applications has also been very limited. For example, most CFD testing under heat transfer conditions (Ambrosini, 2009) demonstrate that the turbulence models do not predict the correct trends under some circumstances. For the present work, we are examining adiabatic SCWR single-phase compressible flow and comparing turbulence modelling options against experimental results.

1.4   Thesis Outline

The thesis is laid out as six chapters. Brief details of each chapter are provided here.

Chapter 2 reviews the critical flow experiments conducted so far under supercritical conditions. It also discusses the application of computational tools such as the one-dimensional codes and the CFD codes to perform thermal-hydraulic simulations. The challenges posed by the computational tools for simulating supercritical conditions are also discussed in this chapter.

Chapter 3 provides an overview of the modelling equations and the details about the computational code employed in this research. A detailed description of the CFD code (STARCCM+) is provided and its limitations to solve supercritical problems are highlighted. The methods investigated and adopted to overcome these limitations are clearly discussed in this chapter.

Chapter 4 provides a brief description about the experimental data chosen in this research to validate the CFD model. It also discusses the steps followed to perform CFD

modelling and emphasises the importance of fine tuning while simulating models under supercritical conditions.

Chapter 5 discusses the nominal case study and provides detailed interpretation of the results obtained for two types of nozzles (Nozzle A and Nozzle B). The validation of the CFD model results with experimental data and the uncertainty in simulation results are elaborated. The sensitivity of the thermal model for various turbulence models (k-epsilon, k-omega, RSM etc), mesh configurations and perturbations in the boundary conditions is also discussed in this chapter.

Chapter 6 draws the conclusions of this thesis. The main contributions of the work are elaborated, and the issues that are outstanding in the research work are pointed out for future work.

2. Literature review

This chapter reviews the modelling methods for predicting critical flow from sub-critical water and then the experiments that were conducted under supercritical conditions. It also provides some details about the computational codes such as one-dimensional codes and computational fluid dynamics (CFD) codes to perform thermal-hydraulic simulations and highlights the challenges encountered while simulating supercritical conditions.

2.1 Background

Water above its critical temperature and critical pressure is referred as supercritical water. The critical point (647.1 K, 22.1 MPa) represents the highest temperature and pressure at which water can exist as a vapor and liquid in equilibrium, i.e., above this point, the substance exists as a fluid without distinct phases. It is neither gas nor liquid, resulting in a single-phase fluid without the occurrence of interfaces. The supercritical region for water is identified in the pressure temperature diagram as shown in Figure 5.

Figure 5. The supercritical region in P-T diagram (De Rosa, 2010)
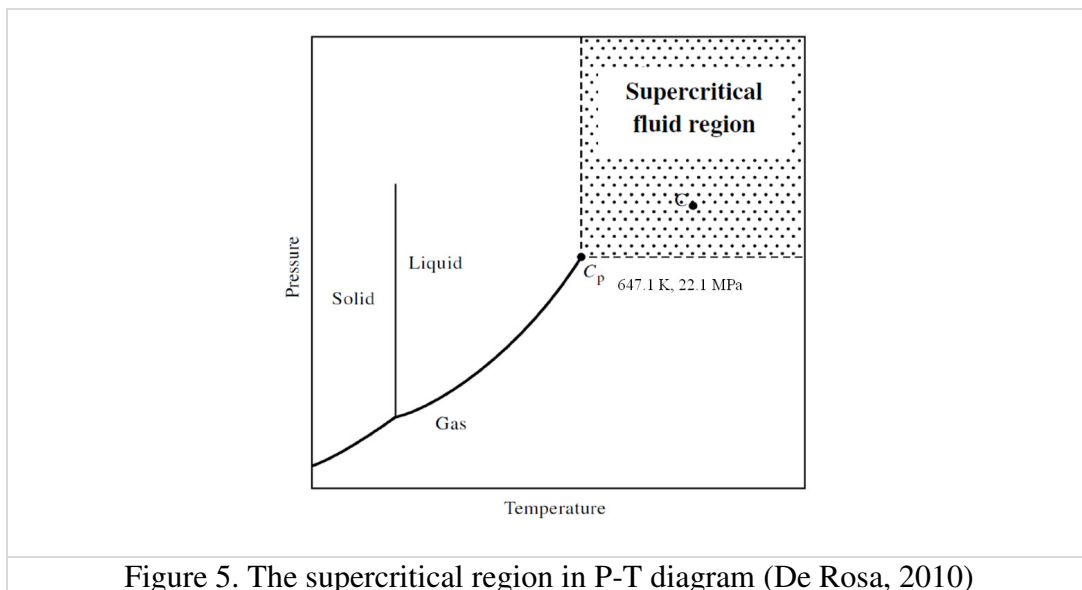
Water at an operating pressure of 25 MPa and temperature in the range of 280 ^{0}C to 550 ^{0}C is considered in the design of Supercritical Water Cooled Reactor (SCWR) systems. The main advantage of this supercritical fluid is that it combines the fluid like (at low-temperature) and gas like (at high-temperature) properties in the same energy cycle because of the large changes in properties near the pseudo-critical point. This is expected to decrease the amount of pump work needed in the pump at low temperatures, while the fluid behaves more like a gas at high temperatures in the turbine. The use of such systems also allows for the use of SCWR turbines, which can achieve a thermodynamic efficiency of over 40%.

Figure 6 presents the thermo-physical properties of water at and above the critical pressures, where the drastic variation in the water properties is clearly seen. The thermodynamic point where the specific heat is maximum (for a given pressure) is called the pseudo-critical point and the related temperature is called pseudo-critical temperature. Density, viscosity, and thermal conductivity all drop significantly at the pseudo-critical points. These large property changes pose significant challenges during thermal-hydraulic simulations. It can be further noted that as the pressure increases, the magnitude of variation in the water properties is reduced. However, at a SCWR design pressure of 25 MPa, there still exists a significant property variation.

Accidental release of water from supercritical conditions to ambient typically results in large pressure differential leading to a maximum discharge flow rate condition called the critical flow (or choked flow). For safety analysis of nuclear power plants, typically the mass discharge rate through a postulated break is determined using empirical models accounting for the pressure, enthalpies and phasic distribution of the flow through the break. Usually, experiments are conducted to evaluate critical flow and provide data for empirical model development or to validate computational codes. The situation is made more complicated due to the potential presence of a two- phase mixture resulting from flashing as the fluid depressurizes, influencing both the velocities and the speed of sound for the discharging fluid. Hence, in most nuclear safety codes (e.g.,

RELAP) critical break flows are predicted using empirically derived models. More details about the critical flow models are discussed in the following section.
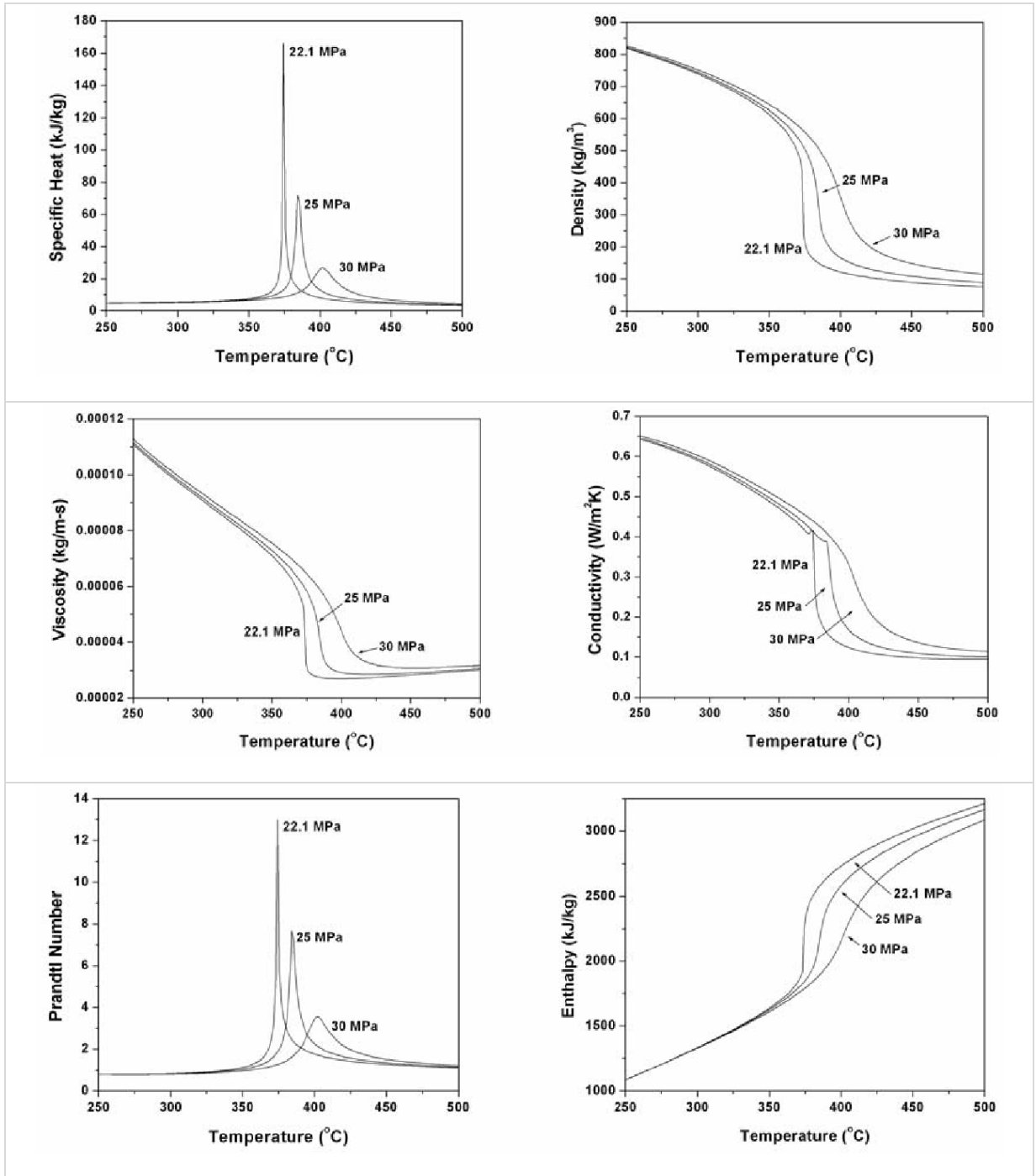
Figure 6. Thermo-physical properties of water at various pressures (Licht et al, 2007)

2.2 Critical Flow Models

There are several critical flow models reported in the literature for single-phase and two-phase releases. However, all the models have been primarily developed for sub-critical conditions and are valid only in those conditions. Their applicability for supercritical conditions needs further development and extensive validation with experimental data. The research is currently ongoing to customize models for supercritical systems. The following sub-sections provide a brief description of the critical flow models for single-phase and two-phase releases, particularly from sub-critical conditions.

2.2.1 *Single-phase Flow*

For single-phase flow, the critical flow can be evaluated using an analytical model for a given geometry and thermodynamic condition. Assuming ideal gas behaviour and isentropic conditions (frictionless and adiabatic), the critical mass flow rate, can be expressed as shown in Equation 2.1.

$$\dot{m} = \frac{AP_0}{RT_0} \sqrt{2C_p T_0 \left[\left(\frac{P_c}{P_0} \right)^{\left(\frac{2}{\gamma} \right)} - \left(\frac{P_c}{P_0} \right)^{\left(\frac{\gamma+1}{\gamma} \right)} \right]}$$

(2.1)

where, the critical pressure ratio is defined as,

$$\frac{P_c}{P_0} = \left(\frac{2}{\gamma+1} \right)^{\left(\frac{\gamma}{\gamma-1} \right)}, \text{ and}$$

$$C_p = \frac{\gamma R}{\gamma - 1}$$

Without the assumption of ideal gas, critical flow can be evaluated using models that solve the three governing equations (mass, momentum and energy conservation equations) at the node of interest. These models typically divide the geometry into several nodes and solves the governing equations at each node to compute critical flow at the

node of interest. One-dimensional computational codes (e.g., RELAP) and three-dimensional computational fluid dynamics (CFD) codes can be used to evaluate critical flow for single-phase releases, with 1-D codes most widely used in the industry.

Significant work has been done (theoretical and experimental) to evaluate critical flow from single-phase releases. It has been established that for single-phase releases, the exit discharge flow rate during choking condition is equal to speed of sound at the exit conditions. Under such circumstances, the downstream pressure information is unable to propagate upstream and the outlet pressure do not affect the discharge flow rate. Therefore, typically during choked flow condition for single-phase releases, we can expect the condition of Mach number equal to unity.

2.2.2   Two-phase Flow

For two-phase releases, the choked flow condition of Mach number equal to unity does not hold because the concept of single sound speed for a mixture of phases do not make sense. There may be more than one sound speed, e.g., one for each phase and one for the mixture depending on the flow pattern and geometry or quality of the mixture. Therefore, the evaluation of critical flow (or choked flow) for two-phase releases is typically carried out using Homogenous Equilibrium Models (HEM) or Non-Homogenous non-equilibrium models.

In the HEM approach, the pressure and temperature between the phases is assumed to be in equilibrium so that the velocity of liquid becomes equal to velocity of vapour. This condition is called a 'no-slip' condition. Several studies have been conducted to compare the critical flow experimental data with the HEM simulation (Moody, 1965, Trapp and Ransom, 1982, Chen et al., 2008). The results indicated that the model typically over predicts the critical flow rate obtained experimentally, because of not considering the pipe friction during simulation. This signifies the importance of friction during the critical flow evaluation.

Non-Equilibrium models relax the assumption of constant temperature, pressure and velocity between the phases (Henry and Fauske, 1971). These models clearly consider the effects of flashing, the growth of vapour phase, nucleation of the bubbles etc., during the two-phase releases. These models solve the three governing equations (mass, momentum and energy equations) without making any assumptions on the two-phases. A good overview of non-equilibrium models is provided by Saha (1978), who classifies the lumped models from the distributed models. Well known one-dimensions codes such as RELAP embed the non-homogenous, non-equilibrium models to evaluate critical flow. Although CFD codes such as STAR-CCM+, FLUENT etc., claim to support multiphase simulation, they are still in the development phase and the research for multiphase CFD simulation of critical flows is currently on-going.

Although, these models are not directly valid for supercritical conditions, efforts are underway to customize the models for supercritical systems. This research is an effort to customize a CFD code to solve thermal hydraulic simulations involving supercritical conditions. In this attempt, the CFD model results have to be validated with experimental data. The next section elaborates the critical flow experiments conducted under supercritical conditions.

2.3   Critical Flow Experiments

Since the introduction of SCWR concept, there has been very limited experimental studies on critical flow of water at supercritical conditions (Chen et al., 2009, Mignot et al., 2007 and Lee et al., 1983). Few relevant experiments were also conducted with CO_2 at supercritical conditions (Mignot et al., 2009, Gebbeken & Eggers, 1996), to provide more insight on the general phenomena of supercritical fluids. The following sub-sections provide a review of the critical flow experiments conducted under supercritical conditions.

2.3.1 CIAE experiments

Chen and co-authors (Chen et al., 2009) at the China Institute of Atomic Energy (CIAE) conducted a comprehensive set of critical flow experiments with water at supercritical pressures and temperatures. The main objective was to investigate critical flow characteristics at supercritical conditions and provide data to validate computational codes that are used for the SCWR safety analysis.

The experimental set up, as shown in Figure 7, was used to conduct the experiments, which were performed by ejecting water at supercritical pressures through the nozzle in vertical direction to replicate a loss of coolant accident (LOCA). A wide range of operating conditions were tested covering a pressure range of 22.1–26.8 MPa and temperature range of 38–474°C. Adiabatic conditions were maintained around the nozzle area, and the tests were conducted at steady state.

1-dumpting tank
2-preheater
3-nozzle test section
4-condenser
5-heat exchanger
6-flowmeter
7-pistom pump
8-water tank
9-valve
10-heat exchanger

Figure 7. Schematic of the experimental setup at CIAE (Chen et al., 2009)
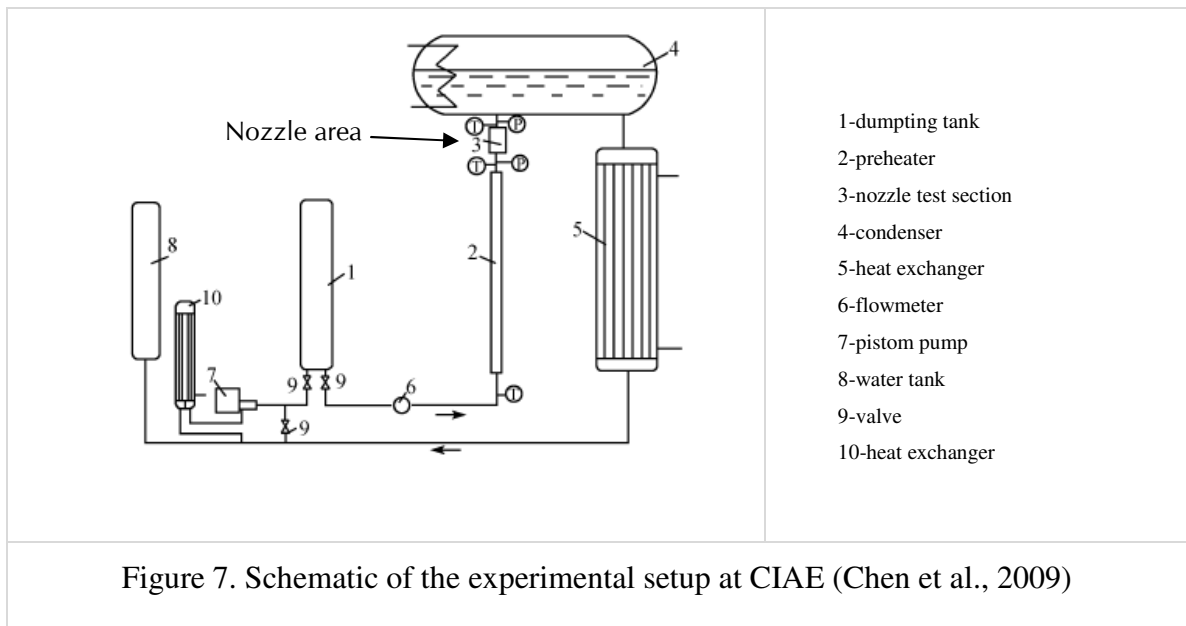
Two types of nozzles were used in the experimentation to study the effects of nozzle entrance geometry on the flow patterns. The schematics of both the nozzles, the rounded-edge (Nozzle-A) and the sharp-edge (Nozzle-B), are shown in Figure 8 and Figure 9 respectively. They have the same diameter of 1.41mm and length of 4.35 mm

but different inlet geometry. The rounded-edge nozzle has a smoothing radius of 1 mm. The parameters and range of conditions used in the experiments are listed in Table 1.

Table 1. Parameters and experiment conditions

Parameters	Conditions
Pressures	22.1–26.8 MPa
Temperatures	38–474°C
Heat mechanism	Adiabatic nozzle section
Expt. Conditions	Steady State
Flow direction	Upward
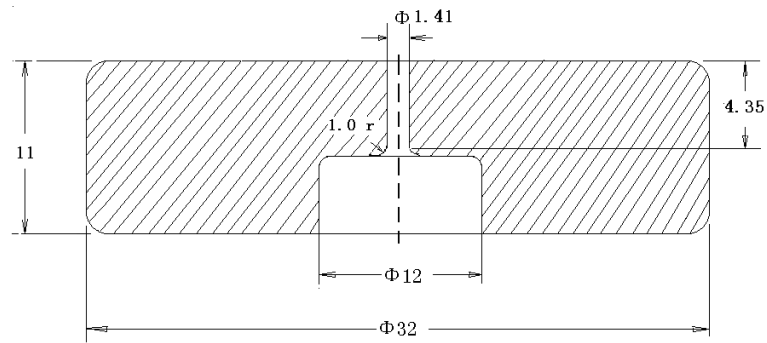
Figure 8. Nozzle A with rounded-edge (Chen et al., 2009)
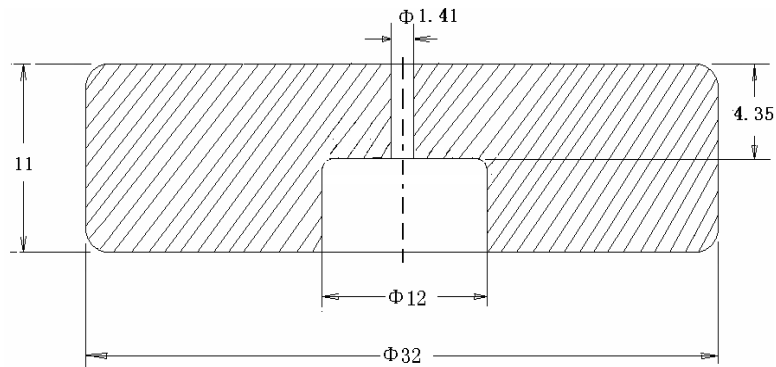
Figure 9. Nozzle B with sharp-edge (Chen et al., 2009)

The experimental data obtained using both the nozzles is reported as mass flux as shown in Figure 10 and Figure 11. The x-axis in the figures is differential temperature (DT_{PC}), which is calculated as pseudo-critical temperature (T_{PC}) less the inlet bulk temperature (T_{in}). Consequently, zero on the x-axis represents the operating condition where inlet temperature is equal to pseudo-critical temperature.

The results indicated that the entrance effects of the nozzles were significant only below the pseudo-critical region ($DT_{PC}>0$), where as in the near or beyond the pseudo-critical region ($DT_{PC}<0$), the results from both the nozzles were very similar, which can be clearly explained from Figure 10 and Figure 11. Particularly, the sharp-edged nozzle exhibited scattered results below the pseudo-critical region and the authors indicated this to be related to hysteresis in the onset of vaporization, describing a bifurcation behaviour. Hence for the sharp-edge geometry boiling/flashing can be initiated at different locations within the nozzle during two-phase discharge. The round-edged nozzle produced more stable results in the sub-critical region, and then shows the drastic change in behaviour in the flow rates near the pseudo-critical region, which is clearly due to the sensitivity of water properties.
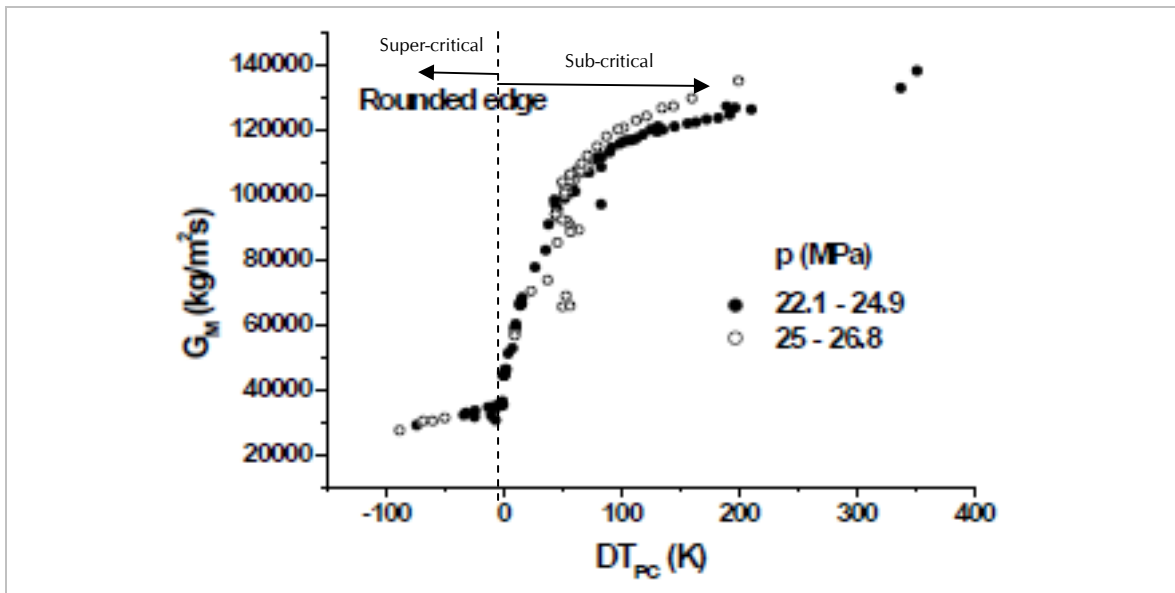
Figure 10. Mass flux data for round edge nozzle (Chen et al., 2009)
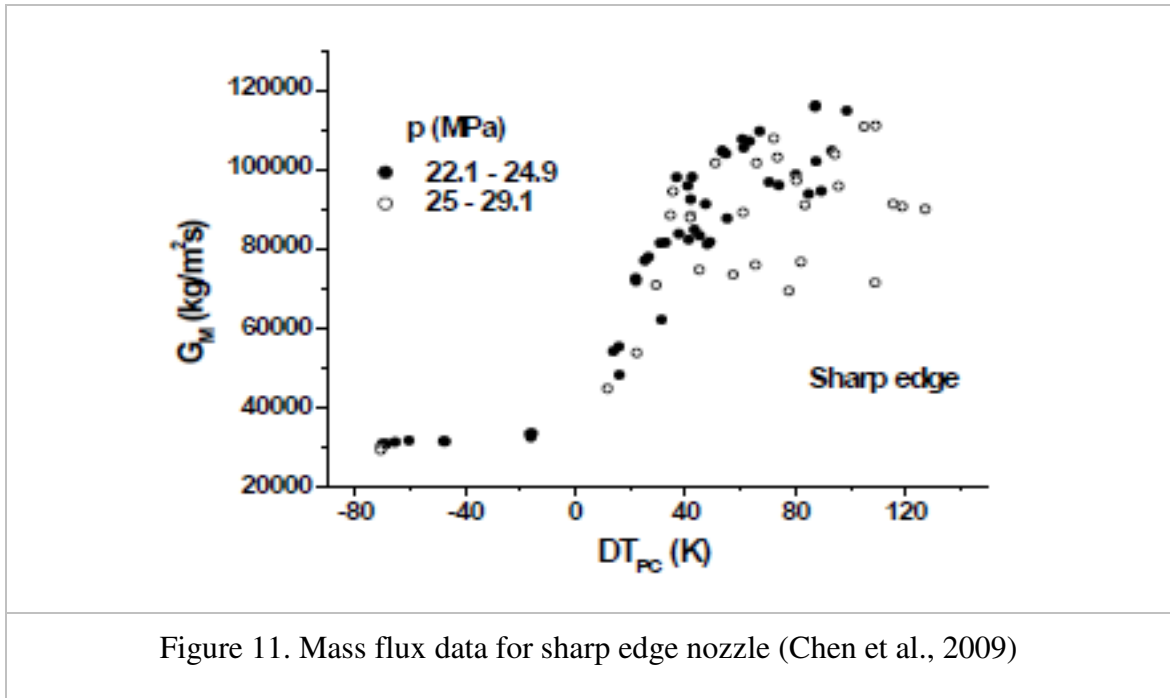
Figure 11. Mass flux data for sharp edge nozzle (Chen et al., 2009)

The authors simulated a one-dimensional Homogenous Equilibrium Model (HEM) equations to reproduce the experimental results. The results indicated that in the region near or beyond the pseudo critical point, thermal equilibrium is dominant and the critical flow rate was estimated by the HEM with good confidence. However below the pseudo critical temperature, the HEM over predicts the critical flow, and the authors postulate this was mainly due to the frictional resistances in the experiments that were not considered in the model.

2.3.2 UW experiments

The experiments at University of Wisconsin (UW) were focused on investigating the heat transfer phenomena, blow down transients and critical flow at supercritical conditions using fluids such as Water and CO_2 (Corradini, 2009 and Mignot et al., 2007 2009). More emphasis was given on studies related to heat transfer phenomena and limited experiments were conducted to evaluate critical flow with water. The details about critical flow experiments are discussed here.

A smooth sapphire tube of 1.59-mm inside diameter and 0.28-m long attached to a cylinder that contained water at supercritical conditions was used to conduct the transient blow down and steady state critical flow experiments with flow in the horizontal direction (Mignot et al., 2005, 2007). A picture of the nozzle area taken during experimentation is shown in Figure 12. The experiments were conducted under adiabatic conditions and covered only a narrow range of operating conditions (24.5-25 MPa and 480 to 520 ^{0}C). The results obtained from the experiments are presented in Table 2.
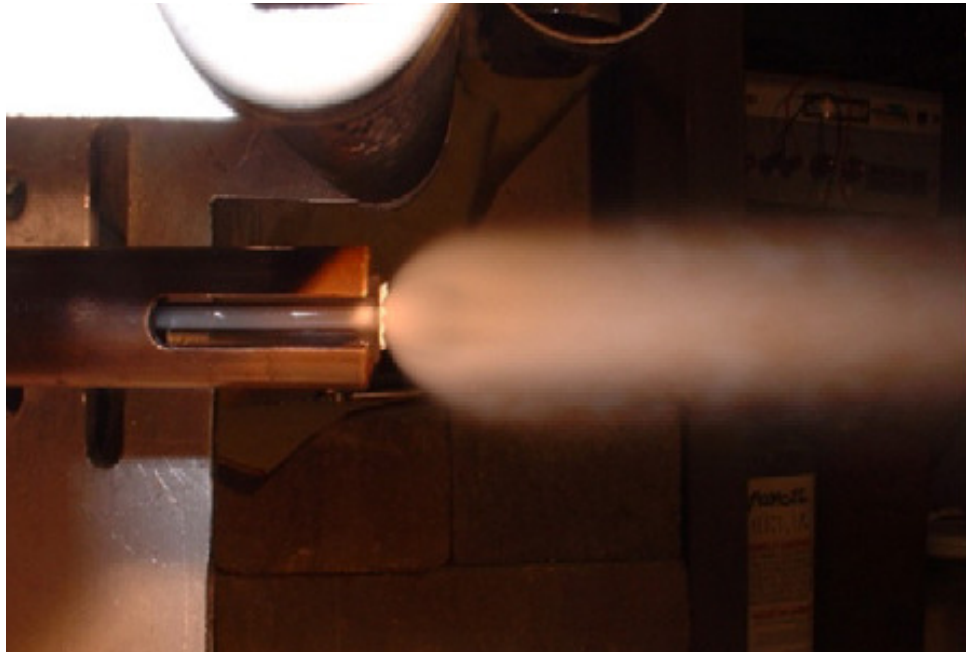
Figure 12. Nozzle used in the experiments (Mignot et al., 2009)

Table 2. Results from supercritical critical flow experiments (Mignot et al., 2007)

Po (MPa)	To (C)	Mass flow rate (Model) (Kg/s)	Mass flow rate (Experiment) (Kg/s)	Tr (T/Tc)	Pr (P/Pc)
24.43	480	0.041	0.048	1.16	1.10
24.72	514	0.040	0.046	1.22	1.12
24.75	479	0.042	0.043	1.16	1.12
24.80	482	0.042	0.050	1.17	1.12
24.92	511	0.040	0.043	1.21	1.13
24.95	514	0.040	0.042	1.22	1.13
25.09	511	0.041	0.042	1.21	1.14

Since, the experiments were conducted well above the pseudo-critical temperature (T_{PC}=385 ^{0}C at 25 MPa), the rapid change in fluid properties was not observed in these tests. Nevertheless, these operating conditions are within the operating range of supercritical water cooled reactors, thus providing valuable information for validating computational codes. The experimental data was compared with the results obtained from a one-dimensional HEM. It was found that the HEM results matched reasonably well with the experimental data. However, a prediction error of about 40% was observed in the results, which was attributed to the frictional effects in the experiment that was not considered in the HEM.

Several other tests were conducted with CO_2 at supercritical conditions to investigate the effect of inlet stagnant conditions, surface roughness and diameter to length ratio on critical flow (Mignot et al., 2009). The results indicated that the critical flow rate increased with a decrease in the temperature for a given pressure. This is expected because the density of the fluid increases quickly as the pseudo-critical point approaches. It was also found that the critical flow increases with a decrease in roughness, which is as expected. The smooth tube obtained critical mass flow rates about 15% higher than the rough tube.

2.3.3 Other experiments

Some of the earliest experiments reported in the literature involving supercritical water were conducted by EPRI (Lee & Swinnerton, 1983). The motivation to conduct these experiments was provided by the lack of data in high-pressure sub-cooled water conditions encountered while investigating anticipated transient without scram (ATWS) phenomena. Since the range of experimental conditions exceeded critical pressure and temperature, the data could be used as a source to validate computational codes at supercritical conditions. A wide range of pressures (4 MPa – 31 MPa) and temperatures (200 C – 400 C) were investigated, with some conditions exceeding the supercritical temperatures for a total of 283 experiments. Also, four different nozzles types (sharp edge, round edge, orifice and baffled) were used during the experiments, starting the idea of investigating the entrance effects on flow patterns.

Gebbeken & Eggers (1996) conducted blow down experiments with supercritical CO_2 to investigate the depressurization of chemical process equipment. The main emphasis of the study was on the pressure and temperature transients inside the pressure vessel during blowdown of CO_2 as this dominates the consequences of an accident. The work also reports the two phase conditions and the corresponding void fraction profiles inside the vessel. The results typically explain the general phenomena of depressurization in a pressure vessel, which could be used to evaluate the response time during an unforeseen event (e.g. LOCA).

In an attempt to obtain more critical flow data for supercritical fluids, École Polytechnique, Canada (Bae et al., 2009) has initiated a research program to experimentally study critical flow phenomenon using water under supercritical conditions. The main aim is to establish a test facility and perform critical flow experiments using different discharge nozzles varying in shape, size and length. As a result, the effect of discharge geometry on the critical flow can also be investigated. This data would be very valuable to validate several computational codes and use in the design of SCWR systems, particularly SCWR CANDU.

2.4   Computational Codes

This section briefly discusses the one-dimensional codes and Computational Fluid Dynamics codes that are used to perform thermal hydraulic simulations and highlights the challenges encountered by the codes while simulating supercritical conditions.

2.4.1   One-dimensional codes

One-dimensional (1D) system codes are most commonly used in the nuclear industry to perform thermal hydraulic simulation for safety analysis and design of Light Water Reactor (LWR) systems. Some of the well known codes include RELAP, CATHENA, TRACE, CATHARE and RETRAN. These codes typically embed a non-homogeneous, non-equilibrium two-fluid model consisting of six main equations to address single and two-phase fluid flow behavior. They have been extensively validated with experimental data, primarily under subcritical operating conditions, and so are widely accepted for accident investigation in LWR systems.

The application of most of these codes for supercritical systems is currently not possible due to numerical solution problems near the critical point, problems in the void fraction formulation near the critical pressure or because the steam stables in the codes do not support supercritical conditions. The evaluation of RELAP code (Riemke et al., 2003) for supercritical conditions indicated execution failures during simulation. Consequently, the code is currently being modified to implement updated steam tables and new methods to deal with the sharp changes in the water properties at pseudo critical conditions. The improvements are underway to completely fix the problems and use RELAP extensively to solve supercritical problems with increased confidence. Similar modifications are necessary for all the other codes as well. Without proper modifications and validation with the experimental data, these codes cannot be used to perform safety analysis for supercritical reactor systems.

On the other hand, a few simplified computational codes have been developed which embed Homogenous Equilibrium Model (HEM) equations and updated steam

tables to account for supercritical conditions (Chen et al., 2009 and Mignot et al., 2007). Although, these codes provided reasonable results in the supercritical region, they led to significant prediction errors in the sub-critical region as the frictional effects, dominant in the sub-critical region, were not modeled.

In general, the one-dimensional codes consume less computational time to perform a simulation as compared to 3D approaches. Consequently, they are the preferred codes to investigate design basis accident response and overall system behavior. Over the last 30 years, these 1-dimensional system codes have formed the basis for safety and licensing of power reactors, and have undergone extensive testing and validation. This validation typically considers experiments at the component level as well as fully integrated sets of tests. However, the major drawback with these codes is their inability to address the three-dimensional effects of fluid flow (e.g., swirling flows, separated flows, flows due to complex geometries where averaging is inappropriate etc.). These effects are often modeled using empirically derived expressions, which are then included within the 1D system codes. Hence, there is a potential to improve the accuracy of predictions by adopting 3D CFD models for components and geometries where the flow conditions may be too complex for the system code approach. Modeling these 3D details could add significant value to the safety analysis. CFD offers some advantages over 1D codes to address these effects.

2.4.2   *Computational Fluid Dynamics codes*

The importance of three-dimensional CFD codes has grown immensely in the last decade to perform thermal-hydraulic simulation studies in the design of nuclear reactor safety systems (Smith, 2010, Mahaffy, 2010 and Hohne et al., 2010). This increasing significance is mainly attributed to its capability to model the three-dimensional effects of fluid flow as mentioned earlier, which cannot be modeled by traditional one-dimensional system codes. These codes typically solves the three main conservation equations (mass, momentum and energy) and other miscellaneous equations in three dimensions to perform fluid flow analysis. The commercial codes are extensively developed for single-

phase fluid flow modeling and have largely been applied successfully. Multi-phase CFD modeling is still immature as a safety and licensing tool in the nuclear industry, but enhancements and validations are underway (Bestion, 2010).

Although, the computer technology has seen rapid developments in the recent times, CFD calculations are still limited by computational power primarily for complex geometries and by the turbulence models employed. Parallel computing has certainly provided a significant improvement in the computational efficiency, but there is still need to further improve the computational power. The different types of errors in CFD simulations include:

- Numerical errors, caused by the discretization of the flow geometry and the model equations, and by their numerical solution,

- Model errors, which arise from the approximation of physical processes by empirical mathematical models and turbulence resolution

Numerical errors can be reduced by defining a proper discretization scheme to an extent that the results do not change by refining the grid further (i.e., obtaining a grid-independent solution). Therefore, proper care should be taken to at least obtain a grid-independent solution that provides a solution within the acceptable range. Addressing modeling errors in critical flow is beyond the scope of this thesis, however this is partially addressed in this work by examining the sensitivity of the results to several of the common turbulence models available in the code.

The commercially available CFD codes include CFX (Cfx, 2009), FLUENT (Fluent Inc, 2004) and STAR-CCM+ (StarCCM+, 2009), although CFX and FLUENT are now distributed as part of ANSYS suite of computational codes. The three major steps involved in using these CFD codes include, (i) CAD modeling, (ii) Meshing, and (iii) Model solving. The ANSYS suite of codes only provide model solving (solver) capabilities, requiring a third party software to perform CAD modeling and meshing. On the other hand, STARCCM+ provides an integrated environment that allows us to

perform multi-dimensional CAD modeling, state-of-the-art meshing, model solving and post processing, all within the same software platform.

Similar to the 1-D codes, the commercial CFD codes are extensively applicable to simulate subcritical conditions. To a large extent, they do not support simulations under supercritical conditions because, the steam tables included in the packages are limited to only the subcritical subset of the thermodynamic properties (IAPWS IF97 (Iapws, 2007)). As a work around, the steam tables can be updated to include supercritical conditions of water and new methods can be implemented to access these steam tables at any thermodynamic state during simulation. By doing so, the CFD codes could be used to perform simulations under supercritical conditions. This implementation requires additional coding through external user-defined routines, and is a major part of the present work.

The commercial CFD codes allow the user to define external routines to implement methods that are not supported by the codes, such as the modification of steam tables. For example, Ambrosini (2009) has demonstrated that instead of using steam tables, the water properties under supercritical conditions can be fitted using higher order polynomials (Spline functions). The resulting polynomial equations can be defined as field functions in STAR-CCM+ to perform simulations related to flow instabilities under supercritical conditions. Similar approach was followed by De Rosa (2011) to study the heat transfer characteristics in supercritical systems. Both these studies were conducted at constant pressure, so that the water properties were defined only as a function of temperature. Consequently, this method is not applicable for systems where both pressure and temperature changes simultaneously. Gallaway et al (2007) proposed a similar polynomial fitting technique to investigate the heat transfer phenomena under supercritical conditions, but extended the applicability of the code to define the water properties as a function of both pressure and temperature. For the present work, it is critical to include thermodynamic properties which are a function of pressure and temperature, since critical flow involves both large pressure and temperature variations.

So far, CFD evaluation of critical flow under supercritical conditions has not been thoroughly investigated. It is important to understand that during critical flow experiments, although adiabatic conditions are maintained along the pipe, the coolant temperature along the length of the pipe decreases due to depressurization. Under supercritical conditions, even a slight change in temperature has to be properly considered, because near the pseudo critical region, a very small change in the temperature could lead to drastic changes in the water properties, which might lead to numerical instabilities during simulation. Therefore, it is required to precisely define the water properties at supercritical conditions as a function of pressure and temperature to evaluate critical flow.

In this thesis, we have developed a 2-D Look-up Table methodology to define the water properties as a function of pressure and temperature and implemented an interpolation scheme in STAR-CCM+ to perform the CFD simulations at supercritical conditions. The 2-D Table methodology replaces the IAPWS –IF97 steam tables currently present in STAR-CCM+. Further details about the 2-D Table method and interpolation scheme are discussed in Chapter 3. It should be noted that as a result of this work, the code developers of STAR-CCM+ are currently developing an internal 2-D interpolation scheme within the code.

2.5   Summary

This chapter briefly discussed the critical flow models (single phase and two phase fluid releases) that are valid for subcritical conditions. The process of extending these models for supercritical conditions is currently ongoing in the research community. In parallel, a few critical flow experiments have been conducted under supercritical conditions to develop and validate critical flow models. Particularly, the experiments conducted at CIAE were found to be most comprehensive at the time of this research. Therefore, these experiments have been adopted to validate the critical flow computational model developed in this research.

A brief description of computational codes (one-dimensional and computational fluid dynamics) was also provided, with main emphasis towards their application for supercritical conditions. It was found that at present, none of the codes are valid directly for supercritical conditions due to the limitations with the default steam tables. The codes (1-D and CFD) can however be made applicable for supercritical systems by updating the steam tables to include supercritical conditions of water. The details about customizing the CFD code to simulate supercritical conditions are described in the next chapter.

3.   Modeling Basis

The key topics covered in this chapter include: the governing equations for Computational Fluid Dynamics (CFD) modeling, description of the CFD code employed in this research to perform thermal-hydraulic simulations, its limitations for supercritical problems and finally a description of the customization of the CFD code to solve supercritical problems in this thesis.

3.1   Governing Equations

The governing equations for Computational Fluid Dynamic (CFD) modeling are nonlinear partial differential equations, which constitute the equations for conservation of mass, momentum and energy. Few other relevant equations are also required to appropriately describe fluid flow and heat transfer that includes turbulence models, near wall treatment etc. A brief description of the three-dimensional modeling equations derived by considering a finite control volume element are provided in the following sections.

3.1.1   Conservation of Mass

The conservation of mass equation for a compressible fluid is shown in Equation 3.1. The first term represents the rate of change of density with time. The second term represents the gradient of mass change along the three spatial coordinates. In this thesis, fluid is considered to be compressible (i.e., fluid density varies) while only steady state simulations are performed (i.e., time gradient disappears). This equation is also the differential form of the continuity equation.

$$\frac{\partial \rho}{\partial t} + \frac{\partial (\rho u_j)}{\partial x_j} = 0 \qquad\qquad (3.1)$$

where ,
ρ : is the fluid density (kg/m^3).
t : time (s).
x_j : spatial coordinates (m) i.e., x, y, z coordinates.

u_j : fluid velocity components (m/s) along the spatial coordinates.

3.1.2 Conservation of Momentum

The three-dimensional conservation of momentum equation in the spatial directions is shown in Equation 3.2. This equation actually constitutes three equations, one each towards a spatial coordinate. The equations are derived by setting the rate of change of the momentum in a particular component direction equal to the net force acting on the element in that direction (due to the surface stress) plus the gravitational and external forces.

$$\frac{\partial(\rho u_i)}{\partial t} + \frac{\partial(\rho u_i u_j)}{\partial x_j} = -\frac{\partial p}{\partial x_j} + \frac{\partial \tau_{ij}}{\partial x_j} + \rho g_i + F_i \tag{3.2}$$

where,

u_i : fluid velocity components u, v and w (m/s) along i.

p : pressure (Pa)

τ_{ij} : shear stress at ij surface (N/m^2)

g_i : the gravitational acceleration (m/sec^2)

F_i : external body force (N/m^3).

The shear stress term in Equation 3.2 is defined as shown in Equation 3.3 :

$$\tau_{ij} = -\rho u_i u_j = -\frac{2}{3} \mu \frac{\partial u_i}{\partial x_i} \delta_{ij} + \mu \left(\frac{\partial u_i}{\partial x_j} + \frac{\partial u_j}{\partial x_i} \right) \tag{3.3}$$

where ,

μ : is the molecular viscosity (Pa. s).

δ_{ij} : is the delta function.

The mass and momentum conservation equations, which form the Navier-Stokes equations are solved simultaneously to describe fluid flow. The most accurate numerical method to solve for turbulent flows is to directly solve the Navier-Stokes equations using

the Direct Numerical Solution (DNS) method without any turbulence model. However, the direct simulation is extremely difficult to solve and often is time consuming and not suitable for practical applications. Also, the approach is applicable only to flows at low Re number with simple flow geometries.

As an alternative, time averaged equations such as the Reynolds-Averaged Navier-Stokes equations (RANS) are used in practical computational fluid dynamics (CFD) applications when modeling turbulent flows. The main assumption in this approach is to decompose the transient velocity into a mean and turbulent fluctuating parts, and solve the resulting simplified equations. As a result of this decomposition, a new set of unknowns called Reynolds stresses arise in the model, which are related to turbulent viscosity. The equations relating to this discussion are presented here.

The decomposition of velocity is done as shown in Equation 3.4.

$$U_i(t) \equiv U_i + u_i(t) \tag{3.4}$$

where,

$U_i(t)$ is the velocity (m/s)

U_i is the mean velocity (m/s)

$u_i(t)$ is the turbulent fluctuating velocity (m/s)

The resulting simplified RANS equations for an incompressible flow under steady state conditions are described using the Equations 3.5 and 3.6.

$$\rho U_k \frac{\partial U_i}{\partial x_k} = -\frac{\partial p}{\partial x_i} + \mu \frac{\partial^2 U_i}{\partial x_j \partial x_j} + \frac{\partial R_{ij}}{\partial x_j} \tag{3.5}$$

$$R_{ij} = -\rho U_i U_j = -\rho \frac{2}{3} k \delta_{ij} + \mu_t \left(\frac{\partial U_i}{\partial x_j} + \frac{\partial U_j}{\partial x_i} \right) \tag{3.6}$$

where μ_t : is the turbulent viscosity (Pa.s)

R_{ij} : Reynolds shear stress.

Turbulence models are used to evaluate turbulent viscosity. There are several methods available for turbulence modeling, such as (i) Linear eddy viscosity models that includes one-equation models (Spalart-Allmaras model, Baldwin-Barth model) and two-equation models ($k - \varepsilon$, $k - \omega$), (ii) Nonlinear eddy viscosity models, (iii) Reynolds Stress Model (RSM), and (iv) Large Eddy Simulation models. The Linear eddy viscosity models, mainly the two-equation models, are mostly used for practical engineering applications. In this research, the CFD model was evaluated with several formulations of $k - \varepsilon$, $k - \omega$ and RSM models. The following section provides a brief description of the two-equation models, particularly $k - \varepsilon$ and $k - \omega$ models.

3.1.2.1 *Turbulence models*

$k - \varepsilon$ and $k - \omega$ models are the most common type of turbulence models employed in general solutions, which have become industry standard to solve most types of engineering problems (Wilcox, 2006). For these two-equation models, the turbulent viscosity is correlated with turbulent kinetic energy (*k*) and dissipation rate (ε or ω) depending on the type of two-equation model selected. For a $k - \varepsilon$ model, the correlation can be represented as follows:

$$\mu_t = \rho C_\mu \frac{k^2}{\varepsilon} \qquad (3.7)$$

Where,

$$k = \frac{U_i U_i}{2}$$

$$\varepsilon = \mu_t \frac{\partial U_i}{\partial x_j} \left(\frac{\partial U_i}{\partial x_j} + \frac{\partial U_j}{\partial x_i} \right), \text{ and}$$

C_μ is a constant.

The transport equations are solved to obtain *k* and ε, for the $k - \varepsilon$ model, so that the turbulent viscosity can be computed for RANS equations. By definition, two-equation

models include two transport equations to represent the turbulent properties of the flow. This allows a two-equation model to account for history effects like convection and diffusion of turbulent energy. One of the transported variables is the turbulent kinetic energy (k) and the second transported variable varies depending on what type of two-equation model is used. The common choices are the turbulent dissipation (ε) for $k - \varepsilon$ model, or the specific dissipation (ω) for $k - \omega$ model. The second variable can be thought of as the variable that determines the scale of the turbulence (length-scale or time-scale), whereas the first variable (k) determines the energy in the turbulence (Wilcox, 2006).

The commercial CFD codes support several turbulence models including the one-equation Sparlart-Allmaras model, the two-equation $k - \varepsilon$ and $k - \omega$ models, and the Reynolds Stress Model (RSM). In the k-epsilon suite of turbulence models, there are Standard k-epsilon model, Realisable k-epsilon model and RNG k-epsilon model. In the k-omega model suite, there are Standard k-omega model, Wilcox's modified k-omega model and SST k-omega model. Sensitivity of the CFD model to some of these turbulence models was evaluated in this research, the details of which are provided in Chapter 5.

The two transport equations for the standard $k - \varepsilon$ model are presented here as shown in Equations 3.8 and 3.9.

$$\frac{\partial}{\partial t}(\rho k) + \frac{\partial}{\partial x_i}(\rho k u_i) = \frac{\partial}{\partial x_j}\left[\left(\mu + \frac{\mu_t}{\sigma_k}\right)\frac{\partial k}{\partial x_j}\right] + P_k + P_b - \rho\varepsilon - Y_M + S_k \tag{3.8}$$

$$\frac{\partial}{\partial t}(\rho\varepsilon) + \frac{\partial}{\partial x_i}(\rho\varepsilon u_i) = \frac{\partial}{\partial x_j}\left[\left(\mu + \frac{\mu_t}{\sigma_\varepsilon}\right)\frac{\partial\varepsilon}{\partial x_j}\right] + C_{1\varepsilon}\frac{\varepsilon}{k}(P_k + C_{3\varepsilon}P_b) - C_{2\varepsilon}\rho\frac{\varepsilon^2}{k} + S_\varepsilon \tag{3.9}$$

where,

$$P_k = -\rho u_i' u_j' \frac{\partial u_j}{\partial x_j},$$

$$S \equiv \sqrt{2S_{ij}S_{ij}},$$

$$P_b = \beta g_i \frac{\mu_t}{Pr_t} \frac{\partial T}{\partial x_i},$$

$$\beta = -\frac{1}{\rho}\left(\frac{\partial \rho}{\partial T}\right)_P, \text{ and}$$

$C_{1\varepsilon}, C_{2\varepsilon}, C_{3\varepsilon}, \sigma_k, \sigma_\varepsilon$ are model constants.

Similarly, the transport equations for standard $k - \omega$ model are expressed as shown in Equations 3.10 and 3.11.

$$\frac{\partial k}{\partial t} + U_j \frac{\partial k}{\partial x_i} = \tau_{ij} \frac{\partial U_i}{\partial x_j} - \beta^* k \omega + \frac{\partial}{\partial x_j}\left[\left(v + \sigma^* v_T\right)\frac{\partial k}{\partial x_j}\right] \tag{3.10}$$

$$\frac{\partial \omega}{\partial t} + U_j \frac{\partial \omega}{\partial x_i} = \alpha \frac{\omega}{k} \tau_{ij} \frac{\partial U_i}{\partial x_j} - \beta \omega^2 + \frac{\partial}{\partial x_j}\left[\left(v + \sigma v_T\right)\frac{\partial \omega}{\partial x_j}\right] \tag{3.11}$$

where,

$$v_T = -\frac{k}{\omega}, \text{ and}$$

$\alpha, \beta, \beta^*, \sigma, \sigma^*$ are model constants.

Another important closure relationship for RANS models is the near wall treatment equations. The near wall region is important in turbulence flow modeling as it is the main source of turbulence generation during fluid flow. Accurate turbulence modeling typically requires successful treatment of the near wall effects. The default near-wall treatment model "All y+ Wall Treatment" available in the STAR-CCM+ code was considered in this research for all the simulations.

3.1.3 Conservation of Energy

The energy equation can be written in two different formulations, i.e., in terms of specific enthalpy or temperature. The choice of one rather than the other form depends on the particular type of problem or numerical considerations. The enthalpy form of the conservation equation is shown in Equation 3.12:

$$\frac{\partial}{\partial t}(\rho H) + \frac{\partial}{\partial x_j}\left(\rho u_j H + F_{h,j} - u_i \tau_{ij}\right) = -\frac{\partial p}{\partial x_j} + s_i u_i + s_h \tag{3.12}$$

where,

$$H = \frac{1}{2}u_i u_i + h$$

$$h = c_p T - c_p^o T^o + H^o$$

Here, the diffusive energy flux ($F_{h,j}$) is given by Equation 3.13, s_h are the energy sources, h is the enthalpy, c_p is the specific heat at constant pressure and temperature T, c_p^o the specific heat at constant pressure at reference temperature (293 K) and H^o is the formation enthalpy of the substance.

$$F_{j,j} = -k\frac{\partial T}{\partial x_j} + \rho u_j' h' \tag{3.13}$$

$$\rho u_j' h' = -\frac{\mu_t}{\sigma_{h,t}}\frac{\partial h}{\partial x_j} \tag{3.14}$$

Also, due to turbulence, a diffusive energy flux appears. This flux is associated with the fluctuations of the enthalpy and velocity average field. In the turbulent viscosity model these average quality are obtained from Equation 3.14. All the equations discussed so far from Equation 3.1 to 3.14 and other relevant equations are solved iteratively to describe the fluid flow and heat transfer behaviour.

3.2   CFD Code used in the research

This section provides a brief description of the commercial CFD code selected for this research work and the limitations of the code for simulating supercritical conditions.

3.2.1   STAR-CCM+

STAR-CCM+ is the commercial CFD software employed in this research to perform thermal hydraulic simulations. It is developed by CD-Adapco to perform three-dimensional modelling of fluid flow and heat transfer in complex geometries

(StarCCM+, 2009). Although, the code supports multi-phase fluid simulations, it is extensively used for single phase simulations. The code is built on a client-server architecture and has parallel processing capabilities to optimize the computational time. The main feature of STAR-CCM+ compared to other solvers such as FLUENT and CFX is its integrated environment that allows us to perform multi-dimensional CAD modeling, state-of-the-art meshing (tetrahedral, polyhedral, hexahedral etc.), model solving and post processing, all within the same software.

STAR-CCM+ supports unstructured meshing and incorporates two types of flow and energy modeling approaches namely, i) Segregated approach, and ii) Coupled approach. Segregated approach uses SIMPLE (Semi Implicit Pressure Linked Equation) algorithm to solve the conservation equations where as Coupled approach uses a time marching methodology (StarCCM+, 2009). A variety of turbulence modeling is supported including several variants of k-ε (standard, realizable, RNG), k-Ω (standard, SST) and Reynolds Stress Model (linear, quadratic). The solver permits control over parameters such as solver iterations, tolerance values and relaxation factors to manage the progress of convergence.

STAR-CCM+ also supports user-defined field functions to implement methods that are not directly supported by the software. Field functions are single-line, C-syntax type statements that allow the manipulation of variables and other field functions to construct complex logical statements.

3.2.2   Code Limitations

STAR-CCM+ has pre-defined steam tables to define the thermo-physical properties of water during simulation. The current version of steam tables (IAPWS-IF97) in the code is only valid for sub-critical conditions of water, i.e., conditions below the critical point (22.1 MPa and 647 K). Consequently, STAR-CCM+ cannot be directly used to simulate models for supercritical conditions. For instance, if supercritical conditions

are encountered during the simulation, STAR-CCM+ produces the error message shown in Figure 13, and quits the simulation.
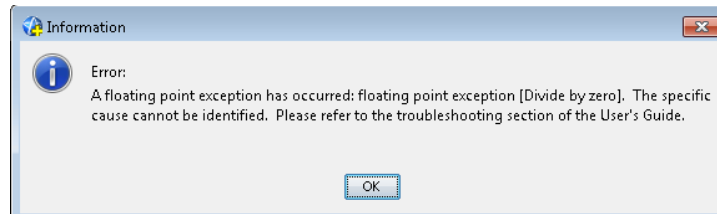
Figure 13. STAR-CCM+ error message for supercritical conditions

After careful examination, it was found that STAR-CCM+ can be customized to simulate supercritical systems by updating the current steam tables to include subcritical as well as supercritical data. The default steam tables (IAPWS-IF97) in the code cannot be altered. Therefore, for successful customization, it is required to perform three main tasks, (1) Create new updated steam tables, (2) Make them accessible to STAR-CCM+ during simulations, and (3) Create a multidimensional interpolation scheme to solve for the water properties at each node. Accomplishing these tasks are the major challenges of this research.

To create steam tables, the data for a wide range of pressures and temperatures can be obtained from the National Institute of Standards and Technology (NIST) database, which is made available to the general users through the following website (http://webbook.nist.gov/chemistry/fluid/).

To make the steam tables accessible to STAR-CCM+ and evaluate the water properties at each node during simulation, two different methods were investigated. They are the interpolating polynomials method and the 2-D Table method. Only these two methods are supported by STAR-CCM+ at the moment, although the STAR-CCM+ developers are currently working to expand the interpolation and properties to the supercritical region. Further details about these methods and the investigation results are presented in the following section.

3.3 Customization of the code for supercritical systems

Typically, Loss Of Coolant Accident (LOCA) simulation scenarios involve changes in both pressure and temperature in the system. Therefore, the new steam tables should define the water properties as a function of both Pressure and Temperature. For the current research, the water property data was obtained for a pressure range of 0.1 MPa to 27 MPa and temperature range of 550 K to 700 K so that the sub-critical region as well as the pseudo-critical region is covered.

This two-dimensional (2D) data should be embedded within STAR-CCM+ so that the data can be accessible to the CFD code during simulation and the water properties can be evaluated at each node for the required thermodynamic state. The two methods considered in this thesis are investigated here. The investigation is carried out to evaluate the best method that ensures reliability during computations and provides a right balance between accuracy, computational burden and programming complexity.

3.3.1 *Interpolating polynomial*

Interpolating polynomials are polynomial functions obtained by fitting two-dimensional data (e.g. steam tables data). A typical polynomial function with respect to Pressure (P) and Temperature (T) is represented as shown in Equation 1. The constants (c_{ij}) in the polynomial function can be obtained by surface fitting algorithms.

$$f(P,T) = \sum_{i}^{m}\sum_{j}^{n} c_{ij} P^{i} T^{j} \qquad [1]$$

Using such polynomial functions, each of water properties (e.g., density, viscosity, thermal conductivity, specific heat etc.) can be fitted as a function of temperature and pressure f(T,P), such that they can be used to evaluate the water properties at any given Pressure and Temperature. These polynomials can eventually be defined as field functions in STARCCM+, so that the CFD code can access the water properties at any thermodynamic state during simulation.

The main objective of this investigation was to evaluate the feasibility of fitting the updated steam stables as an interpolating polynomial. The goodness-of-fit for the interpolating polynomial typically represents how well the polynomial fits the data. This is an important parameter, because poor goodness-of-fit could lead to large interpolation errors. For the current research, highly accurate polynomials are required because in the pseudo-critical region (i.e., Pressure range of 22 – 27 MPa and Temperature range of 645 to 660 K), even small changes in the pressure and temperature could result in rapid changes in the water properties.

The 2-D data for water density with respect to pressure and temperature is represented as a surface plot as shown in Figure 14. Clearly the water density at subcritical conditions (i.e., less than 22 MPa) is quite linear; however, in the pseudo-critical region (i.e., above 22 MPa and between 645 - 660 K) water density is very nonlinear due to the pseudo-critical transition. Similar kind of non-linearity can be observed for other water properties as well. It is very challenging to fit such non-linear data using interpolating polynomials
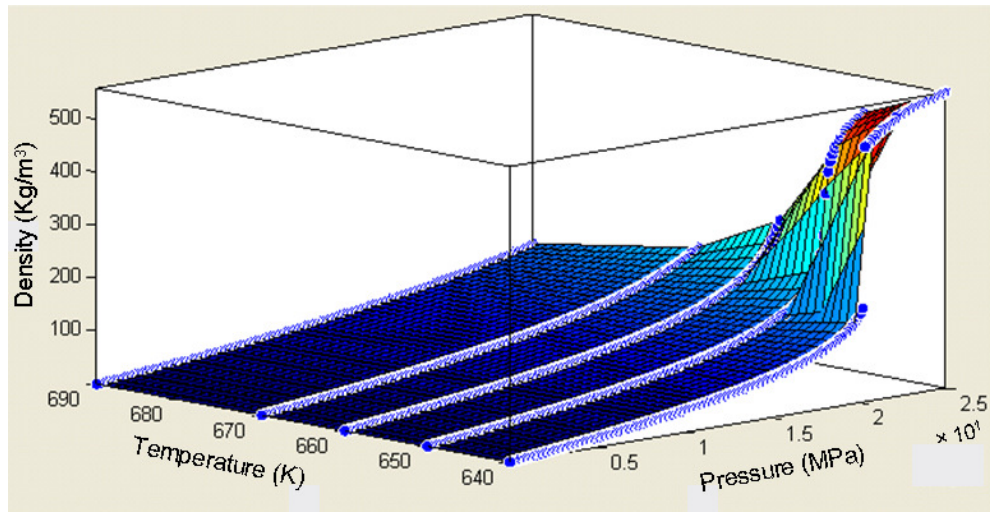
Figure 14: Surface plot for water density

Although, several attempts were made to fit this surface data, it was difficult to obtained a good fit over the entire range of conditions, which is primarily attributed to the

non-linearities in the pseudo-critical region. The best fit obtained had a goodness-of-fit value of about 80%, which means that interpolation error using these polynomials is about 20%. This error is quite large for the current context and consequently, it was concluded that the interpolating polynomial approach may not be suitable to represent the 2-D steam tables in the current research.

3.3.2   2-D Look-up TABLE method

In the 2-D Look-up Table method, firstly the water properties (e.g., density, viscosity, thermal conductivity, specific heat etc.) are defined as separate 2-dimensional tables over a defined range of pressure and temperature, so that the data covers sub-critical as well as super-critical conditions. A typical 2-D table for water density is shown in Figure 15. These 2-D tables can be made accessible to STAR-CCM+ using external user-defined routines. The routines are implemented in a way that STAR-CCM+ can access the 2-D tables to retrieve the water properties at any pressure and temperature during simulation. Typically, the default steam tables in STAR-CCM+ are replaced by this method to solve supercritical scenarios.

Pressure (MPa)	Temperature (K)									
	550	600	610	620	630	640	.	.	690	700
0.10	0.40	0.36	0.36	0.35	0.34	0.34	.	.	0.31	0.31
0.20	0.79	0.72	0.71	0.70	0.69	0.68	.	.	0.63	0.62
0.30	1.19	1.09	1.07	1.05	1.03	1.02	.	.	0.94	0.93
0.40	1.59	1.45	1.43	1.40	1.38	1.36	.	.	1.26	1.24
0.50	1.99	1.82	1.79	1.76	1.73	1.70	.	.	1.57	1.55
0.60	2.40	2.18	2.15	2.11	2.08	2.04	.	.	1.89	1.86
0.70	2.80	2.55	2.51	2.47	2.43	2.39	.	.	2.21	2.17
0.80	3.21	2.92	2.87	2.82	2.78	2.73	.	.	2.53	2.49
0.90	3.62	3.30	3.24	3.18	3.13	3.08	.	.	2.84	2.80
1.00	4.04	3.67	3.61	3.54	3.48	3.42	.	.	3.16	3.12
.	.	.	.	.	.	.	.	.	.	.
.	.	.	.	.	.	.	.	.	.	.
.	.	.	.	.	.	.	.	.	.	.
26.90	784.33	692.79	669.19	642.50	611.34	572.91	.	.	160.62	145.00
27.00	784.37	692.87	669.29	642.62	611.50	573.15	.	.	161.12	145.39

Figure 15: 2-D table for Water Density

This method is similar to a 2-D table lookup approach, where the updated steam tables are first defined as 2-D tables and then STAR-CCM+ retrieves the required data during simulation by performing 2-D interpolation over pressure and temperature. Unfortunately, STAR-CCM+ does not support 2-D interpolation by default. As a result, user-defined routines were implemented in STAR-CCM+ using the available field functions to perform the 2-D interpolation over all the water property tables. For instance, when a fluid property has to be evaluated at a given thermodynamic state (i.e. Temperature and Pressure), the routine first performs a 1-D interpolation over the temperature grid to obtain a column of data for various pressures and then finally performs an interpolation over the pressure grid to obtain the fluid property at the required temperature and pressure.

It is well known that the water properties in the sub-critical region are quite linear. However, in the transition from sub-critical to supercritical region (i.e., in the pseudo-critical region), they are highly non-linear. Therefore, proper care should be taken while implementing 2-D interpolation routines. Due to the complexity involved in implementing non-linear interpolation routines in STAR-CCM+, only linear interpolation was implemented in this research. Appropriate care was taken to minimize the error due to linear interpolation by defining a smaller grid spacing (along temperature and pressure grids) in the pseudo-critical region (645 K - 660K and 22 – 27 MPa) as compared to the other regions. For clarity, the pressure and temperature grids in the 2-D table are shown in Figure 16.

Pressure (MPa)	Temperature (K)									
	550	600	610	620	630	640	.	.	690	700
0.10						Temperature grid				
0.20										
0.30										
0.40										
0.50										
0.60										
0.70										
0.80										
0.90										
1.00										
.										
.										
.										
26.90										
27.00										
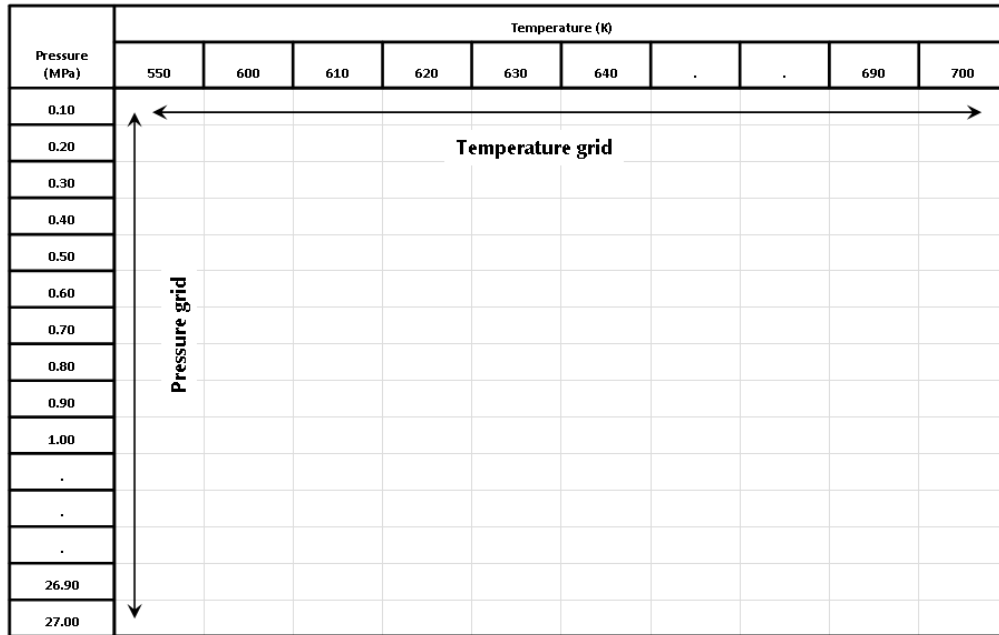
Figure 16: Pressure and Temperature grids

Since, the water properties in the sub-critical region are quite linear, a coarse grid spacing is sufficient in this region, whereas a fine grid spacing is required for the pseudo-critical region to ensure that the interpolation errors are minimum. A uniform grid spacing of 0.1 MPa was chosen for the pressure grid, whereas a non-uniform spacing was used for the temperature grid such that coarse grid spacing is maintained in the subcritical region and fine grid spacing in the pseudo-critical region. Using such grid formulation was found to provide a good balance between programming burden and accuracy of routine implementation.

For temperature, a grid spacing of 1 K was used for the coarse grid (i.e. in the subcritical region) and 0.25 K was used for the fine grid (i.e. in the pseudo critical region). It was found that the fine grid spacing of 0.25 K was the most appropriate in this research that ensured the interpolation errors near the pseudo-critical transitions are minimum (typical maximum difference in density for any given interpolation condition is about 3.5%; i.e., interpolation error is less than 3.5%). The details about the effect of grid spacing on the interpolation error can be found in Appendix A.

Obtaining an optimal grid spacing over both the dimensions (Pressure and Temperature) was the most challenging task of this method. Once, it was accomplished, this method was found to provide good results without reporting any execution failures during simulation. This method could therefore, be the most appropriate to define the updated steam tables and make them accessible for STAR-CCM+ to simulate supercritical conditions.

3.4   Summary

This chapter describes the governing equations and main features of the CFD software STAR-CCM+ that was selected to perform thermal-hydraulic simulations in this research. After several simulation trials, it was confirmed that STAR-CCM+ do not support thermal-hydraulic simulations for supercritical conditions of water. The reason was because the default steam tables (IAPWS-IF97) are valid only for subcritical water properties. Our investigation has revealed that if updated steam tables (that includes subcritical and supercritical data) are created and embedded in STAR-CCM+, the code can be used to solve supercritical problems. To address this issue, two different approaches (Interpolating polynomials and 2-D Look-up Table method) were investigated in this research to customize the new steam tables in STAR-CCM+, and it was found that 2-D Table method is the most appropriate method to customize the CFD code to solve supercritical problems.

Consequently, the 2-D Look-up Table method was chosen for this research work and implemented in STAR-CCM+ through several user defined routines. The implementation was tested for several case studies and confirmed that there were no issues with the 2-D Table approach. Following the successful implementation, all the supercritical simulation scenarios considered in this thesis were simulated without any reported issues. The details about CFD modeling procedure followed in this thesis are described in the next chapter.

4. Experimental Data and CFD Modeling procedure

This chapter presents the experimental data that was selected to test the CFD model and validate its results. It also provides an overview of the steps involved in CFD modeling and simulation. The details related to each step are discussed and the importance of fine tuning in CFD simulation is highlighted.

4.1 Experimental Data considered in this research

The experimental data reported by China Institute of Atomic Energy (CIAE) (Chen et al., 2009) that was discussed in Section 2.3.1, has been chosen in this research to evaluate the CFD model and validate the simulation results. The experiments were performed at steady state and adiabatic conditions by ejecting water at supercritical pressures through two types of nozzles to represent a loss of coolant accident (LOCA) and study the effects of nozzle entrance geometry on the flow patterns.

The schematics of both the nozzles, the smooth-edge (Nozzle-A) and the sharp-edge (Nozzle-B) are shown in Figure 17 and Figure 18 respectively. They have the same diameter of 1.41mm and length of 4.35 mm but different inlet geometry. The rounded-edge nozzle has a smoothing radius of 1 mm.
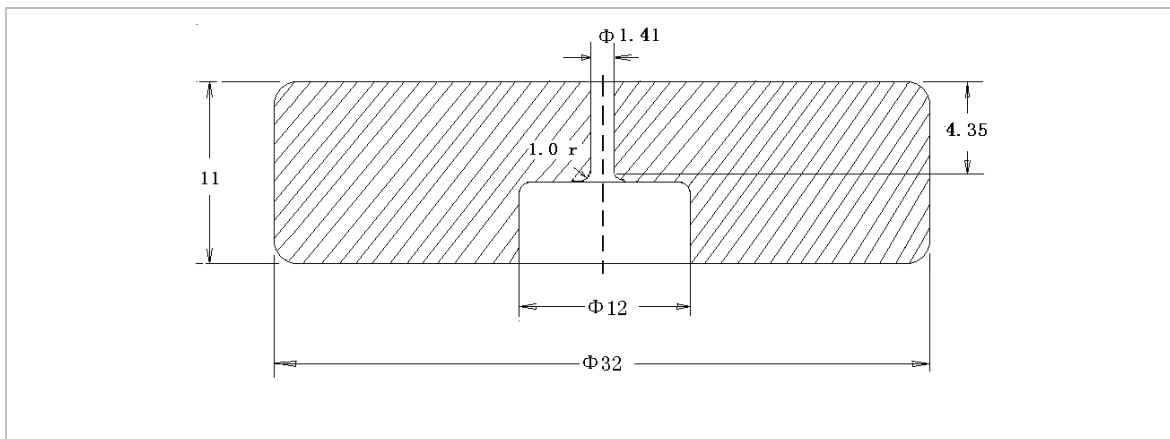
Figure 17. Nozzle A with rounded-edge (Chen et al., 2009)

Figure 18. Nozzle B with sharp-edge (Chen et al., 2009)
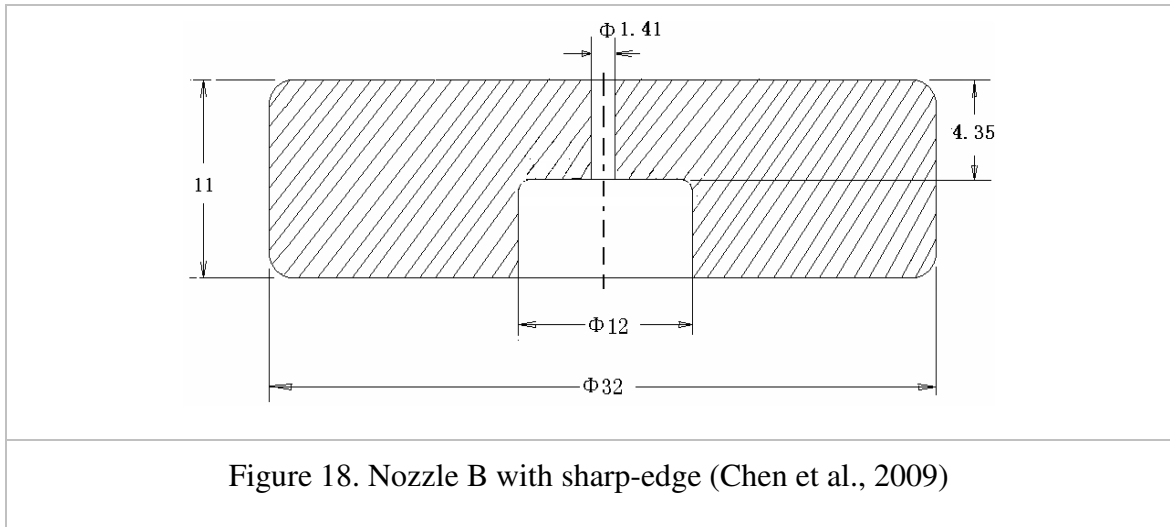
In this research, the thermal models were developed for both these nozzles and the steady state simulation was performed for various scenarios of inlet pressure and temperature to reproduce the experimental data. The details about CFD modeling and the steps involved in the simulation procedure are discussed in the following sections.

4.2   CFD Modeling Procedure in STAR-CCM+

Computational Fluid Dynamic (CFD) modeling and analysis in STAR-CCM+ comprises of building a three-dimensional thermal model and simulating the postulated case studies. The steps followed to perform CFD analysis include:

- Creating CAD models,
- Meshing the model,
- Selecting Physics models,
- Defining Initial and Boundary conditions,
- Specifying Convergence criteria, and
- Running the simulation.

Relevant details of these steps are elaborated in the following sections.

4.2.1   CAD modeling

The first step in CFD analysis is to develop a 3-D CAD model. For this research, CAD models for the two nozzles (Nozzle A and Nozzle B) were developed in STARCCM+ as shown in Figure 19 and Figure 20 respectively. The length of pipes leading to the nozzles was altered (as opposed to original designs discussed in Section 3.4.1) in order to achieve fully developed flow in the pipes before the fluid exits through the nozzle. This was done in order to ensure that the critical flow is not affected by flow irregularities in the pipe.

After performing several simulations, it was verified that a length of at least 20 cm would guarantee fully developed flow in the pipe under supercritical conditions. Therefore, a pipe length of 20 cm was chosen for the CAD model. It is important to understand that altering the length of the pipe does not affect the critical flow from the nozzle. It is the nozzle geometry that is of prime interest for interpreting the simulation results.

20 cm Flow direction	Flow direction
Figure 19. CAD model for Nozzle A	Figure 20. CAD model for Nozzle B
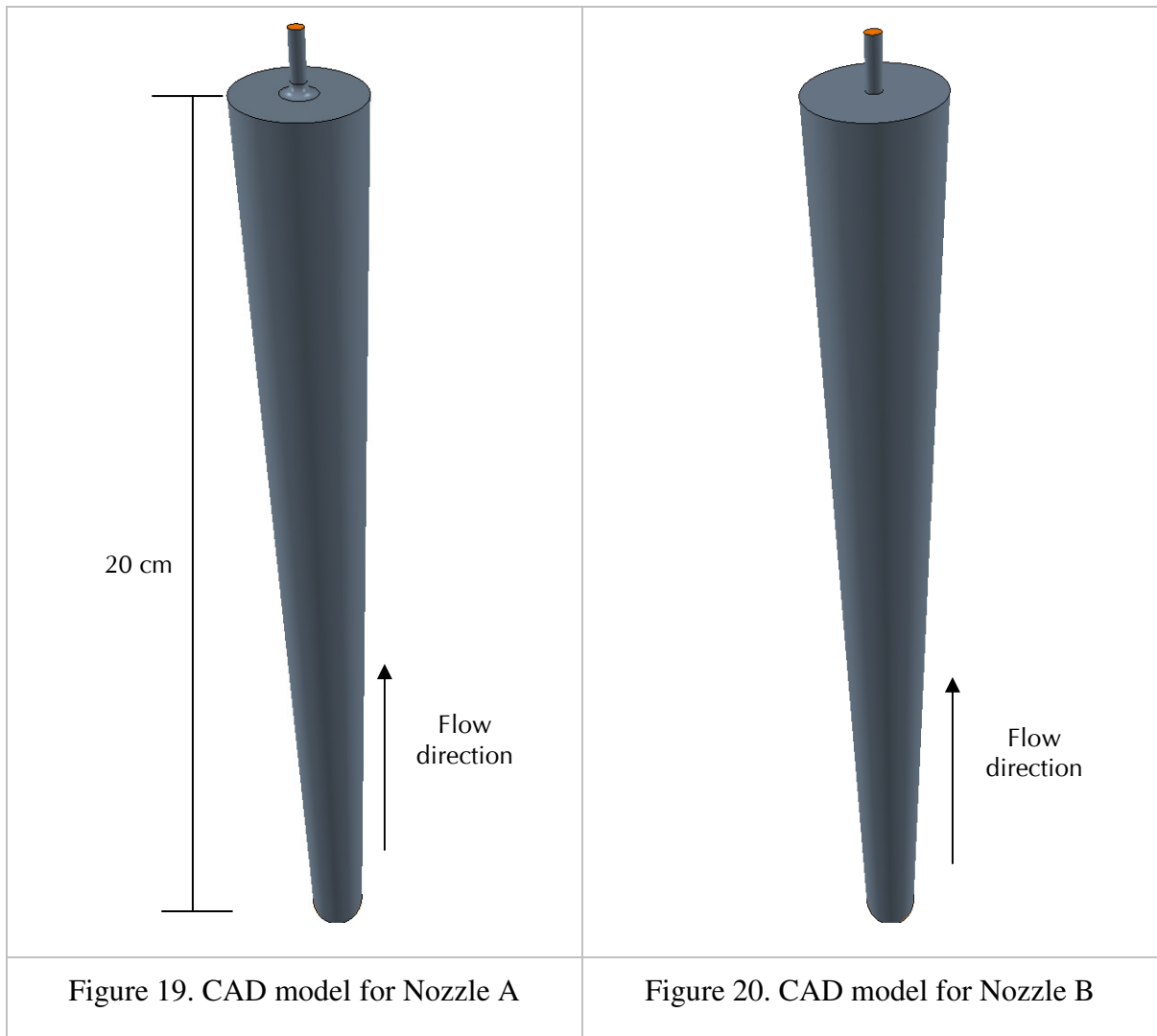
4.2.2 Meshing

Meshing in an important step of CFD analysis because an inappropriate mesh configuration could lead to a bad solution. It is well known that a coarse mesh requires less computational time but provides less accurate results, whereas a finer mesh requires more computational time but provides better results. Therefore, an optimal mesh configuration is required that provides a balance between computational time and solution accuracy. A balance of meshing techniques involves choosing appropriately

small grid spacing in regions of greatest gradients (i.e., near walls and constrictions), and selecting larger spacing for the far field.

A typical mesh configuration for Nozzle-A and Nozzle-B are shown in Figure 21 and Figure 22 respectively. This was created in STARCCM+ and consisted of 1259523 cells, 8730423 faces and 7472079 vertices for Nozzle-A. In order to optimize the mesh configuration, surface wrapping was used and polyhedral volume mesh was implemented. Customized mesh was generated with finer mesh in the nozzle area (the area of interest), and coarse mesh in the pipe section. This reduces the total number of cells in the mesh and hence improves the computational time.

Figure 21. Mesh details around the nozzle area for Nozzle A
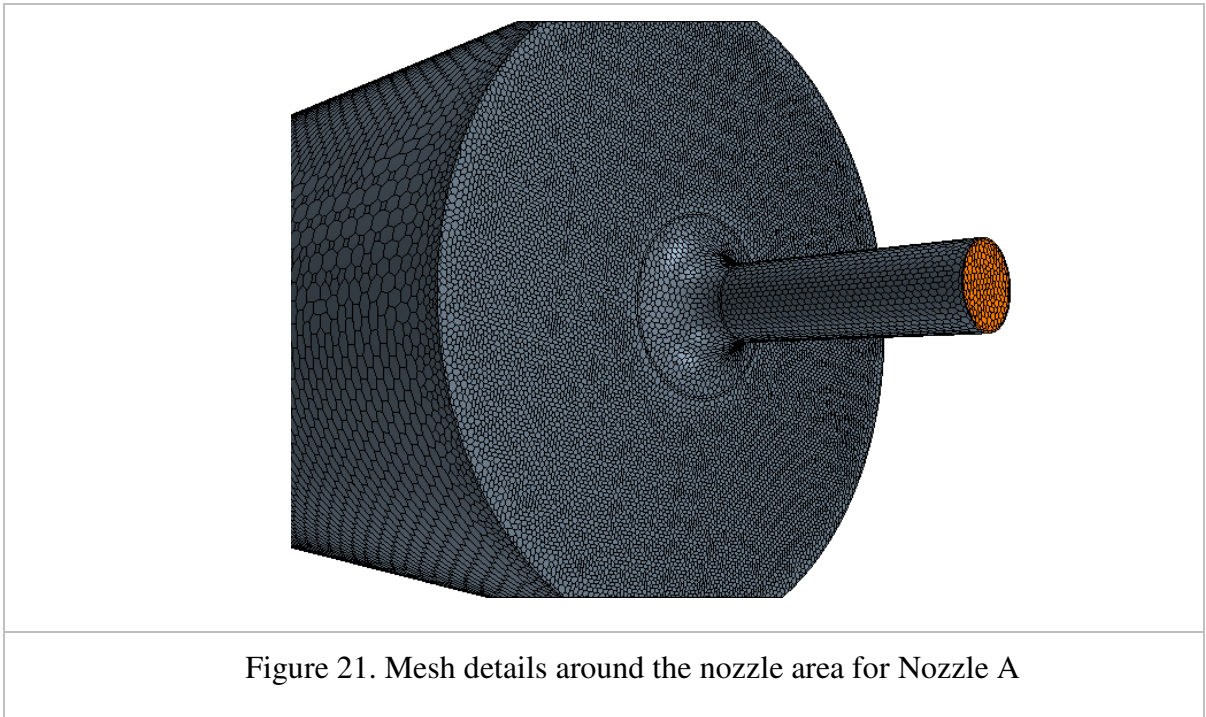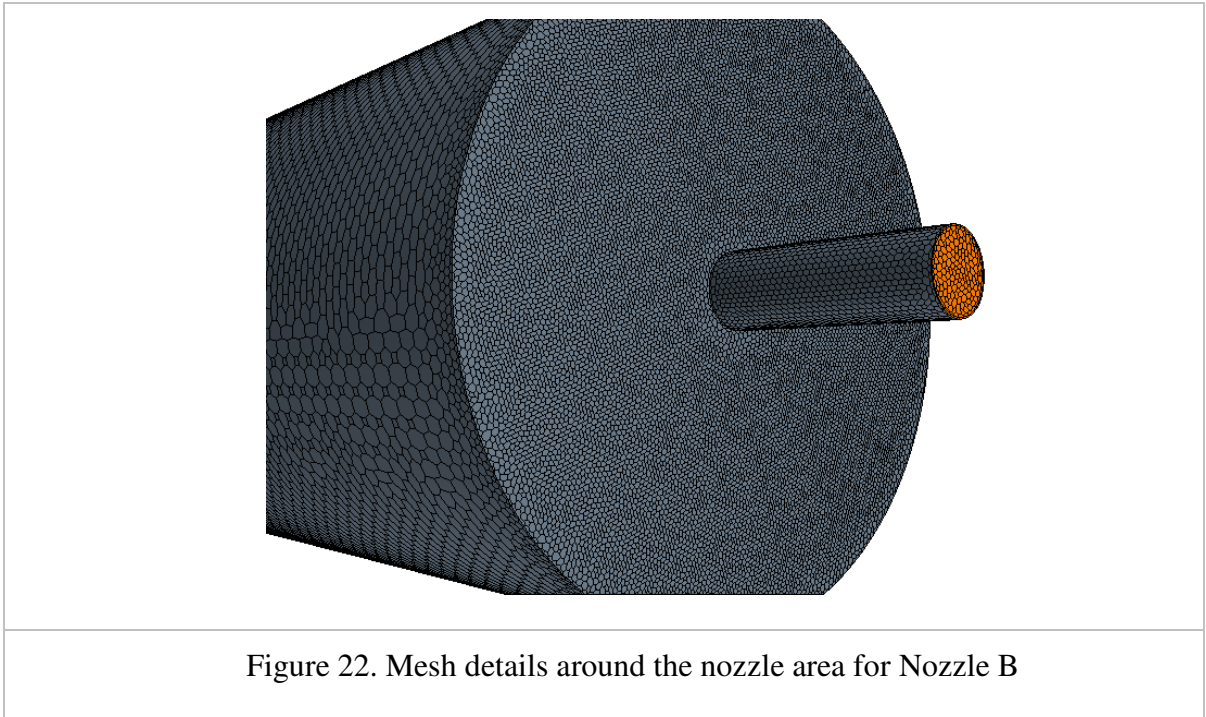
Figure 22. Mesh details around the nozzle area for Nozzle B

A comprehensive sensitivity analysis was performed in this research to determine the best mesh configuration for the nozzles. Four different mesh configurations with varying grid densities were tested and the results obtained from the analysis are discussed in section 5.3.2.1.

4.2.3 Physics models

The physics models also form an integral part of the CFD simulation. These models are used to define the fluid type, flow modeling, energy modeling, turbulence modeling, thermo-physical properties, discretization schemes and simulation conditions. Proper knowledge of these models will help define the simulation conditions appropriately. The physics models shown below were used to perform the case studies.

- Single phase fluid (H_2O)
- Segregated flow model
- Segregated Fluid Temp model
- Reynolds-Averaged Navier-Stokes
- Turbulence model (k-epsilon, k-omega or RSM)

- All y+ Wall Treatment
- User defined properties (density, viscosity, thermal conductivity)
- No slip - shear stress
- Rough wall surface
- Adiabatic wall surface
- Gravity
- Upward flow
- Steady State simulation
- Discretization schemes
  - Flow loop: Second-order upwind convection scheme
  - Energy loop: Second-order scheme

4.2.4 Boundary/Initial conditions

The boundary conditions and initial conditions for the CFD model are set according to the postulated case study. The initial conditions typically play a major role in the progress of convergence. A better initial guess would definitely help converge faster than a bad guess. Depending on the turbulence model, in some cases, a bad initial guess could lead to diverging solution. Therefore, it is advisable to use a better initial guess. For example, a solution from a coarse mesh model could be used as an initial guess for a fine grid model to obtain better results.

4.2.5 Convergence criteria

CFD problems solve the conservation equations, which are non-linear, and the solution techniques use an iterative process to successively improve a solution, until 'convergence' is reached. The criteria for convergence is typically decided based on knowledge of the problem and the CFD code. During the solution procedure it is often preferred to plot the residuals (the amount by which the discretized equations are not satisfied) as function of iteration number. By doing so it is possible to visualize how the residuals are developing with iterations.

The reduction in the residuals indicate the progress towards convergence. However, once the residuals are reduced to a certain level, they exhibit minor random fluctuations, which are caused by the numerical round off errors associated with the CFD codes level of precision. Ideally, it is preferred to perform iterations until this level of convergence is reached. A sample residual convergence plot for a case study simulated in this thesis is shown in Figure 23, which illustrates this behaviour.
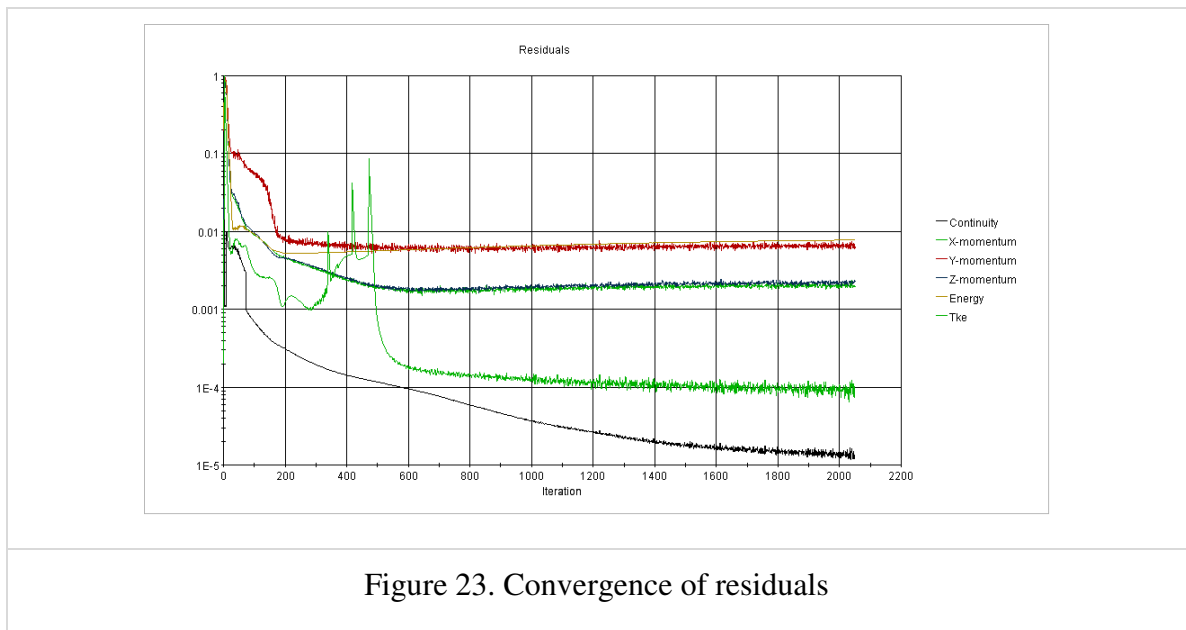
Figure 23. Convergence of residuals

On the other hand, user experience suggests that the reduction of residuals to a level of 10^{-6} guarantees convergence to a sufficient level, but it is often impossible to reach these values because of the complexity of the problem under investigation. Also, one should understand that residuals are linked with the initial guess for the CFD problem. For example, if the results from a coarser grid model are used as the initial guess for a fine grid model, the residuals will not reduce greatly after few iterations because the continuity is already relatively well converged. Therefore, the criteria for convergence should be based on experience and knowledge of the model. Besides the residuals, it is preferred to monitor the variables of interest after every few iterations to see if a stable solution is reached, which then also helps us to confirm convergence.

The best practice followed in this research was to firstly monitor the residuals until they reached a point of sufficient convergence represented by steady fluctuations followed by monitoring the variables of interest, such as pressure, velocity and physical properties of water for an extended period of time to confirm steady solution. When both these criteria are satisfied, we confirm sufficient convergence has been attained. For example, the outlet pressure and velocity as a function of solver iterations depicted in Figure 24 and Figure 25 were used to confirm convergence.
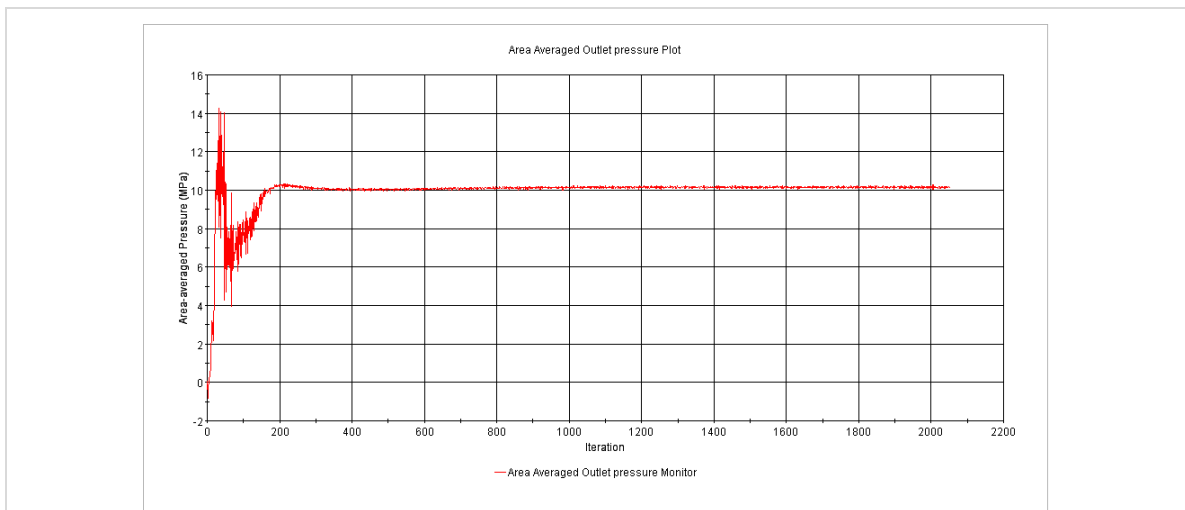
Figure 24. Convergence of oulet pressure
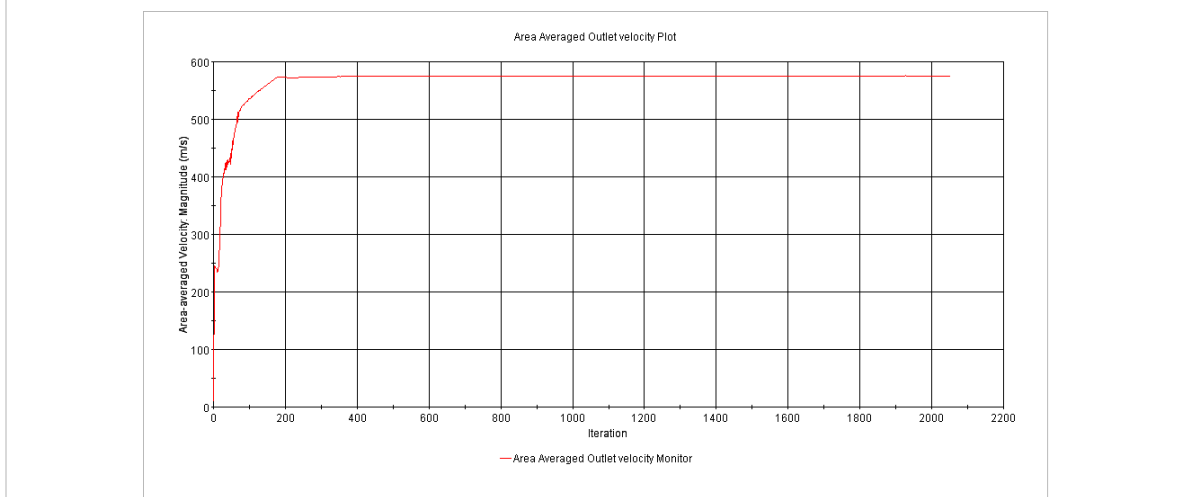
Figure 25. Convergence of discharge velocity

4.3   Parallel Computing

In the recent times, computer technology has seen rapid developments. However, CFD simulations are still limited by computational power primarily for complex geometries. Parallel computing is a recent breakthrough in the computational domain, where multiple processors (on a single computer or different computers) are used to share the computational burden while solving complex models. STAR-CCM+ supports parallel computing, so that multiple processors can be used to perform a simulation. This has certainly provided a significant improvement in the computational efficiency for the present work. A total of six (6) processors were used in this thesis to perform the simulations. The effect of parallel computing on the computational time was not investigated in this research.

4.4   Fine Tuning

Solution stability and convergence are important issues during CFD simulation that needs careful attention. Several stability and convergence issues were encountered during the initial stages of research when supercritical case studies were simulated. It was believed that the drastic changes in the thermo-physical properties of water near the pseudo critical points as well as the solver parameters form the main reasons to trigger such issues. A small change in the operating conditions around the pseudo critical line results in a drastic change in the water properties. During simulation, such conditions could exist in the adjacent cells, resulting in large variations in the thermo-physical properties in those cells, thus leading to stability and convergence issues.

Segregated Flow and Energy modeling combined with SIMPLE (Semi Implicit Pressure Linked Equation) solution algorithm provides the flexibility to fine tune the solver parameters, primarily the relaxation coefficients in the velocity, pressure and energy loops. From computational experience, it was found that fine tuning during the progress of simulation is very essential to guarantee stability and convergence. The default solver parameters in STARCCM+ (velocity coefficient = 0.7 and pressure

coefficient = 0.3) typically resulted in unstable solution or diverging residuals within few iterations.

It is well known that higher values of relaxation coefficients makes the solver aggressive, while lower values makes it less aggressive and more stable. The default solver parameters are quite aggressive for the supercritical problem, therefore lower values of relaxation coefficients are preferred in the initial stages of the simulation (more like a passive approach). This makes the solver stable and although it takes more computational time for convergence, it guarantees convergence and stability during the simulation.

Besides lowering the relaxation coefficients, it was also found that solving the flow and energy models in two stages was more efficient than solving them at the same time. The advantage of segregated modeling is the flexibility to solve flow and energy loops in succession. The best procedure would be to solve the flow model first and then solve the energy model once flow is converged.

The common practice followed in this research to fine tune the relaxation coefficients and solve the CFD model in two stages is presented here. It is recommend to follow this procedure primarily for case studies involving supercritical conditions to obtain better results.

- Stage 1: Disable the Energy loop and solve the Flow model.
    - Energy loop is disabled by setting the relaxation coefficient for energy as 0.
    - Set the relaxation coefficients for Flow loop as follows: velocity loop = 0.15 and pressure loop = 0.075.
    - Let the solver iterate. Monitor the residuals and variables of interest.
    - Check for convergence using the criteria described in section 4.2.5. Pressure and velocity loops should converge, while temperature remains constant in the pipe.

o   Once convergence is verified, go to Stage 2.

- Stage 2: Enable the Energy loop while keeping the Flow loop active.
  o   Do not modify the relaxation coefficients for velocity and pressure loop.
  o   Energy loop is enabled by setting the relaxation coefficient as 0.01.
  o   Let the solver iterate. Monitor the residuals and variables of interest.
  o   After few iterations, increase the relaxation coefficient to 0.1.
  o   If the energy residuals are still decreasing, increase the coefficient to 0.5 and finally to 0.9. This will speed up the convergence of energy loop. The velocity and pressure solution will also adjust accordingly.
  o   Check for convergence using the criteria described in section 4.2.5.
  o   Stop the solver once convergence is confirmed.

4.5   Summary

This chapter presents the experimental data considered in this research to validate the CFD model and describes the CFD modeling procedure followed. All the steps involved in CFD modeling and simulation are clearly discussed, with emphasis on meshing, physics models and the proposed convergence criteria. Although, the 2-D Look-up Table method was developed to customize the CFD code for supercritical systems, it is rather challenging to simulate supercritical conditions because of the rapid property changes in the pseudo-critical regime.

Parallel computing was found to reduce the computational burden to a great extent. However, it was found that careful attention should be given while simulating supercritical problems. The simulations have to be monitored continuously iteration by iteration because the solver was found to diverge in many instances, which we believe is due to the non-linearity in the thermo-physical properties. After several attempts, it was found that fine tuning during the simulation is very essential to solve supercritical problems. We proposed a fine-tuning scheme, which was followed to simulate all the simulations in this thesis. The scheme was specific for the problem considered in this

thesis, therefore it may be required to slightly tweak the relaxation coefficients and adopt the procedure for any supercritical problem in general. The details about the simulation case studies and the relevant results are presented in the next chapter.

5.   Results and Discussion

This chapter presents the CFD evaluation of critical flow from supercritical conditions through small nozzles, which are meant to represent the piping breaks considered in LOCA scenarios. Sensitivity of the CFD model for mesh size, turbulence model and perturbation in boundary conditions are also evaluated and discussed in this chapter. The results for two types of nozzles (round-edge and sharp-edge) are discussed and compared to interpret the effects of nozzle geometry on the CFD model results.

5.1   Critical Flow Evaluation

As per the definition, critical flow (or choked flow) is the maximum discharge flow rate (of coolant during a LOCA), which no longer increases with decreasing downstream pressure. To evaluate if a choked flow condition occurs during an accidental coolant release of water from supercritical conditions, the inlet pressure in the thermal model was maintained at a constant supercritical pressure and the outlet pressure was slowly decreased until a maximum discharge velocity was obtained.

Nozzle A (Round-edge) was used to perform this evaluation. The simulation results are typically presented as (i) one-dimensional profiles, and (ii) two-dimensional contours to provide a better interpretation of the results. The 1-D profiles are the values taken along the central axis of the nozzle as shown in Figure 26, and the 2-D contours are the results on the plane as shown in Figure 27.

Figure 26. 1-D nodes along the central axis	Figure 27. 2-D plane along the central axis
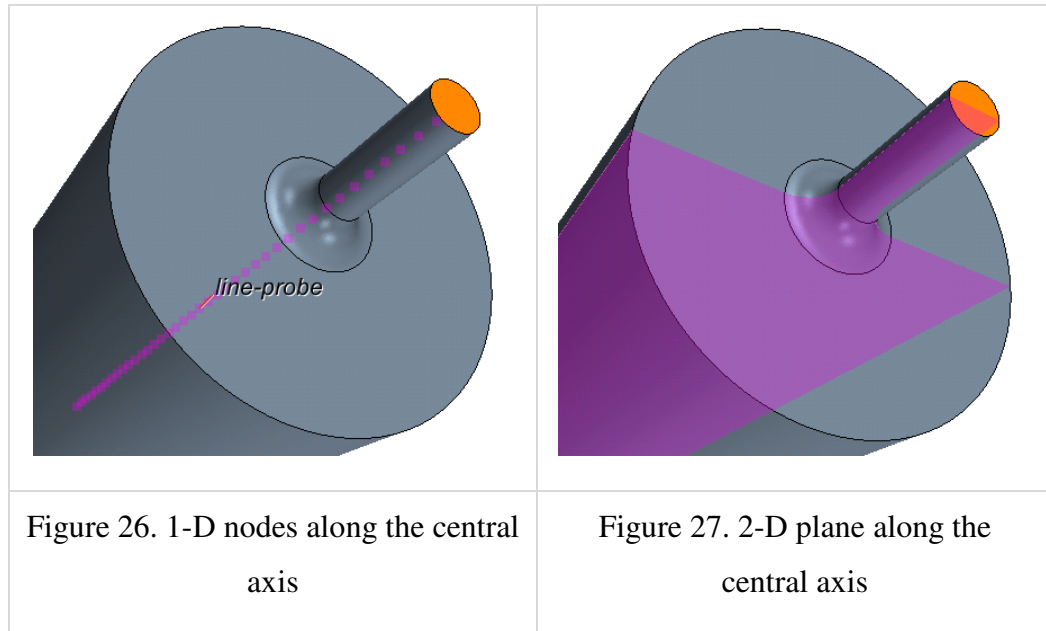
For the critical flow evaluation, the inlet pressure of Nozzle A was held at 25 MPa and the outlet pressure was slowly decreased in eight (8) stages (23 MPa, 22 MPa, 20 MPa, 17 MPa, 15 MPa, 13 MPa, 11 MPa and 0.1 MPa), each of which represents a separate simulation experiment.

The steady state profiles of pressure and velocity for all the 8 experiments along the length of the nozzle are plotted as shown in Figure 28 and Figure 29 respectively. Since the nozzle area is the most important part of the model, the results only in the vicinity of the nozzle are presented for clarity (i.e. from 2 cm upstream of the nozzle). The simulation results indicated that as the outlet pressure was slowly decreased in each experiment, the corresponding discharge velocity increased and eventually when the outlet pressure reached 11MPa, the velocity reached a maximum value, not increasing any further for any reduction in the outlet pressure.

This justified the occurrence of choked flow condition for a coolant release from supercritical conditions. By carefully examining the results, it was found that the discharge velocity was equal to the speed of sound at the pipe outlet, confirming discharge velocity to be sonic velocity (i.e, Mach number equal to 1). This is true for a

single phase fluid. Since, this result was reproduced by CFD, it justifies the use of CFD for critical flow evaluation.
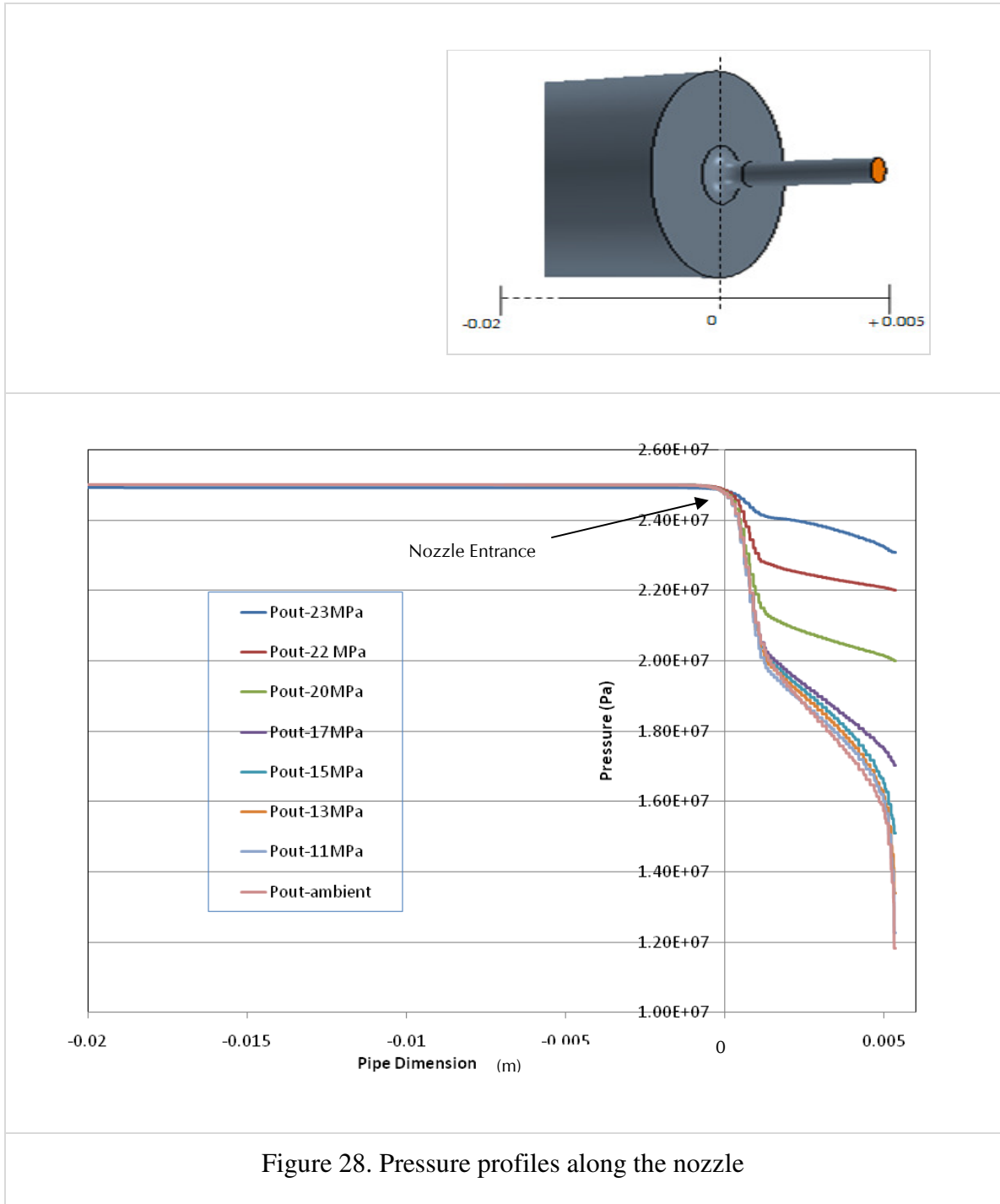
Figure 28. Pressure profiles along the nozzle

Figure 29. Velocity profiles along the nozzle
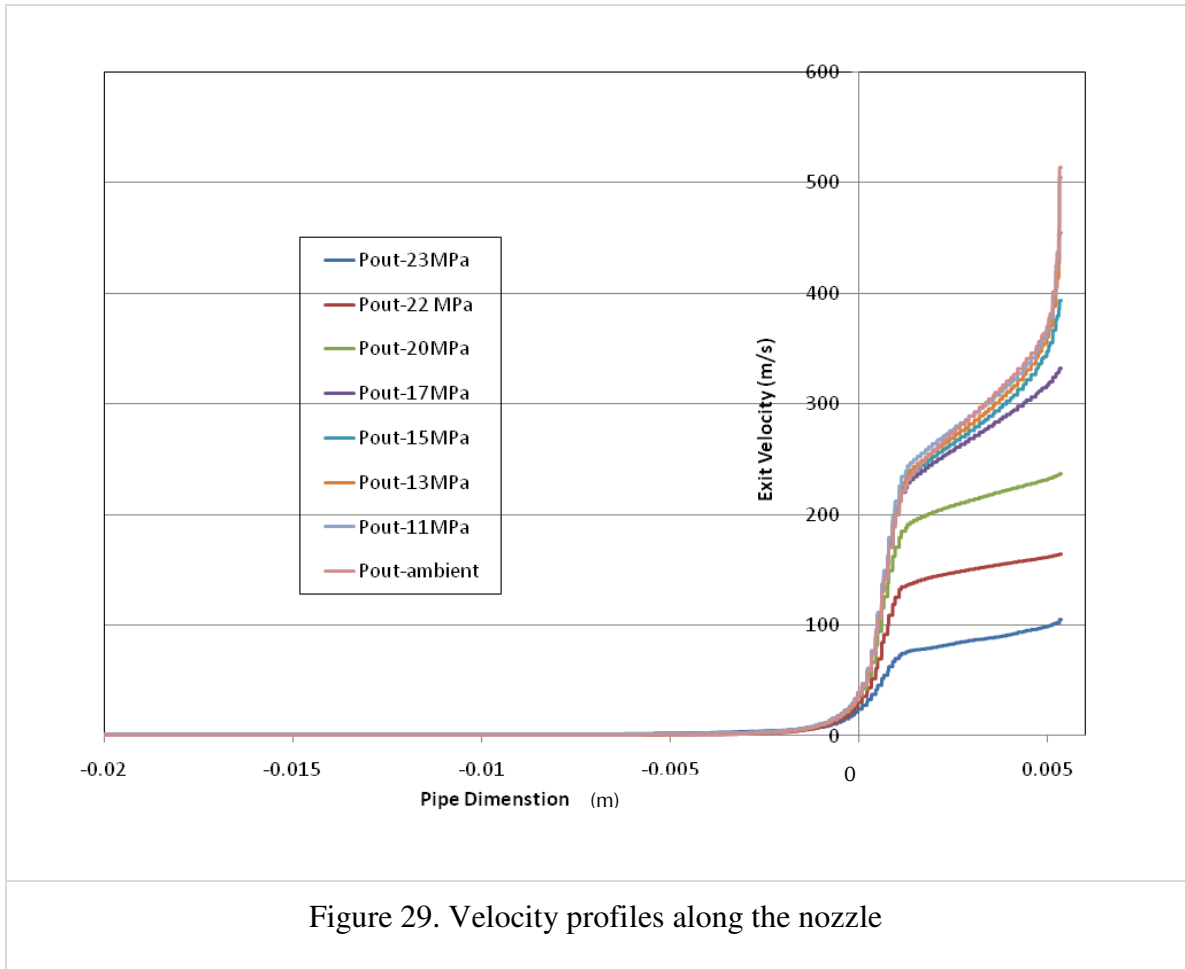
Figure 30 depicts the discharge velocity as a function of outlet pressure. It can be clearly seen that as the outlet pressure decreases the discharge velocity increased and when the outlet pressure reached about 11 MPa, the discharge velocity has attained a maximum value confirming it to be critical velocity.

Figure 30. Discharge Velocity as a function of Outlet Pressure
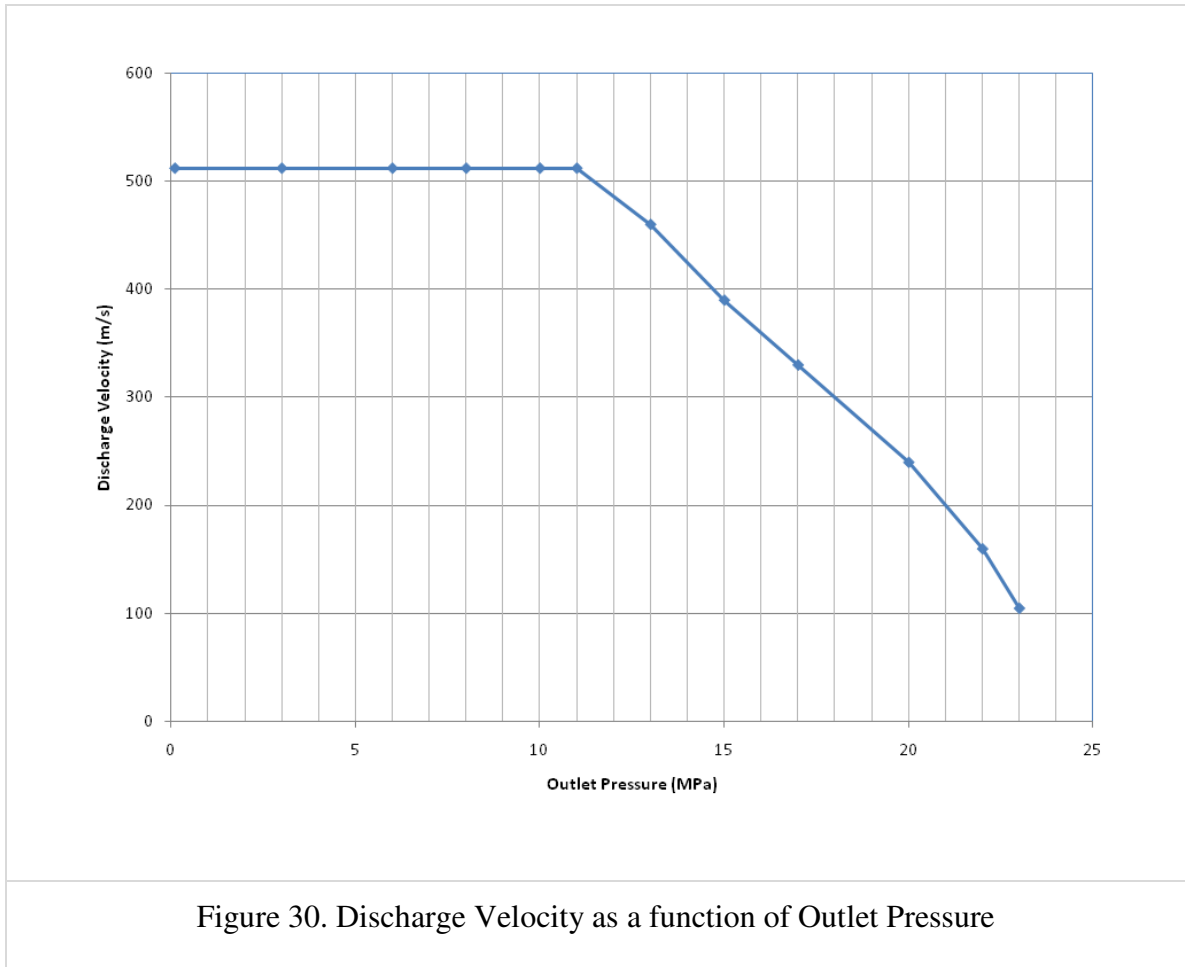
5.2   Description of Nominal Case Study

A nominal case study has been selected to evaluate the CFD model and validate the results with the experimental data. The case study includes ejecting supercritical water through a small nozzle to mimic the flow through a break during a Loss Of Coolant Accident (LOCA) in a typical reactor Heat Transport System (HTS).

Adiabatic conditions are maintained in the pipe and nozzle area and unlimited coolant inventory is assumed. Typically, when a break event occurs, the coolant releases to the ambient and quickly reaches a steady state (maximum velocity) if the conditions and the inventory permits. In a real case, the pressure in the HTS would eventually start

to decrease as the inventory is depleted. For the purpose of this study and the experimental investigation, it is assumed that the HTS inventory is sufficiently large relative to the break flow rate, such that the system pressure remains largely unaffected by the discharge flow. The nominal case study simulates the steady state condition that is achieved when supercritical water releases through a nozzle. The boundary conditions for this case study are defined as shown in Table 3.

Table 3. Boundary conditions for the case study

Parameters	Values
Pin	25 MPa
Tin	657 K
Pout	0.1 MPa
Tout	300 K

Both the nozzles (Nozzle A and Nozzle B) are simulated for this nominal case study. Furthermore, sensitivity analysis was performed with Nozzle A to study the sensitivity of thermal model to various mesh configurations, turbulence models and perturbations in the boundary conditions. The results obtained from the simulations are discussed in the following sections

5.3   Nozzle-A

The boundary conditions and the physics models selected to simulate the nominal case study are depicted in Figure 31. The default turbulence model (K-Epsilon Realizable 2-layer) and wall treatment model (All y+ Wall Treatment 2-layer) in STARCCM+ were used for this simulation. The mesh configuration consisted 1,259,534 cells, 8,730,423 faces and 7,472,079 vertices. The steady state results obtained by simulating this case study are discussed as follows.

Outlet (P = 0.1MPa, T = 300 K)

Physics Models
- Single phase fluid
- Segregated flow model
- Segregated Fluid Temp model
- Reynolds-Averaged Navier-Stokes
- K-epsilon Realisable 2-layer turbulence model
- All y+ Wall Treatment (2-Layer)
- User defined water properties (Rho, Mu, TC)
- No slip - shear stress
- Rough wall surface
- Adiabatic wall surface
- Discretization schemes
  - Flow: Second-order upwind convection scheme
  - Energy: Second-order scheme
- Steady State

Flow direction

Inlet (P = 25 MPa, T = 657 K)

Figure 31. Simulation conditions for the case study

5.3.1 Discussion of Results

The steady state profiles of pressure, temperature, density, viscosity, velocity and speed of sound along the length of the nozzle are shown in Figure 32 to Figure 37. The results clearly indicate that there are three (3) stages of property variation in the nozzle area. The three stages are highlighted on the pressure profile, as shown in Figure 32, and interpreted as follows.

- Stage 1: The sharp pressure drop of about 5 MPa in this stage over a length of 1 mm in the nozzle is due to the pseudo-critical transition of water. This conclusion is justified by examining the density and viscosity profiles as shown in Figure 34 and Figure 35, where they drop significantly in this stage. For instance, water density drops from 360 Kg/m3 to about 120 Kg/m3. Such a drop is typically seen during the pseudo-critical transition.

- Stage 2: Water at supercritical conditions at the nozzle entrance transforms to vapour phase before entering stage2 and continues to be in this phase. This was verified by examining the water density and steam tables. In this stage, the pressure drops about 5 MPa, but rather slowly over 3 mm length of the nozzle, which could be attributed to the very little change in the water properties in this stage as per Figure 34. (If the water properties are maintained constant, then pressure would probably decrease linearly)

- Stage 3: In this stage, the pressure again appears to drop drastically at the nozzle exit. The water properties (density and viscosity) in this stage drop slightly, but considering the pipe length over which it changes, the drop is quite significant. As a result, velocity increases sharply in this stage and attains a maximum discharge flow rate at the nozzle exit (critical flow). The speed of sound at the nozzle exit (Figure 36) was compared with the discharge flow rate at the nozzle exit to verify if choked conditions existed and the results clearly indicated the choked behaviour.

Although, the exit boundary condition for pressure was specified to be 0.1 MPa, it appears that after 11 MPa, pressure doesn't seem to have any effect on the velocity. This again justifies the choked behaviour, because at choking conditions the downstream pressure does not have any effect on the flow rate. The outlet pressure eventually converges to about 11 MPa under these conditions. Therefore, this indicates that an inlet to outlet pressure ratio of 2.27 (25/11 MPa) is required for supercritical water to attain critical flow.
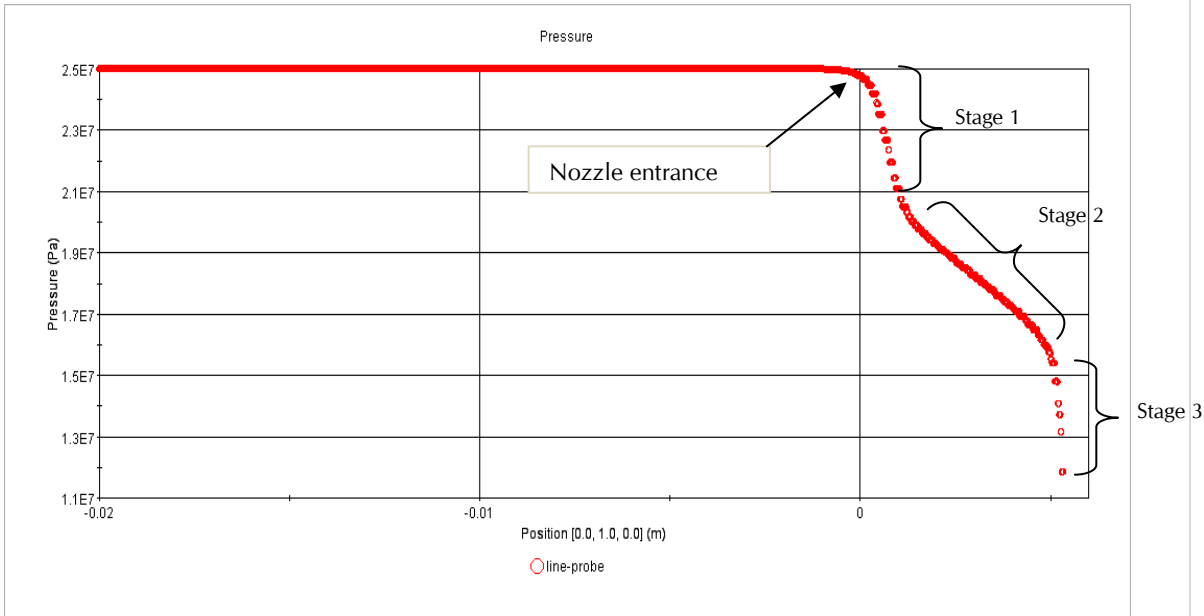
Figure 32. Pressure profile along the central axis of Nozzle A
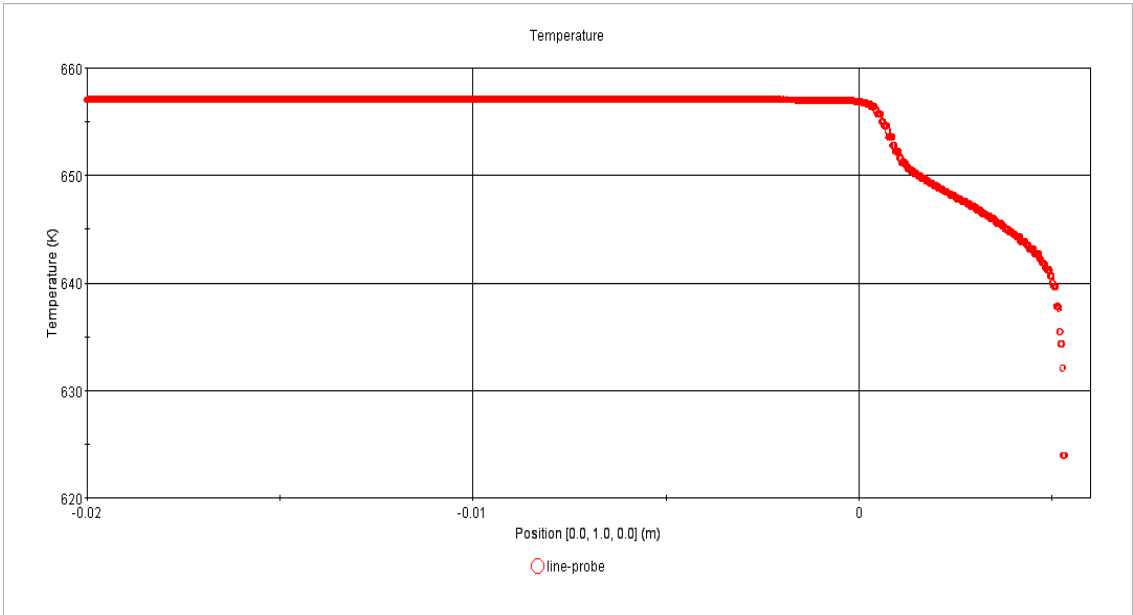
Figure 33. Temperature profile along the central axis of Nozzle A
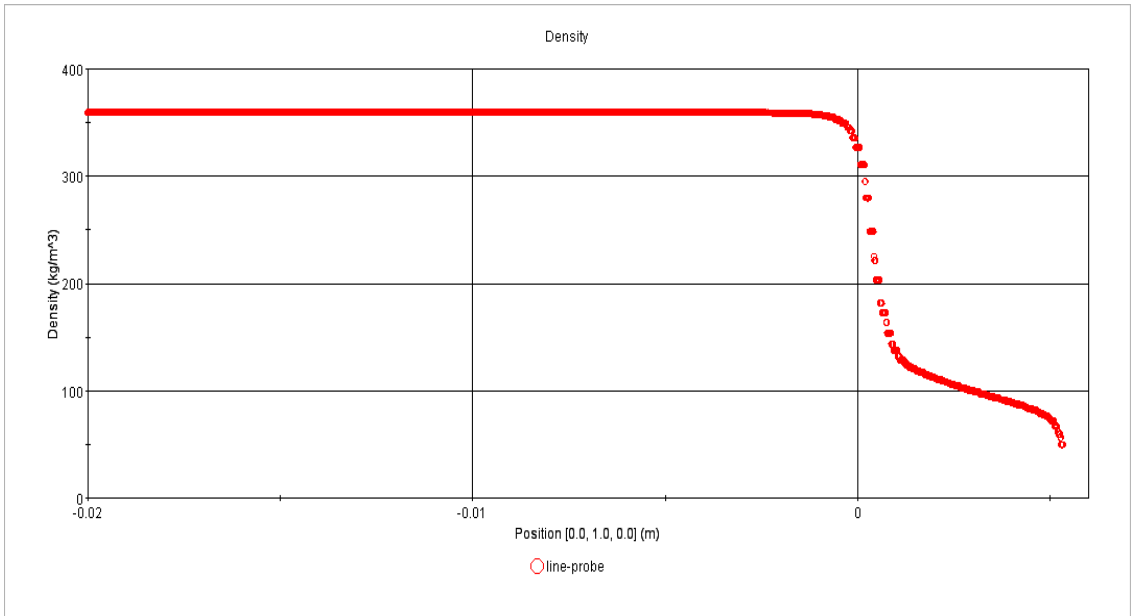
Figure 34. Density profile along the central axis of Nozzle A
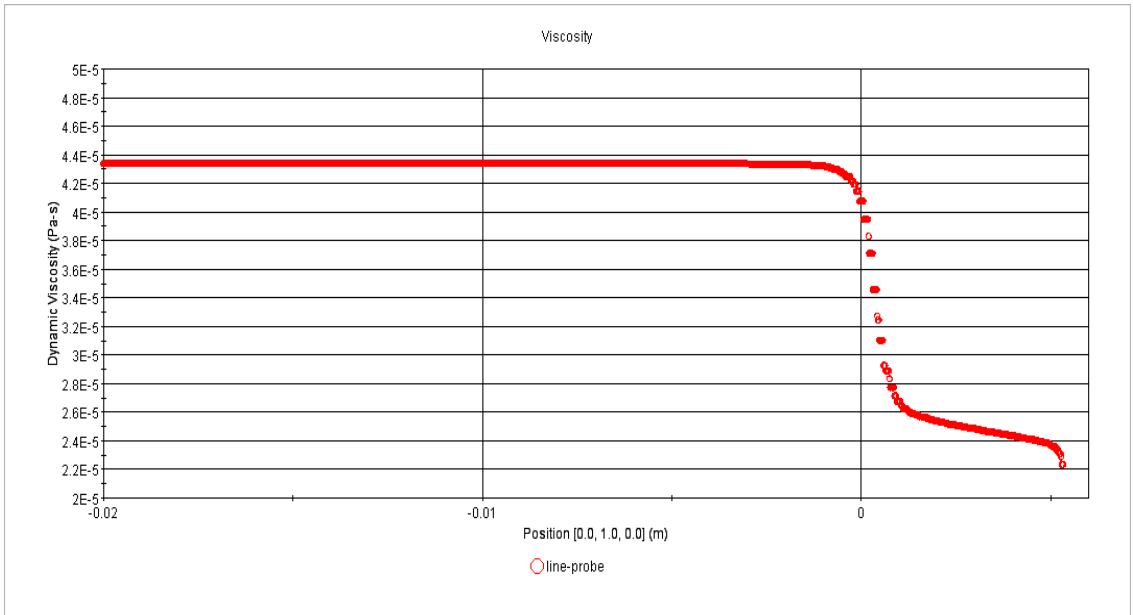
Figure 35. Viscosity profile along the central axis of Nozzle A
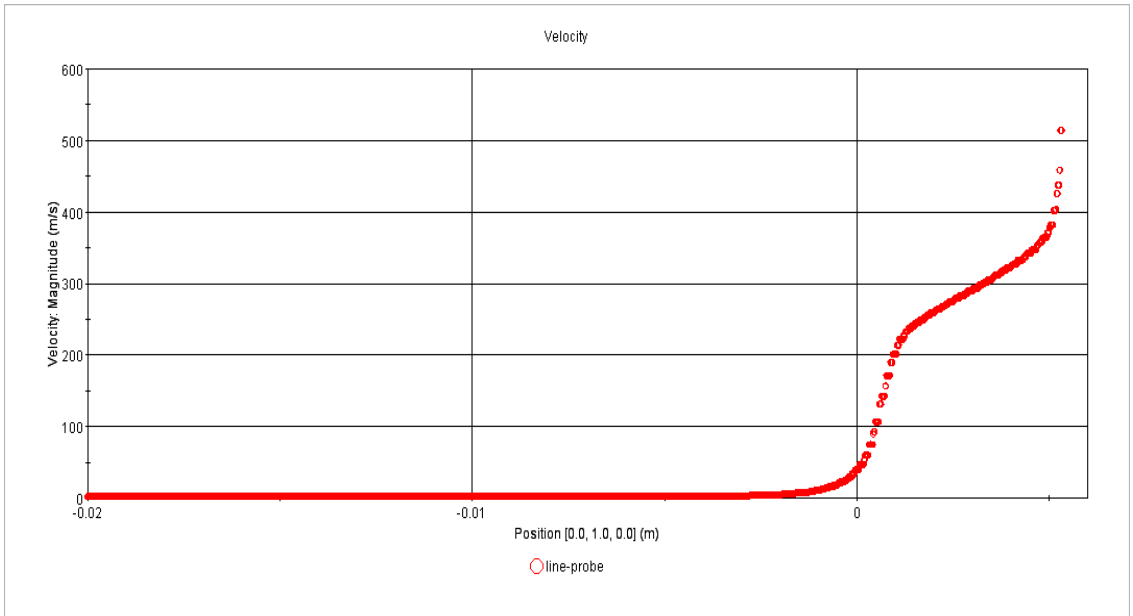
Figure 36. Velocity profile along the central axis of Nozzle A
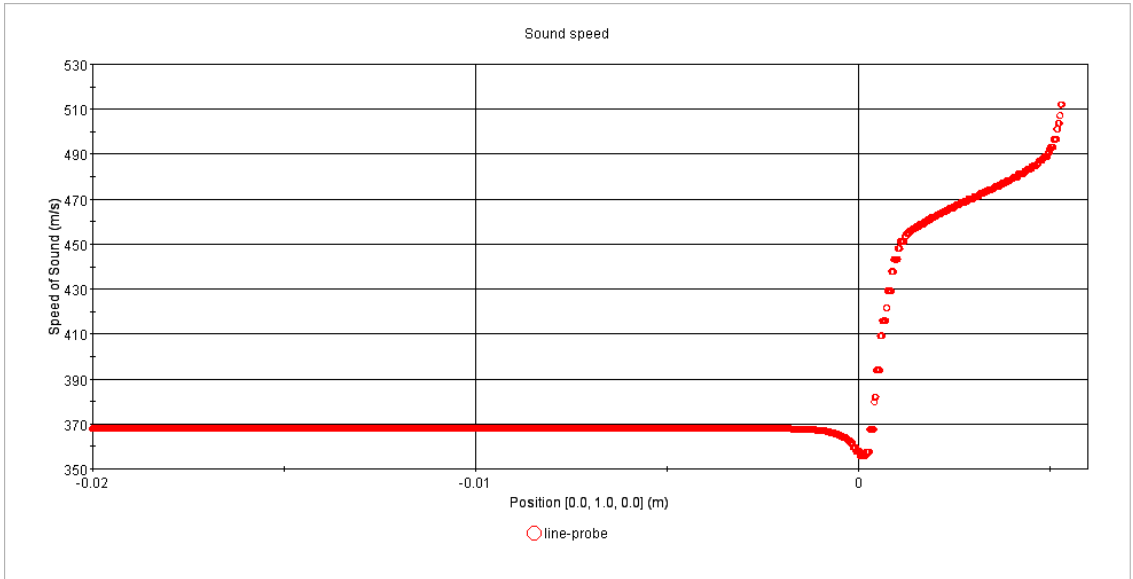
Figure 37. Speed of sound along the central axis of Nozzle A

Although adiabatic conditions were maintained along the pipe and nozzle area, the temperature profile as shown in Figure 33 indicates a 30 K drop in the temperature in three stages along the length of the nozzle. This temperature drop is believed to be due to depressurization effect. Although, the temperature drop along the length of the nozzle was small, it had a significant effect on the fluid properties because the change in temperature lead to a pseudo-critical transition in the nozzle area. As noticed in the above results, the temperatures and the corresponding pressures in stage 1 has initiated a pseudo-critical transition, resulting in significant variation in the water properties.

The profiles of water properties (density and viscosity) as shown in Figure 34 and Figure 35 clearly indicate the significant variation along the length of the nozzle. It can be noticed that density of water dropped from 360 Kg/m3 to about 50 Kg/m3 and viscosity drops by half its value before exiting the nozzle. This drastic change in the water properties explains the difficult phenomena that exists in the coolant release scenarios from supercritical conditions. The density profile as shown in Figure 38 highlights the phases of water and transitions along the nozzle length. It is clear that supercritical water at the nozzle entrance changes to vapour after undergoing the pseudo-critical transition and stays in the vapour phase until exiting the nozzle. Two phase mixture could possibly exist in this region but it is not evident in the CFD prediction and couldn't be verified from this analysis.
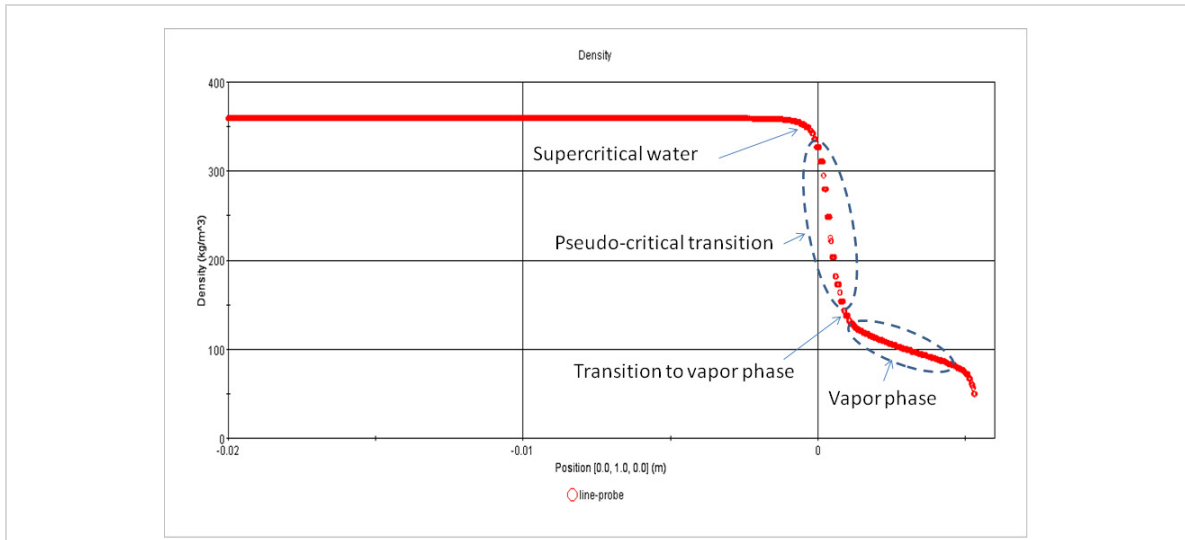
Figure 38. Water density profile interpretation

The steady state profiles of velocity and speed of sound along the nozzle are shown in Figure 36 and Figure 37 respectively. It can be noticed that the velocity in the nozzle increased in three (3) stages reaching a maximum, which was identified as sonic velocity by comparing it with the speed of sound at the nozzle outlet. This velocity is the critical velocity, which was found to be 512 m/s. The corresponding mass flux at the outlet of the nozzle was calculated to be 29657 kg/m2s. By comparing it with the experimental mass flux (33,000 kg/m2s), the prediction error of the thermal model was calculated to be about 10% for the current scenario.

The two-dimensional contours for the simulation variables along the central plane of the nozzle are shown in Figure 39 to Figure 43. These contours provides us a better picture of property variation in the vicinity of the nozzle area. It is clear from the results that the pressure drop, velocity rise and water property variation in the round-edge nozzle occurs inside the nozzle mainly due to reduction in the diameter.

The turbulence models and wall models are essentially developed for single phase flow modeling. The 2-D contours here revealed that the pseudo-critical transition takes place far away from the wall. Therefore, the boundary layer flow largely remains single phase and hence the turbulence models and wall models have produced reasonable results.
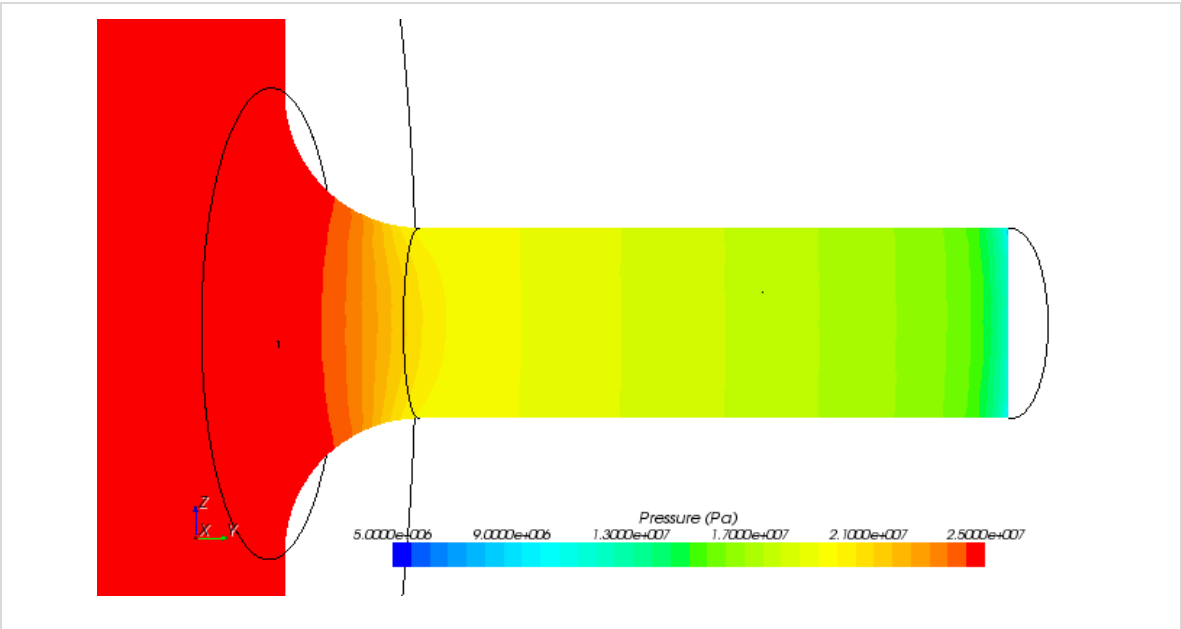
Figure 39. Pressure contours along the nozzle area for Nozzle A
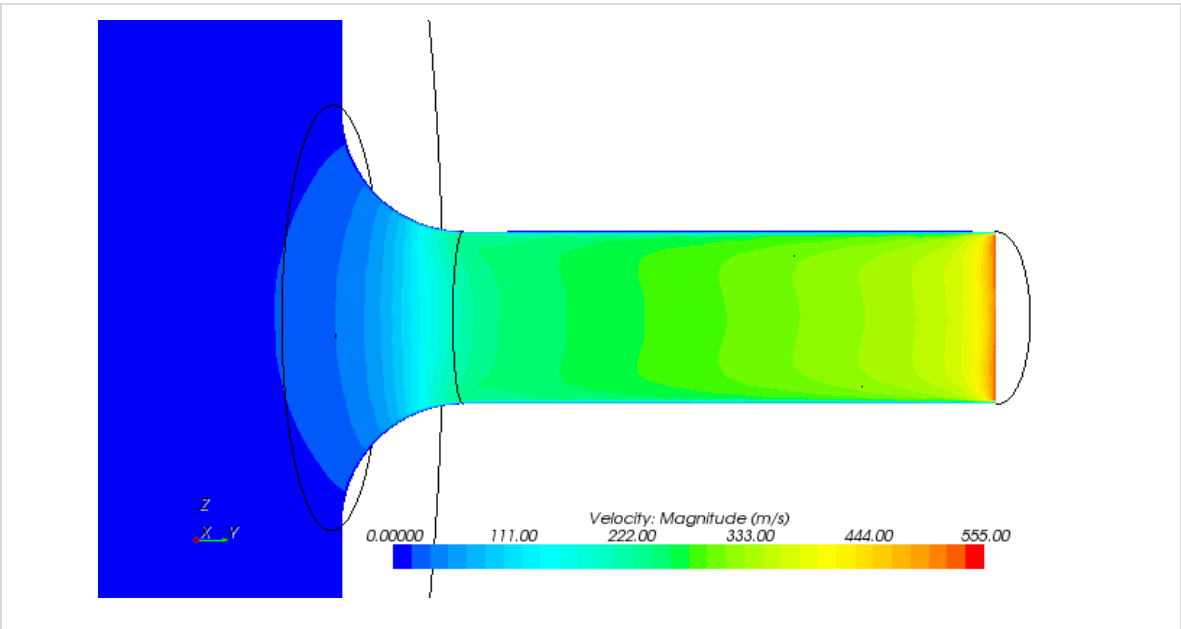
Figure 40. Velocity contours along the nozzle area for Nozzle A
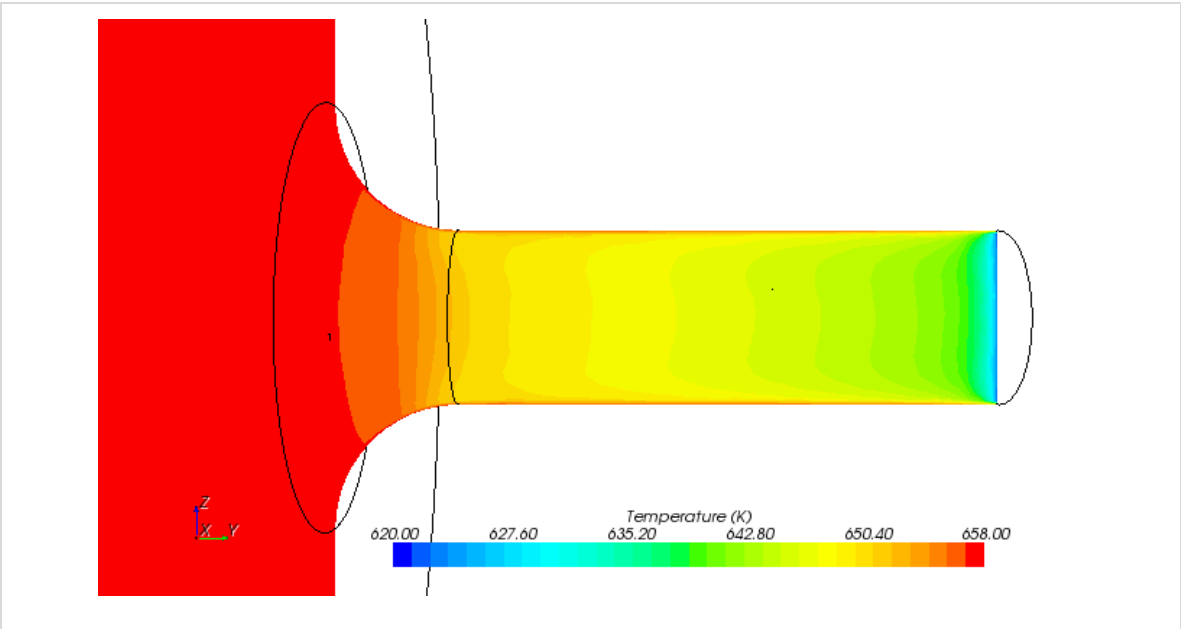
Figure 41. Temperature contours along the nozzle area for Nozzle A
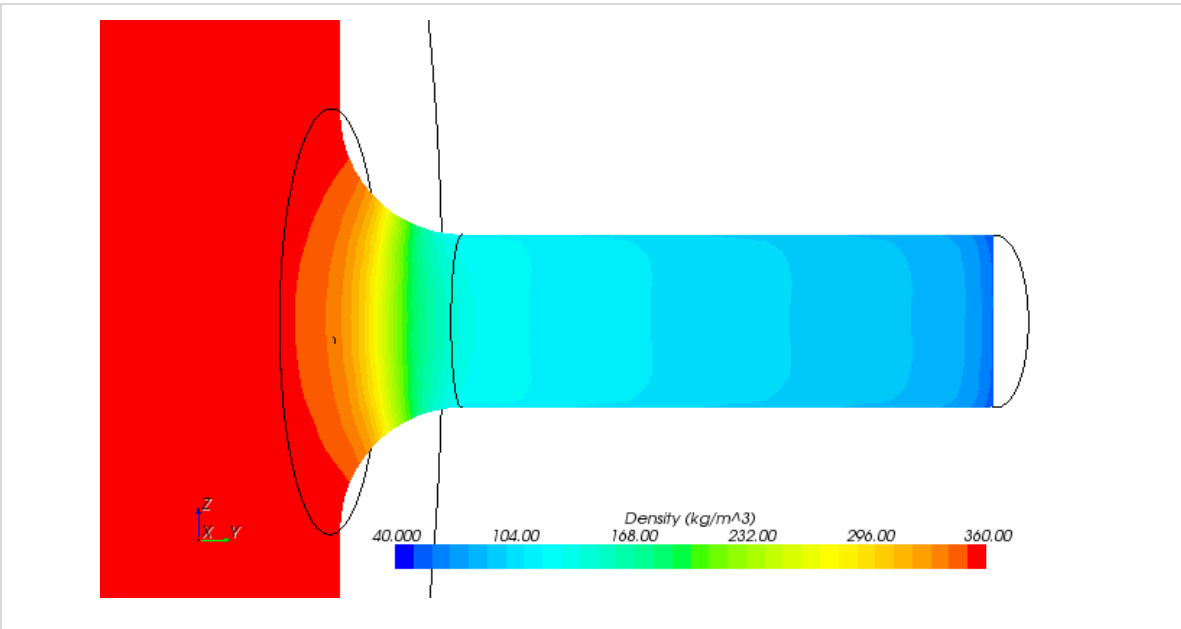
Figure 42. Water Density contours along the nozzle area for Nozzle A

Figure 43. Water Viscosity contours along the nozzle area for Nozzle A
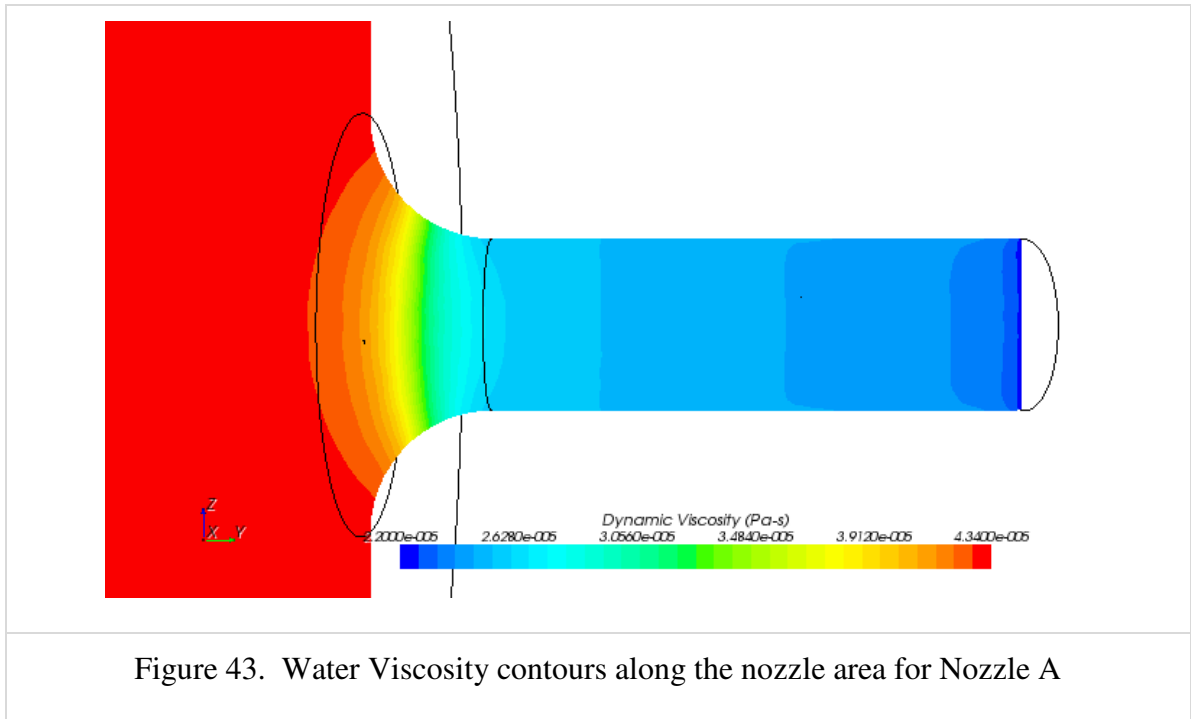
5.3.2 Sensitivity Analysis

Sensitivity analysis of the thermal model was performed for different mesh configurations, turbulence models and perturbations in boundary conditions to identify the best parameters and models required for CFD simulation under supercritical conditions. The details of the sensitivity analysis are discussed in the following sections.

5.3.2.1 Mesh size

To evaluate the sensitivity of the thermal model, four different mesh configurations with varying grid densities were considered. The cells, faces and vertices for the meshes are shown in Table 4. Clearly Mesh1 has least number of cells indicating a coarse mesh and Mesh4 has the most cells representing a fine mesh. Mesh2 and Mesh3 are intermediate meshing configurations.

Table 4. Mesh parameters

	Cells	**Faces**	**Vertices**
Mesh 1	802,206	5,648,705	4,547,562
Mesh 2	1,259,534	8,730,423	7,472,079
Mesh 3	2,141,545	14,889,127	12,749,461
Mesh 4	6,758,695	47,584,880	40,830,303

The boundary conditions and the physics models selected for this analysis are shown in Figure 31. The default turbulence and wall treatment models recommended by STARCCM+ (K-Epsilon Realisable 2-layer turbulence model and All y+ wall treatment 2-layer) were used.

In general, a coarse mesh requires less computational time to converge but provides less accurate results, whereas a finer mesh requires more computational time to converge but provides better results. Therefore, the best mesh configuration should ideally provide a balance between computational time and solution accuracy. The results obtained by simulating the four mesh configurations separately are shown in Table 5. The experimental value of mass flux is taken from the China paper (Chen et al., 2009) and the percent error in the simulation result is calculated using the estimated value and the experimental value. The computational time required per iteration is also shown for each mesh type. A total of about 1500 iterations were required to attain convergence for all these cases.

Table 5. Mesh analysis results

Mesh Type	**CFD Estimated Mass flux (Kg/m²s)**	**Experimental Mass Flux (Kg/m²s)**	**% Error**	**Computational time/iteration (secs)**	**Total Computational time (mins)**
Mesh 1	27012	33000	18.1	4	100
Mesh 2	29203	33000	11.5	13	325
Mesh 3	29273	33000	11.3	250	6250
Mesh 4	29274	33000	11.3	600	15000

By examining the results, it is clear that Mesh1 (coarse mesh) produces about 18% error in the simulation results but requires only 4 seconds for each iteration. Mesh2 produces about 11.5% error in the computed results requiring 13 seconds per iteration. The remaining mesh configurations (Mesh3 and Mesh4) do not improve the accuracy of the results any further, in addition requiring more computational time. Therefore, we can conclude that Mesh2 is the best configuration that provides the required accuracy without demanding significant computational time.

5.3.2.2   *Turbulence models*

There are several turbulence models available in STARCCM+ to perform sensitivity analysis, which are shown in Table 6

Table 6. Suite of turbulence models in STARCCM+

Turbulence models	Different types
K-Epsilon Turbulence	▪ Standard K-Epsilon ▪ Standard K-Epsilon Low-Re ▪ Standard K-Epsilon Two-Layer ▪ Realizable K-Epsilon ▪ Realizable K-Epsilon Two-Layer*
K-Omega Turbulence	▪ SST (Menter)* ▪ Standard (Wilcox)
Reynolds Stress Turbulence	▪ Linear Pressure Strain ▪ Linear Pressure Strain Two-Layer* ▪ Quadratic Pressure Strain
Spalart-Allmaras Turbulence	▪ High-Reynolds Number Spalart-Allmaras ▪ Standard Spalart-Allmaras*

* Default selection in STARCCM+

Few turbulence models were selected from this suite to perform sensitivity analysis. The selected turbulence models and the corresponding wall treatment models

used for the simulations are shown in Table 7 . The wall treatment models were the default ones that would go along with the selected turbulence models. Since, all the wall treatment models are similar, this provides consistency in the turbulence model sensitivity analysis. The effect of wall treatment on the thermal model results was not investigated exclusively in this research, but few preliminary simulations have indicated that the effect was not significant.

Table 7. Chosen Turbulence and Wall treatment models for sensitivity analysis

	Turbulence model	Wall treatment model
1	Laminar	N/A
2	k-epsilon (standard)	All y+ Wall Treatment
3	k-epsilon (Standard 2-layer)	All y+ Wall Treatment (2-Layer)
4	k-epsilon (Realizable 2-layer)	All y+ Wall Treatment (2-Layer)
5	k-omega (Standard)	All y+ Wall Treatment
6	k-omega (SST)	All y+ Wall Treatment
7	Reynolds Stress Model (RSM)	All y+ Wall Treatment (2-Layer)

The boundary conditions, as defined in the postulated case study (Section 5.2), were used for the thermal model simulation. The physics models selected for the simulation as shown in Figure 31. The best mesh configuration (Mesh2) was selected to perform this analysis. The sensitivity of the thermal model to the turbulence models listed in Table were investigated.

The results for the seven simulations are shown in Table 8 along with the corresponding experimental mass flux and the percent error in the results. The results clearly indicate that except for Laminar and k-epsilon (standard) models, all the other turbulence models did reasonably well with all of them producing a prediction error of around 10%.

Table 8. Turbulence model analysis results

		CFD Estimated Mass flux (Kg/m^{2}s)	Experimental Mass Flux (Kg/m^{2}s)	% Error
1	Laminar	25669	33000	22.2
2	k-epsilon (Standard)	27549	33000	16.5
3	k-epsilon (Standard 2-layer)	29203	33000	11.5
4	k-epsilon (Realizable 2-layer)	29657	33000	10.1
5	k-omega (SST)	29803	33000	9.7
6	k-omega (Standard)	29704	33000	10.0
7	Reynolds Stress Model (RSM)	29808	33000	9.7

In the K-Epsilon turbulence models, both Standard 2-layer and Realizable 2-layer models provided good prediction results. Of these models, Realizable 2-layer model appeared to be more robust because it guaranteed convergence for several kinds of initial guesses (some bad and some good) to start the simulation. For similar reasons, K-Omega (SST) model was found to be more robust than K-Omega (standard). The standard k-epsilon and k-omega models needed a good initial guess to converge relatively quickly.

On the other hand, Reynolds Stress Model (RSM) required a good initial guess to converge and often diverged if the initial guess was far from the real solution. Any bad guess would cause severe computational problems during convergence. Often the residuals diverged and the software would terminate with a floating point error caused due to exceptionally high residuals. While it did provide good results, it is less robust than the other models in terms of convergence.

From this analysis, we can conclude that K-Epsilon (Realizable 2-layer) and K-Omega (SST) models are the most robust. All the other turbulence models required a good initial guess to successfully converge, otherwise the simulation showed signs of

divergence. Therefore, either k-epsilon (realizable) or k-omega (SST) could be used for supercritical flow simulations.

5.3.2.3   *Perturbations in Boundary conditions*

The sensitivity of CFD model was evaluated for slight perturbations in the boundary conditions such as Pressure, Temperature and Wall roughness. The results obtained for the perturbations are depicted in Table 9. The nominal case study was used as the base case to compare the results and calculate the percent error in the results due to the perturbations. For the nominal case, Pressure of 25 MPa, Temperature of 657 K and Wall roughness of 5E-5m was used and the discharge mass flow rate was found to be 29657 Kg/m^{2}s.

Table 9. Perturbations in Boundary conditions results

Condition	Pressure (MPa)	Temperature (K)	Wall Roughness (m)	Estimated Mass flux (Kg/m2s)	% Error from Nominal
Pressure perturbation	25.5	657	5 E-5	26770	9.7%
Temperature perturbation	25	659	5 E-5	25701	11%
Wall Roughness perturbation	25	657	10 E-5	29837	1%

The results indicate that for Pressure and Temperature perturbations, the CFD model produces about 10% error in the simulation results when compared to the nominal case. Although, the perturbations are quite small (i.e., 0.5 MPa Pressure and 2 K Temperature), one should understand that in the pseudo-critical region, even a small change in the boundary conditions could lead to significant effect on the discharge flow rate. This behaviour is clearly seen in the results. The experimental uncertainties in inlet temperature could be as high as 0.5 C, and as such this represents the single largest

sensitivity observed and may account for a majority of the differences observed between the CFD model and experiment. The perturbations in the wall roughness did not seem to have a large effect on the CFD model, which is probably due to highly turbulent flow inside the pipe.

5.3.3 Summary

The sensitivity of the CFD model was evaluated for various mesh configurations, turbulence models and perturbations in the boundary conditions to identify the best settings and conduct simulations in this research. It was found that Mesh2 was the best configuration that provides the required accuracy without demanding significant computational time. Therefore, Mesh2 configuration was used to conduct all the simulations in this research. Regarding the turbulence model, it was found that k-epsilon (Realizable 2-layer) and k-omega (SST) were the best models that provided consistent results for any set of initial conditions. For the current research, k-epsilon turbulence model was selected to conduct simulations.

5.4   Nozzle-B

The best mesh configuration (Mesh2) and turbulence model (K-Epsilon realisable 2-layer) obtained from the sensitivity analysis were chosen to simulate nominal case study using Nozzle-B. The boundary conditions and the physics models chosen for simulation are shown in Figure 44. The inlet conditions represent supercritical water and the outlet is defined as ambient pressure and temperature. The results obtained by simulating these conditions are discussed in the following section.

Figure 44. Simulation conditions for the case study
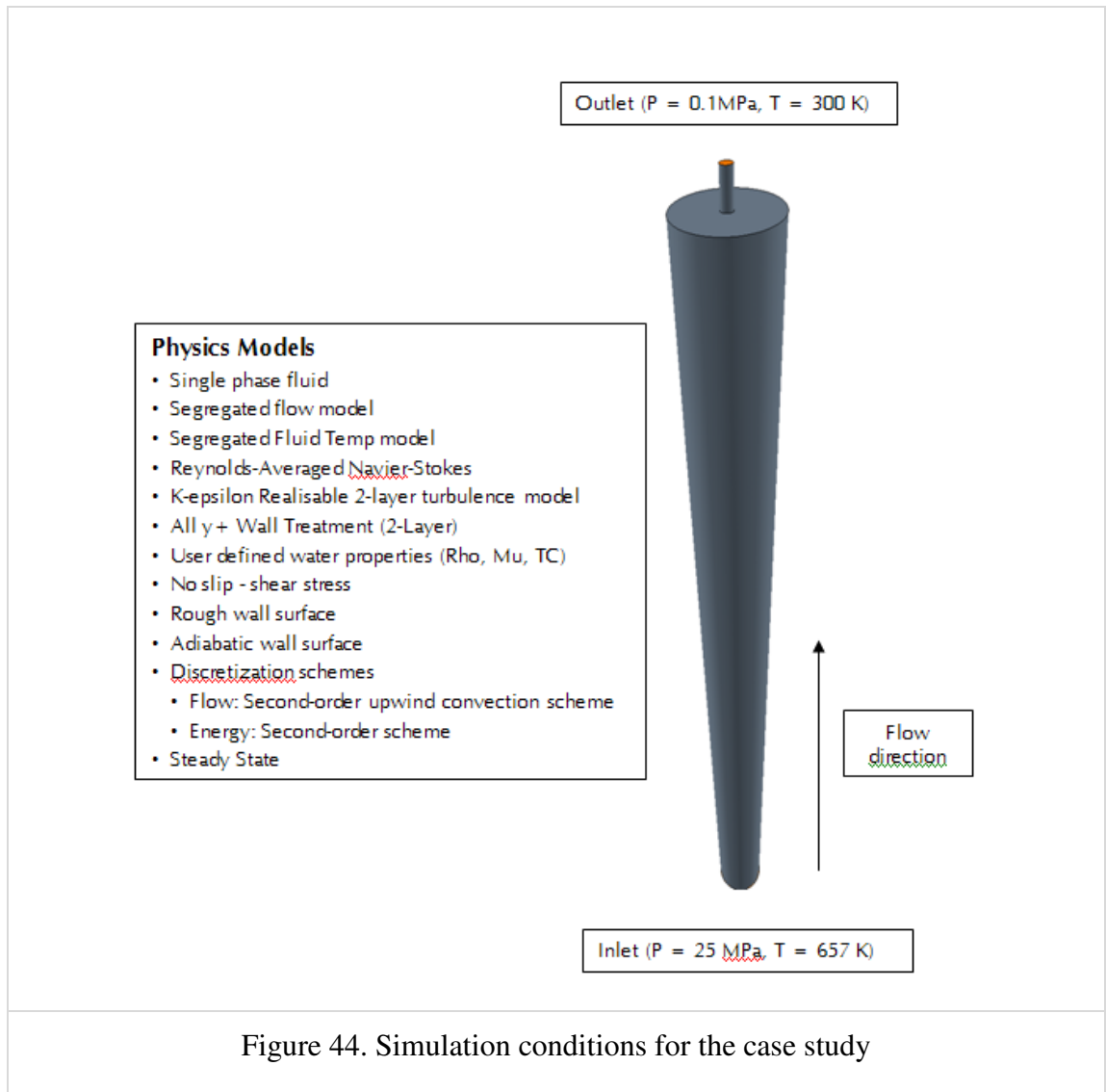
5.4.1 Discussion of Results

The steady state profiles of pressure, temperature, density, viscosity, velocity and speed of sound along the length of the nozzle are shown from Figure 45 to Figure 50. The results are quite similar to those of Nozzle-A, clearly indicating the three (3) stages in the nozzle area. The only significant difference in the profiles is seen in Stage1, where the pressure drops just before the nozzle entrance, as opposed to slightly after the entrance in Nozzle A. The same behaviour is seen in all the profiles.

It is believed that the sharp nozzle geometry creates extra mixing and turbulence around the edges, resulting in such behaviour. However, this had very little effect on the discharge velocity, which was found to be 535 m/s. As a result of higher mixing and turbulence effects due to the sharp edges, the discharge velocity is slightly greater than it is seen in round edge nozzle. The corresponding mass flux at the outlet of the nozzle was calculated to be 29960 kg/m^{2}s. By comparing it with the experimental mass flux (33,000 kg/m^{2}s), the prediction error of the thermal model was calculated to be about 9.2% for the current scenario.

Figure 45. Pressure profile along the central axis of Nozzle B
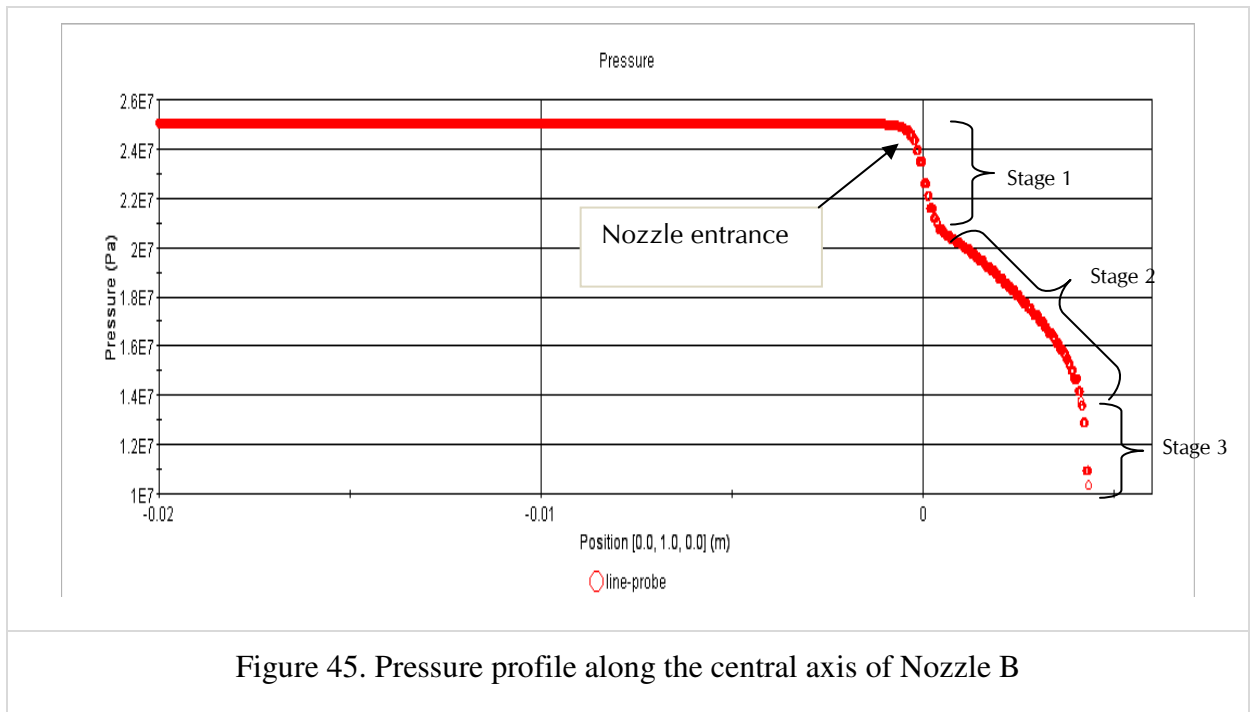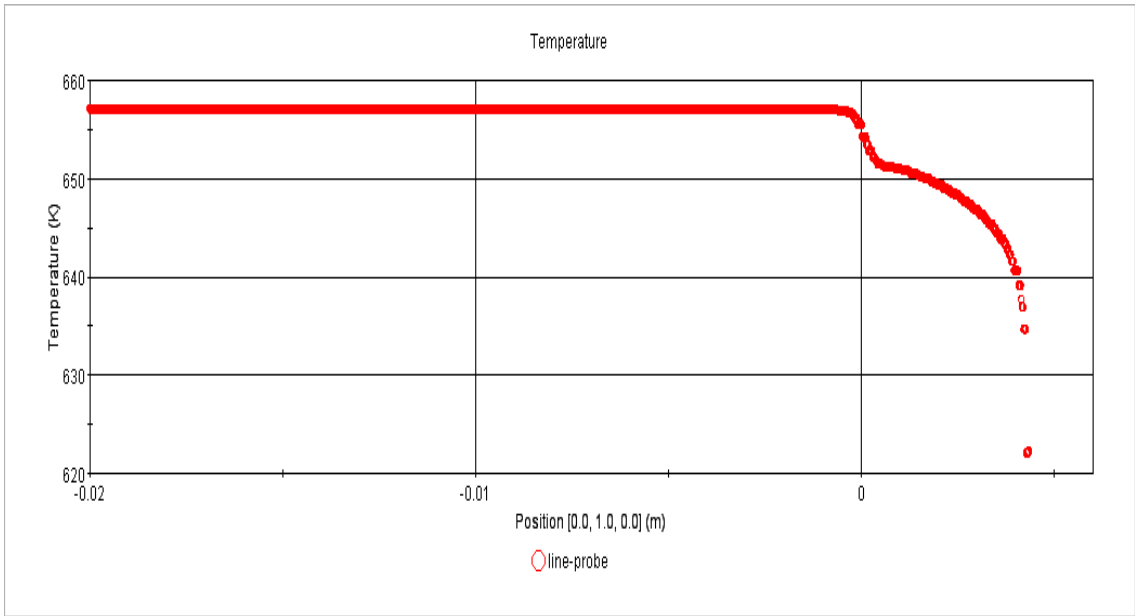
Figure 46. Temperature profile along the central axis of Nozzle B
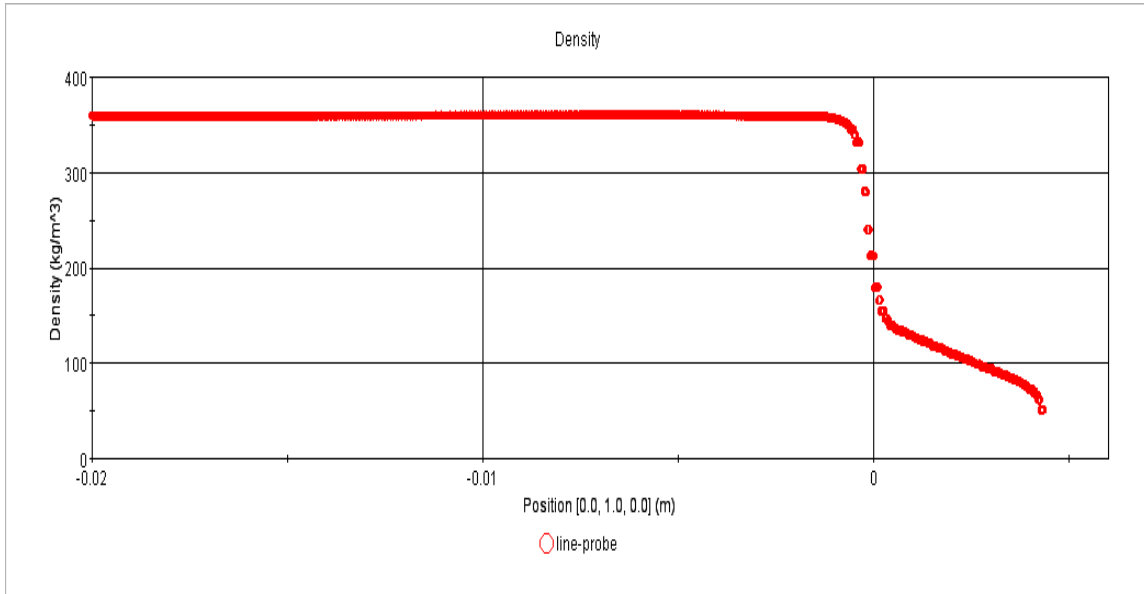
Figure 47. Density profile along the central axis of Nozzle B
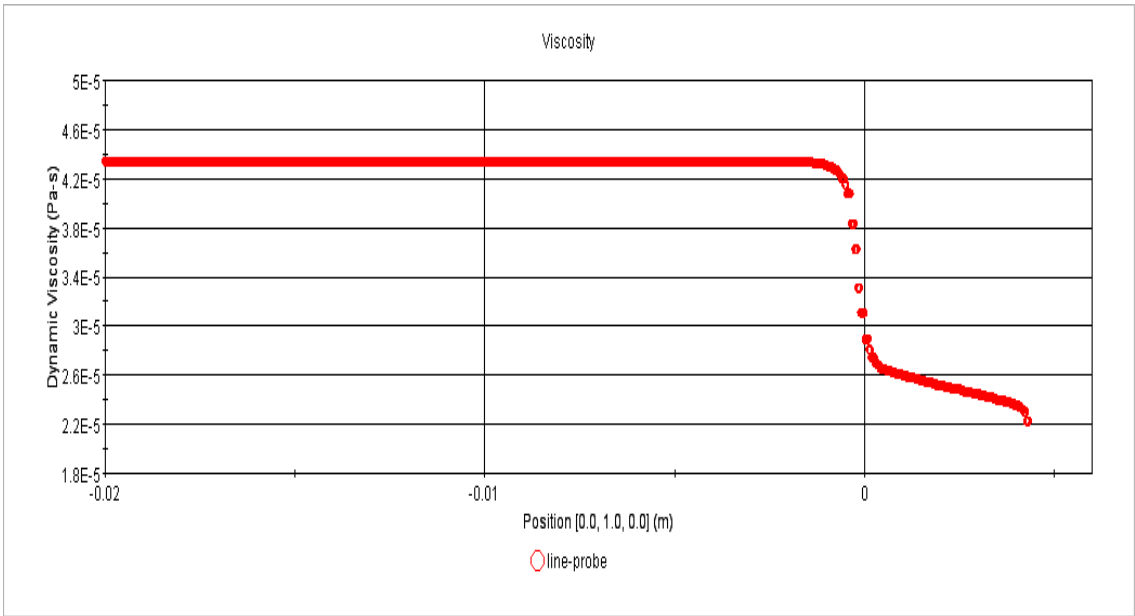
Figure 48. Viscosity profile along the central axis of Nozzle B
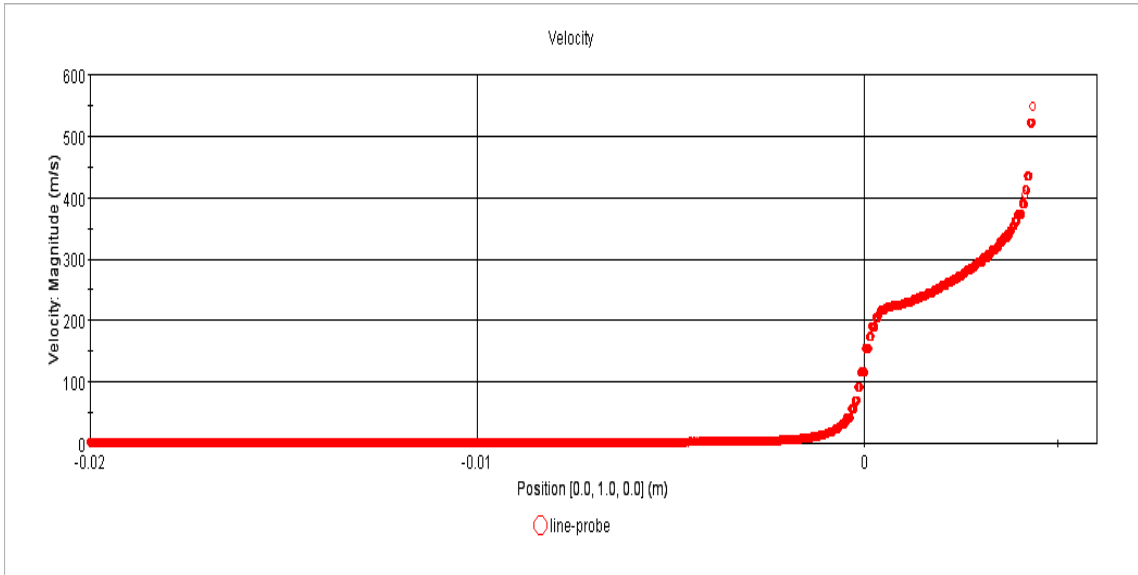
Figure 49. Velocity profile along the central axis of Nozzle B
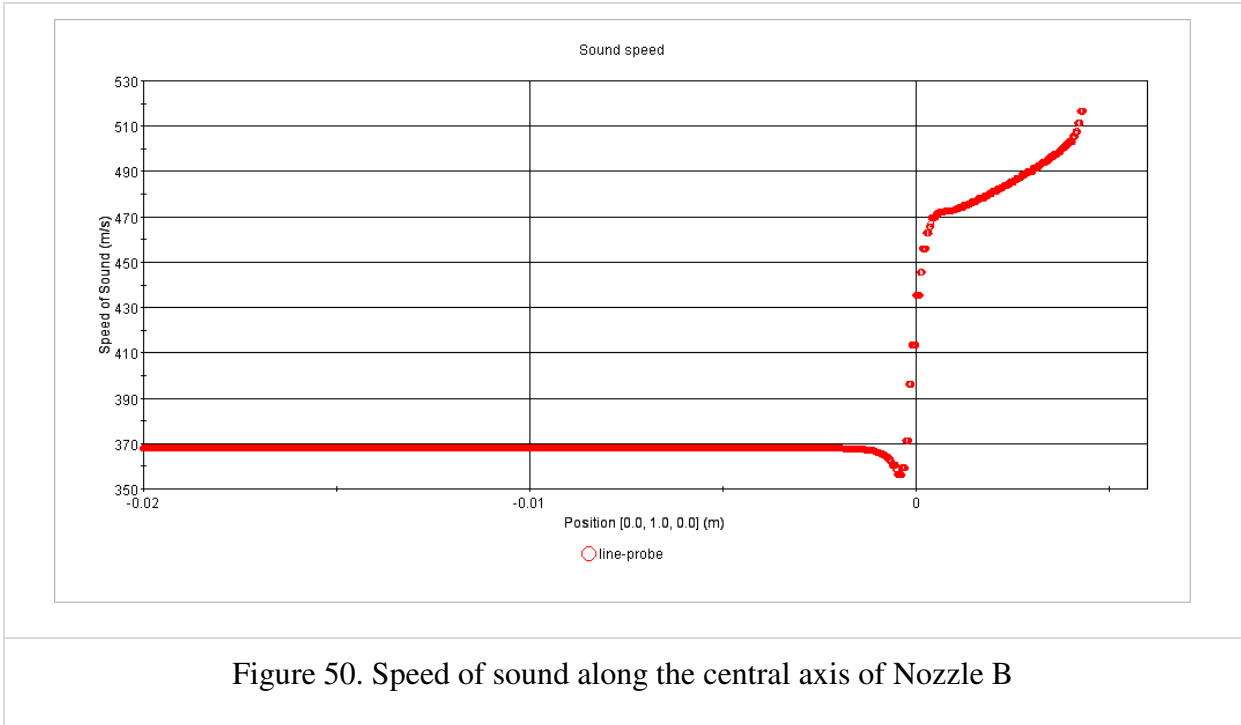
Figure 50. Speed of sound along the central axis of Nozzle B

The two-dimensional contours for the simulation variables along the central plane of the nozzle are shown in Figure 51 to Figure 55. The effect of sharp edges on the pressure drop and flow patterns can be clearly seen in these 2-D contours. As opposed to the round edge nozzle, here the water properties change upstream of the nozzle entrance, indicating the effect of sharp edge causing upstream effects (likely originated by shock formation).
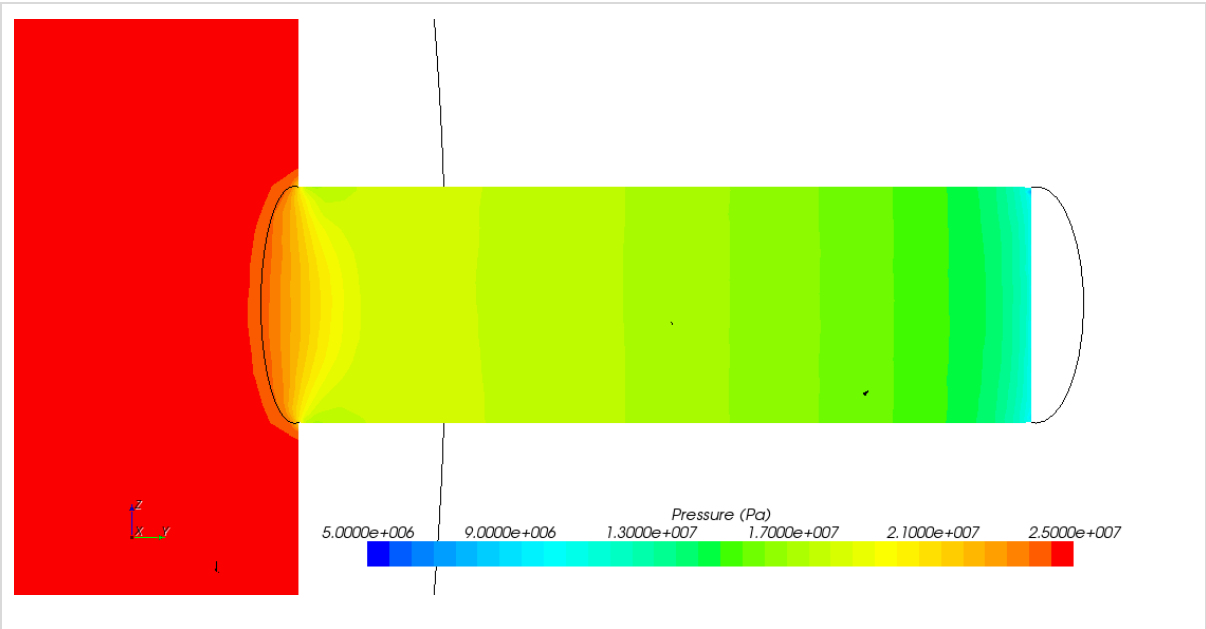
Figure 51. Pressure contours along the nozzle area for Nozzle B
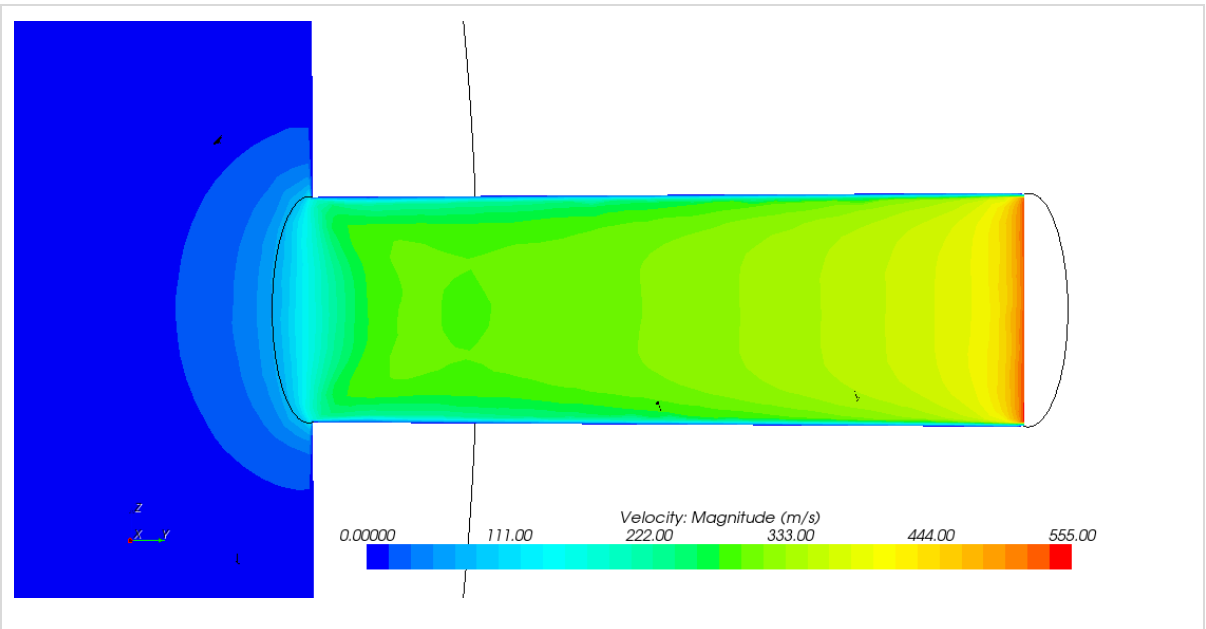
Figure 52. Velocity contours along the nozzle area for Nozzle B

Figure 53. Temperature contours along the nozzle area for Nozzle B

Figure 54. Density contours along the nozzle area for Nozzle B

Figure 55. Viscosity contours along the nozzle area for Nozzle B
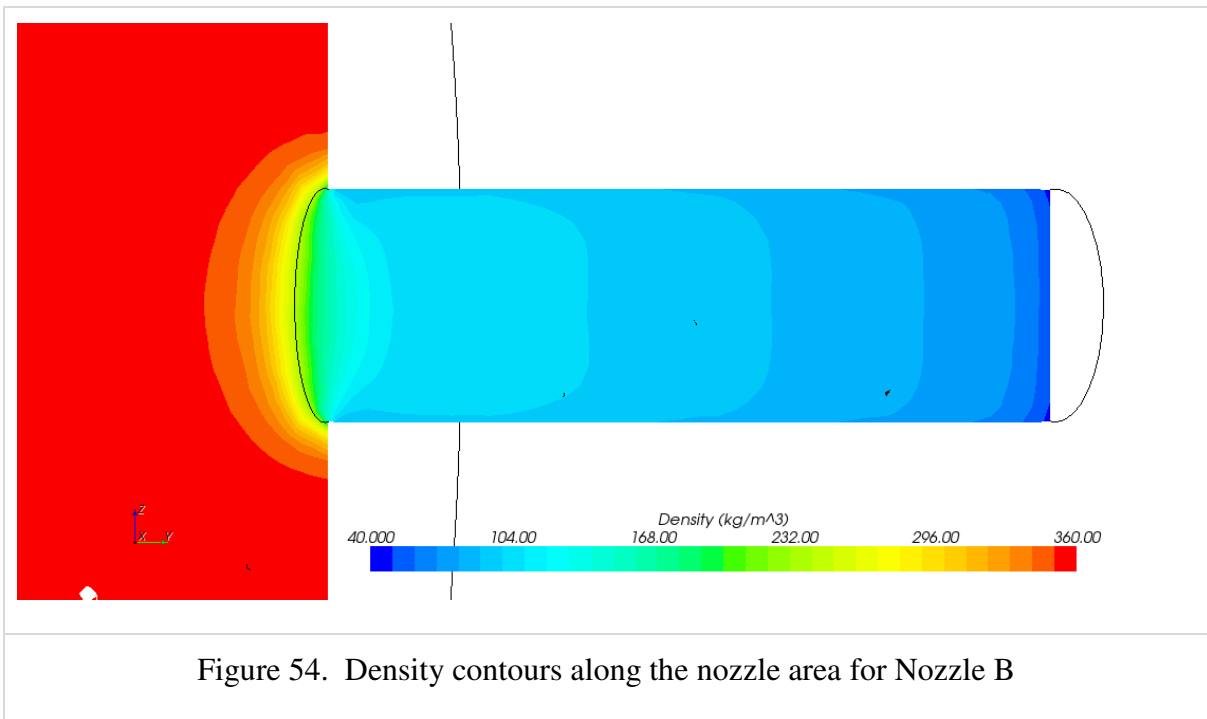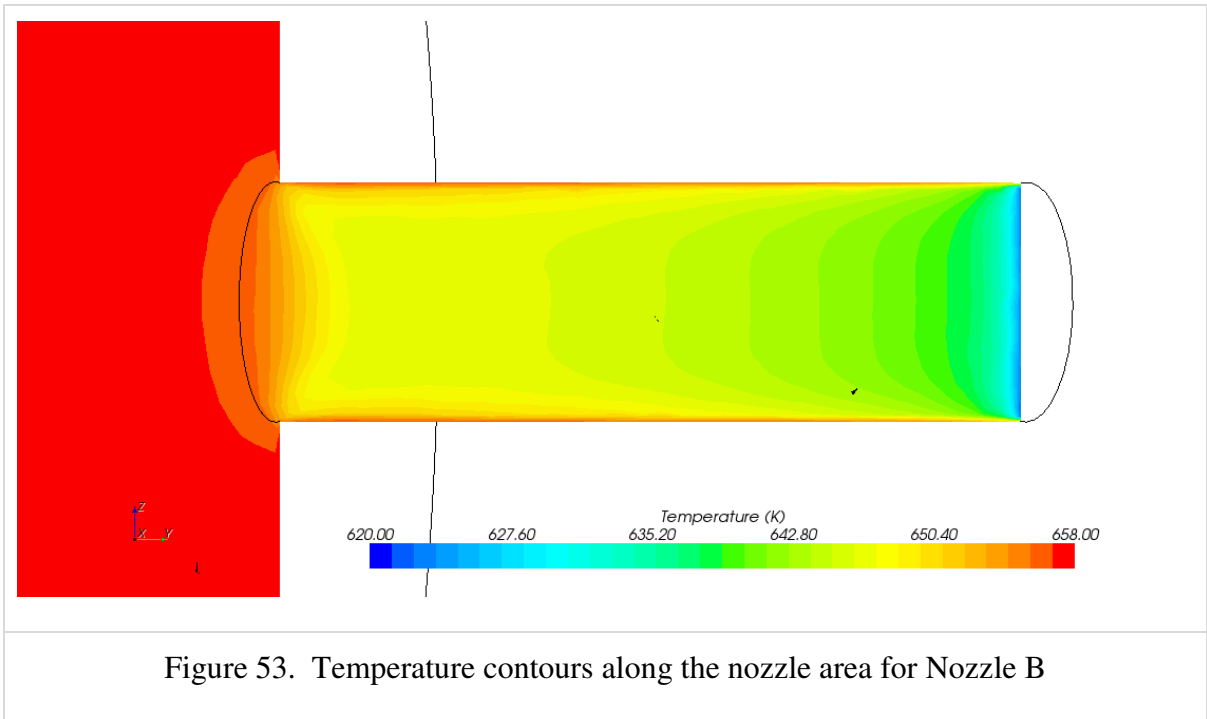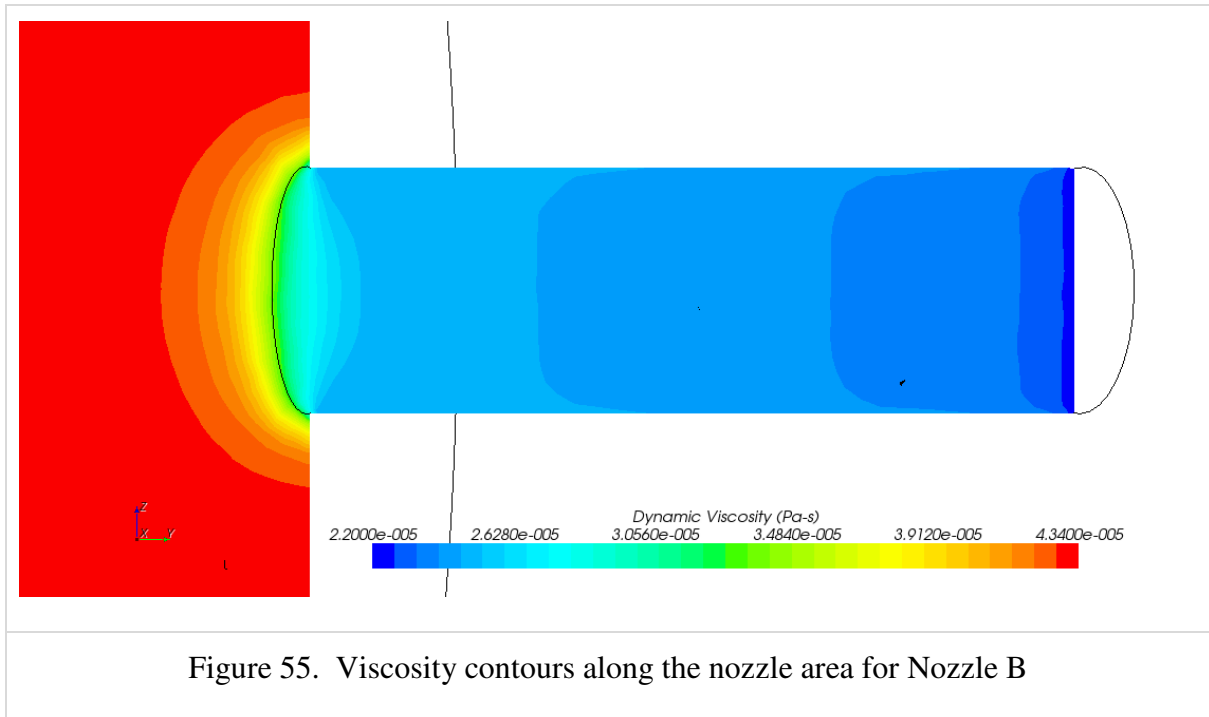
5.5 Interpreting the Effect of Nozzle Geometry

To gain more insight on the effect of nozzle geometry on the simulation results, the pressure and velocity contours for both round-edge and sharp edge nozzle are shown in Figure 56 to Figure 61 for quick comparison. These contours provide a clear picture of the nozzle geometry and the effects on the pressure drop and fluid velocity. Providing such intuitive figures is one of the advantages of CFD, which could not be obtained from 1-D simulation.

The results are self explanatory. It is clear that for the round edge nozzle, the pressure drop occurs inside the nozzle where diameter changed, indicating that the nozzle geometry does not have a profound effect on the results. On the other hand, the pressure drop in the sharp edge nozzle occurs right at the sharp edge of the nozzle, resulting in higher velocities compared to rounded edge nozzle. We believe that this change in flow may be due to the vena contracta effect as seen in Figure 59. A dotted line was drawn on the flow contours to highlight the flow patterns which appeared like the vena contractra

effect. The turbulent kinetic energy contours for both the nozzles (Figure 60 and Figure 61) indicate that there could be some effect of turbulence as well on the flow patterns.

Due to these effects primarily in the sharp edge nozzle, the velocity appears to be slightly higher in the sharp edge nozzle area compared to the round edge. As a result, the discharge velocity at the nozzle exit was also slightly more in the sharp edge nozzle (about 4%) compared to the round edge nozzle. By considering the supercritical simulations carried out in this thesis, it was found that the nozzle geometry does not have a great effect on the discharge flow rate, although it does seem to slightly affect the flow patterns upstream of the nozzle. This result was confirmed by the experiments (Chen et al., 2009), where it was found that for releases from supercritical conditions, the nozzle geometry does not have a substantial effect on the discharge flow rate, where as for releases from subcritical conditions it has a greater effect.

Figure 56. Pressure contours along the nozzle area for Nozzle A	Figure 57. Pressure contours along the nozzle area for Nozzle B
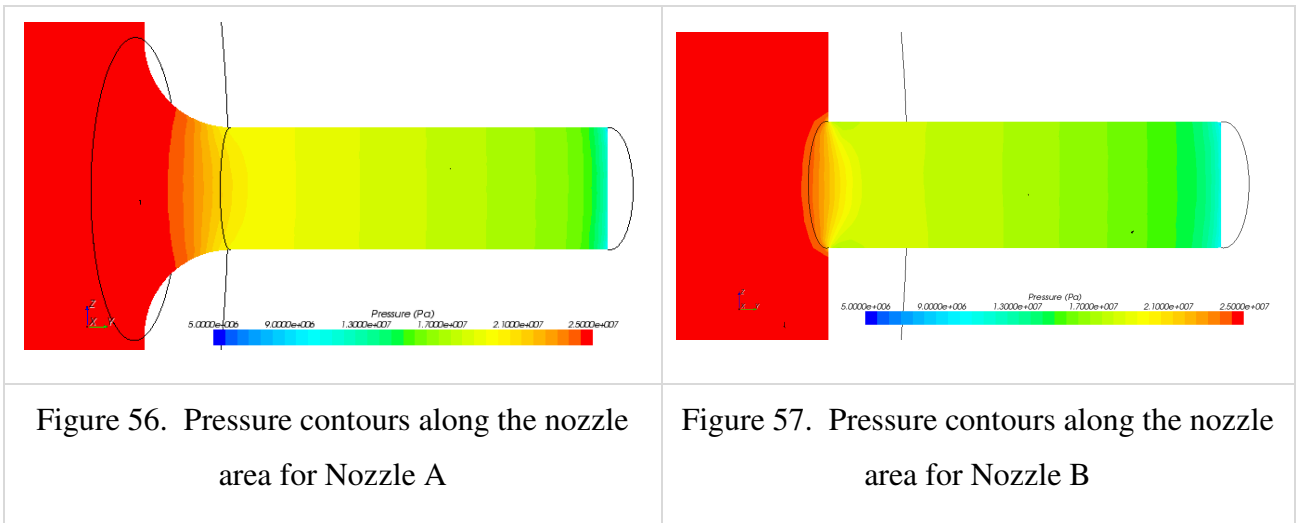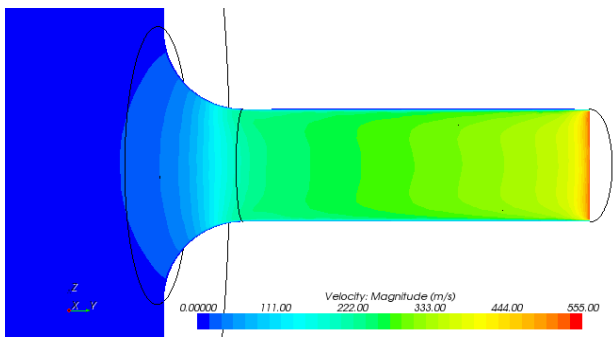
Figure 58. Velocity contours along the nozzle area for Nozzle A
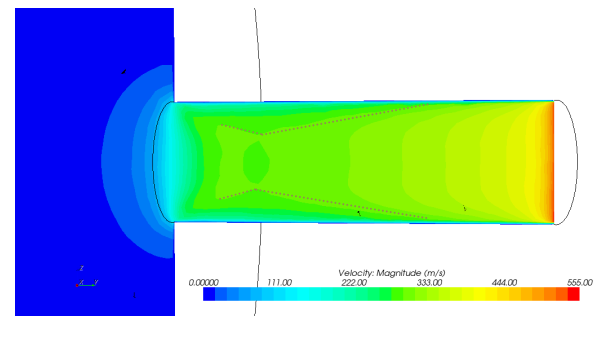
Figure 59. Velocity contours along the nozzle area for Nozzle B
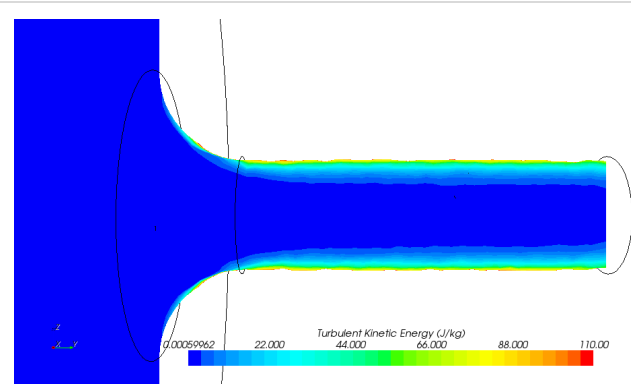
Figure 60. Turbulent Kinetic Energy along the nozzle area for Nozzle A
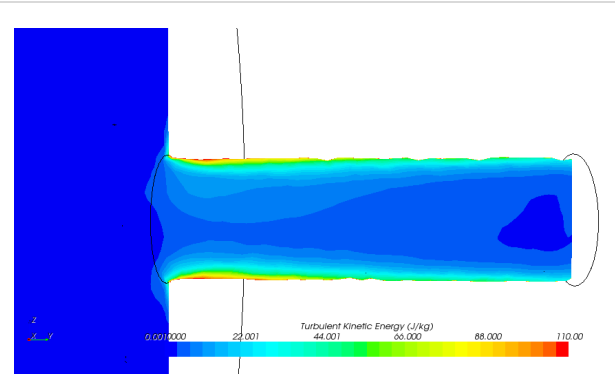
Figure 61. Turbulent Kinetic Energy along the nozzle area for Nozzle B

5.6   CFD Model Validation with Experimental Data

The validation of CFD model results with experimental data was performed only for Nozzle A. Several simulations were performed for the specified inlet Pressure and Temperature conditions and the results obtained were compared with the experimental data (Chen et al., 2009). To perform the simulations, the best settings for meshing and physics models, obtained from sensitivity analysis, were employed. The results obtained

from the simulations indicate that the CFD model predicts the experimental data within about 10% as shown in Table 10.

Table 10. CFD model validation with experimental data

	Pressure (MPa)	Temperature (K)	Reynolds Number	Experimental Mass Flux	CFD Estimated Mass Flux	% Estimation Error
1	25	650	1910720	34000	29855	12.2
2	25	655	1907264	33500	29801	11.1
3	25	657	1804800	33000	29657	10.1
4	25	660	1897792	33000	29653	10.2
5	25	665	1733312	32600	27083	16.9
6	25	670	1780480	32000	27820	13.1

The prediction error was found to be less than 17% for all the simulation cases; however, given the extremely high sensitivity to upstream temperature discussed earlier, these accuracies fall within those expected for such a configuration. Chen et al., (2009) reported that during accidental coolant release (LOCA) from supercritical conditions, a second phase would probably appear in the nozzle area. In this research, although a single-phase CFD modeling was used to simulate the accidental release scenario, the results obtained are promising and quite reasonable. This further confirms that CFD modeling is an excellent tool to perform thermal hydraulic simulations for supercritical systems.

5.7   Summary

This chapter primarily discusses the results obtained from the CFD simulation scenarios considered in this thesis. The simulation results for the nominal case study (accidental release of coolant from supercritical condition) revealed that the pressure and

velocity profiles along the length of the nozzle changed in three distinct stages, which were also clearly visible in all the water properties.

The sensitivity of the CFD model was evaluated for various mesh configurations, turbulence models and perturbations in the boundary conditions. Consequently, the best settings were obtained from the analysis that ensured best performance. These settings were then used to perform all the simulations in this thesis. By comparing the CFD model results with the experiential data, it was found that the predication error is less than 17% for the simulation cases considered in this thesis. This is an exceptional result given that single-phase CFD modeling and simulation was performed to capture the accidental release events, which potentially gives rise to two-phases.

Two types of nozzle geometries (Nozzle A and Nozzle B) were investigated to evaluate the effect of nozzle geometry on the flow patterns and the exit discharge flow rate. The results revealed that the nozzle geometry has a very little effect on the fluid flow particularly for releases from supercritical conditions. The experiments have confirmed the same results, thus providing additional evidence that CFD is a practical technique to perform thermal hydraulic simulations.

6.   Conclusions and Future work

The main aim of this research work was to investigate the ability of CFD code STAR-CCM+ to perform critical flow evaluation due to accidental coolant release from supercritical conditions and to identify the computational challenges encountered while achieving the goal. This chapter provides a brief summary of the work done in this thesis followed by the conclusions and recommendations for future work.

The major challenge encountered in this research work was the inability of STAR-CCM+ to support simulations under supercritical conditions, which was mainly because of the steam tables included in the package that are limited to only the subcritical subset of the thermodynamic properties. Updating the steam tables (including subcritical and supercritical water properties) and implementing them within STAR-CCM+ using external user-defined routines resolved the issue and allowed us to perform simulations involving supercritical conditions.

To perform critical flow evaluation and validation of the CFD model with experimental data, three-dimensional CFD models were developed for rounded-edge and sharp-edge nozzles according to the CIAE experiments (Chen et al., 2009). Solution stability (or convergence) issues were encountered during simulation, which is mainly due to the rapid changes in water properties in the pseudo-critical region. As a result, a step-by-step simulation procedure was proposed that guaranteed convergence. Sensitivity of the CFD model was evaluated and the best mesh configuration and turbulence model was used to carry out the simulations. The validation results revealed that the CFD model produced results that were in good agreement with experimental data with only about 10% prediction error for most cases. Furthermore, the results obtained in this thesis were in good agreement with the theoretical expectations. For instance, the choked flow condition for single phase flow where the discharge velocity equals to the sonic velocity, was reproduced by the CFD model. This confirms that CFD, with appropriate

customization, can be used as a practical approach to perform thermal hydraulic simulations for design and safety analysis of supercritical nuclear reactor systems.

The major conclusions and contributions of the research and the recommendations for future work are discussed in the following sections.

6.1 Conclusions

- The work carried out in this thesis confirmed that STAR-CCM+ can be used to perform thermal hydraulic simulations under supercritical conditions with appropriate customization. The major challenges encountered in the present work were related to the customization of CFD code for supercritical conditions and overcoming the solution instability (or convergence) issues during the simulations. Methods were proposed to resolve these issues, which allowed us to complete all the case studies in this thesis successfully.

- STAR-CCM+ was customized to support thermal hydraulic simulations involving supercritical conditions by updating the steam tables and embedding them within the CFD code. A 2-D Look-up Table approach, which performs 2-D interpolation to retrieve the water properties at any thermodynamic condition during CFD simulation, was found to be the most appropriate method for customization that ensured reliability during computations and provided a right balance between accuracy, computational burden and programming complexity. With an appropriate grid spacing (temperature and pressure points) in the steam tables, the supercritical simulations were performed without any reported problems.

- A step-by-step simulation procedure was proposed to overcome the convergence issues encountered while solving supercritical simulations. The procedure was to solve the flow loop first, while disabling the energy loop. Once the flow is converged the energy loop is solved. The relaxation coefficients played a significant role during this process. The default

relaxation coefficients for flow and energy were found to be very aggressive leading to an unstable solution. Therefore, fine tuning of the relaxation coefficients was necessary and consequently a passive approach was proposed, where lower values of relaxation coefficients were used during the initial stages of the simulation and then slowly they were increased after overcoming the stability issue to achieve faster convergence. The best set of relaxation coefficients and the overall procedure illustrated it this thesis proved to be robust for all the simulations carried out in the present work.

- Several case studies were simulated using a rounded-edge nozzle to perform critical flow evaluation due to accidental release of coolant from supercritical pressures (25 MPa). The results revealed that choked flow conditions were observed when the downstream pressure was about 11 MPa. At this point, the discharge velocity reached a maximum value and did not change for any further intentional decrease in the downstream pressure. This led to a conclusion that for supercritical water, an upstream to downstream pressure ratio of at least 2.27 is required for choked conditions to appear.

- Sensitivity analysis was performed to evaluate the sensitivity of the CFD model for various mesh configurations, turbulence models, and perturbations in the boundary conditions. The results indicated that out of the four mesh configurations investigated in this research, Mesh 2 was the best configuration as it provided the required accuracy without much computational burden. Among the turbulence models, k-epsilon (realizable 2-layer) and k-omega (SST) were found to be the most robust as they guaranteed convergence for several initial guesses (some bad and some good). The perturbations in inlet temperature and pressure led to about 10% error in the simulation results, while the wall roughness did not have any significant effect.

- A nominal case study representing an accidental leak from supercritical conditions was simulated and the results indicated that pressure, velocity and

water property profiles along the nozzle varied in three distinct stages. The most drastic change in these variables was seen in the nozzle area in the first stage, where pseudo-critical transition of water took place. In the second stage, the fluid properties were linear and so all the profiles varied linearly, In the third stage, the velocity increased sharply to attain choked flow condition, while the other variables varied only slightly.

- The model results for two types of nozzles (rounded-edge and sharp-edge) were compared to investigate the effect of nozzle geometry on the discharge flow rate. The results indicated that the nozzle geometry did not have a significant effect on the discharge flow rate for releases from supercritical conditions, although it does play some role in the internal flow upstream of the nozzle. These results were confirmed by the experiments as well. The discharge velocity for rounded-edge nozzle and sharp-edge nozzle were found to be about 512 m/s and 535 m/s respectively. The slightly higher velocity for sharp-edge nozzle may be due to the vena contracta effect as well as higher mixing and turbulence effects due to the sharp edges.

- The validation of CFD model with experimental data has indicated that a prediction error of at the most 17% was observed for the case studies considered in this thesis. Given the extremely high sensitivity of the CFD model to upstream temperatures, this accuracy falls within the expected result for such a configuration. Furthermore, the use of single-phase CFD modeling for supercritical releases that might potentially result in two-phases inside the nozzle explains that the prediction error is quite reasonable.

6.2   Recommendations for Future work

- 2-D Look-up Table method refinement: In this thesis, a 2-D Look-up Table method was proposed to customize the CFD code STAR-CCM+ to support supercritical simulations. Although, the method worked well for all the simulations considered in this thesis, it can be further refined to provide better

results by incorporating more temperature and pressure points in the steam tables and improving the 2-D interpolation routine. We requested CD-Adapco (developer of STAR-CCM+) to incorporate a 2-D interpolation routine within the code. Upon its development, it will be interesting to use their routine in the proposed method and verify if any improvements can be achieved.

- Near-wall treatment models: The near wall region is important in turbulence flow modeling as it is the main source of turbulence generation during fluid flow. In this thesis, the default near-wall treatment models in STAR-CCM+ (All y+ Wall Treatment) were used while evaluating the sensitivity of the CFD model for various turbulence models. Although, we believe that the default models would provide acceptable results, it may be worth evaluating the sensitivity to the CFD model to various near-wall treatment models available in STAR-CCM+.

- Transient simulation: This thesis has mainly concentrated on steady state simulations. However, a couple of transient simulations (Edward's-Obrien pipe blowdown simulation from supercritical conditions) were also performed as discussed in Appendix B. Computational difficulties (convergence issues) were encountered during the transient simulations. Therefore, we believe that further investigation is required for the applicability of STAR-CCM+ for transient supercritical simulations.

- Two-phase CFD simulation: It has been reported that a second phase appears in the nozzle area during accidental release of coolant from supercritical conditions (Chen et al., 2009). To model the two-phase behaviour of the fluid in the nozzle area, it is required to use multi-phase CFD simulation. Although, STAR-CCM+ supports multi-phase fluid modeling, it is still pre-mature and requires further development for full-fledge applicability. Therefore, two-phase CFD modeling will be a topic for future exploration.

References

1. GIF (2011). http://www.gen-4.org/

2. Department of Energy (DOE). (2003). A Technology Roadmap for Generation IV Nuclear Energy Systems, March 2003.

3. GIF. (2009). Generation IV International Forum (GIF) Annual Report 2009.

4. Bae Y.Y., Leung, L/K.H., Lycklama, J.A., Nijeholt, A., Andreani, A., Schulenberg, T., Oka, Y. (2009). Status of ongoing research on SCWR Thermal-Hydraulics and Safety, Proceedings of GIF Symposium, Paris, France, 9-10 September 2009.

5. Sakurai, S., Shinichi, H., Katsumi, Y., and Kazuaki, K. (2009). SCWR (Supercritical Water-cooled Reactor) fuel an core design study, Proceedings of GIF Symposium, Paris, France, 9-10 September 2009.

6. Shan, J.Q., Leung, L.K.H. (2009). Subchannel Analysis of CANDU-SCWR Fuel, Progress in Nuclear Energy, Vol 51, 799-804.

7. Torgerson, D.F. , Shalaby, B. A., and Simon, P. (2006). CANDU technology for Generation III+ and IV reactors, Nuclear Engineering and Design, 236, 1565–1572.

8. Licht, J., Mark Anderson, M., Corradini, M. (2008). Heat transfer to water at supercritical pressures in a circular and square annular flow geometry, International Journal of Heat and Fluid Flow, 29, 156–166.

9. Gallaway, T., Antal, S.P., Podowski, M.X. (2008). Multi-dimensional model of fluid flow and heat transfer in Generation-IV Supercritical Water Reactors, Nuclear Engineering and Design 238, 1909–1916.

10. Corradini, M. (2009). Transport phenomena in supercritical fluid in Gen-IV reactor designs, Nuclear Technology, 167, 145-156.

11. Menter, F. (2002). CFD Best Practice Guidelines for CFD Code Validation for Reactor Safety Applications, ECORA FIKS-CT-2001-00154, 2002.

12. Smith, B.L. (2010). Assessment of CFD codes used in Nuclear reactor safety simulation, Nuclear Engineering and Technology, 42, 4, 339-364.

13. Nagatsuka, T., Misawa, T., Yoshida, H., Takase, K. (2009). Numerical simulation of Heat Transfer experiment of Supercritical water by Two-Fluid model code ACE 3-D, Proceeding of 4th International Symposium on Supercritical Water-cooled Reactors, Germany 8-11 March 2009.

14. Parry, W. T., Bellows, J. C., Gallagher, J. S., Harvey, A. H. (2000). ASME International Steam Tables for industrial use: Based on the IAPWS International Formulation 1997 for the thermodynamic Properties of Water and Steam (IAPWS-IF97), CRTD- 58, ASME, 2000.

15. Jeremy R. Licht, Mark H. Anderson, Michael L. Corradini, Riccardo Bonazza. (2007). Heat Transfer Phenomena in Supercritical Water Nuclear Reactors, Final Technical Report, DE-FG07-04ID14602.

16. Mattia De Rosa. (2010). Computational Fluid Dynamics Analysis of Experimental Data on Heat Transfer Deterioration with Supercritical Water, PhD Thesis, University of Pisa.

17. Yuzhou Chen, Chunsheng Yang, Shuming Zhang, Minfu Zhao, Kaiwen Du, Xu Cheng. (2009). Experimental study of critical flow of water at supercritical pressure, Frontiers of Energy and Power Engineering in China, 3, 175-180.

18. Mignot, G., Anderson, M., Corradini, M. (2007). Critical flow experiment and analysis for Supercritical fluid, Nuclear Engineering and Technology, 40, 133-138.

19. Mignot, G., Anderson, M., Corradini, M. (2009). Measurement of supercritical CO2 critical flow: Effects of L/D and surface roughness, Nuclear Engineering and Design, 239, 949-955.

20. Bernhard Gebbeken, Rudolf Eggers. (1996). Blow down of Carbon dioxide from initially supercritical conditions, Journal of Loss Prevention in Process Industries, 9, 285-293.

21. Richard A. Riemke, Cliff B. Davis, Richard R. Schultz. (2003). RELAP5-3D code for supercritical pressure, light water cooler reactors, International Conference on Nuclear Engineering, Tokyo, Japan.

22. Lee, D.H., Swinnerton, D. (1983). Evaluation of critical flow for supercritical steamwater, EPRI-NP-3086.

23. Corradini, M. (2009). Transport Phenomena in Supercritical fluids in Gen-IV reactor designs, Nuclear Technology, 167, 145-156.

24. Mignot, G., Anderson, M., Corradini, M. (2005). Initial study of Supercritical fluid blow down, Fusion Science and Technology, 47, 574-578.

25. Bae, Y.Y, Leung, L.K.H. , Lycklama, J.A, Nijeholt, A, Andreani, M, Ishiwatari, Y., Oka, H. Mori, K. E. (2009). Status of ongoing research on SCWR Thermal-hydraulics and safety, GIF Symposium, Paris (France), 9-10 September, 2009

26. Smith, B.L. (2010). Assessment of CFD Codes Used in Nuclear Reactor Safety Simulations, Nuclear Engineering and Technology, 42, 4, 339-364.

27. Bestion, D. (2010). Extension of CFD Codes Application to Two-Phase Flow Safety Problems, Nuclear Engineering and Technology, 42, 4, 365-376

28. Mahaffy, J. (2010). Development of Best Practice Guidelines for CFD in Nuclear Reactor Safety Nuclear Engineering and Technology, 42, 4, 377-381

29. Hohne, T., Krepper, E., Rohde, U. (2010). Application of CFD Codes in Nuclear Reactor Safety Analysis, Science and Technology of Nuclear Installations, Volume 2010, Article ID 198758, 8 pages.

30. Cfx. (2009). CFX user Guide, www.ansys.com.

31. Fluent Inc. (2009). Fluent user Guide, www.ansys.com.

32. StarCCM+. (2009). STAR-CCM+ user Guide, www.cd-adapco.com.

33. Iapws. (2007). International Association for the Properties of Water and Steam, Revised Release on the IAPWS Industrial Formulation 1997 for the Properties of Water and Steam, IAPWS Secretariat, Lucerne, Switzerland, www.iapws.org.

34. Tara Gallaway, Steven P. Antal, Michael Z. Podowski. (2007). Multi-dimensional model of fluid flow and heat transfer in Generation-IV Supercritical Water Reactors, Nuclear Engineering and Design, 238 (2008), 1909–1916

35. Levy, S., Abdollahian, D., Healzer, J. (1982). Critical–flow data review and analysis. EPRI-NP-2192.

36. Saha, P. (1978). A review of two-phase steam-water critical flow models with emphasis on thermal non-equilibrium. BNL-NUREG-50907.

37. Moody, F. J. (1965). Maximum flow rate of a single component, two-phase mixture. ASME Transactions, Journal of Heat Transfer, 87(1): 134–142

38. Henry, R. E., Fauske, H. K. (1971). The two-phase critical flow of one component mixtures in nozzles, orifices, and short tubes. ASME Transactions C, Journal Heat Transfer, 93(2): 179–187

39. Chen Yuzhou, Yang Chunsheng, Du Kaiwen (2008). An experimental study of critical flow of water at steady-state with pressure of up to 22 MPa. In: Proc 7th International Symposium of Heat Transfer, Beijing.

40. Trapp, J. A., Ransom, V. H. (1982). A choked-flow calculation criterion for non-homogeneous, non-equilibrium, two-phase flows. International Journal of Multiphase Flow, 8(6): 669–681

41. Ambrosini, W. (2009). Continuing assessment of system and CFD codes for heat transfer and stability in supercritical fluids, 4th International Symposium on Supercritical Water-Cooled Reactors March 8-11, Heidelberg, Germany.

42. Wilcox, D. C. (2006). Turbulence modeling for CFD, 3rd Edition, DCW Industries Incorporated, USA.

Appendix A

2D Table interpolation method – Effect of grid spacing on the results

A.1   Effect of grid spacing in the 2D Look-up Table interpolation method

In the present work, updated steam tables were created as 2-D tables for each water property (e.g. density, viscosity, thermal conductivity, specific heat etc) for a pressure range of 0.1 MPa to 27 MPa and temperature range of 550 K to 700 K so that both sub-critical as well as the super-critical regions are covered. The sample 2-D table for water density is shown in Figure 62. As discussed in the chapter 3, all the steam tables were created with uniform pressure grid spacing of 0.1 MPa, whereas a non-uniform temperature grid spacing was used with coarse spacing in the subcritical region and fine spacing in the pseudo-critical region (i.e., Pressure range of 22 – 27 MPa and Temperature range of 645 to 660 K).

Pressure (MPa)	Temperature (K)									
	550	600	610	620	630	640	.	.	690	700
0.10	0.40	0.36	0.36	0.35	0.34	0.34	.	.	0.31	0.31
0.20	0.79	0.72	0.71	0.70	0.69	0.68	.	.	0.63	0.62
0.30	1.19	1.09	1.07	1.05	1.03	1.02	.	.	0.94	0.93
0.40	1.59	1.45	1.43	1.40	1.38	1.36	.	.	1.26	1.24
0.50	1.99	1.82	1.79	1.76	1.73	1.70	.	.	1.57	1.55
0.60	2.40	2.18	2.15	2.11	2.08	2.04	.	.	1.89	1.86
0.70	2.80	2.55	2.51	2.47	2.43	2.39	.	.	2.21	2.17
0.80	3.21	2.92	2.87	2.82	2.78	2.73	.	.	2.53	2.49
0.90	3.62	3.30	3.24	3.18	3.13	3.08	.	.	2.84	2.80
1.00	4.04	3.67	3.61	3.54	3.48	3.42	.	.	3.16	3.12
.	.	.	.	.	.	.	.	.	.	.
.	.	.	.	.	.	.	.	.	.	.
.	.	.	.	.	.	.	.	.	.	.
26.90	784.33	692.79	669.19	642.50	611.34	572.91	.	.	160.62	145.00
27.00	784.37	692.87	669.29	642.62	611.50	573.15	.	.	161.12	145.39

Figure 62: 2-D table for Water Density

The fine grid spacing for temperature in the pseudo-critical region plays an important on the interpolation accuracy. Therefore, to investigate the effect of temperature grid spacing on the interpolation accuracy, two types of grid spacing were tested. They are:

(i)   Scenario 1: A spacing of 0.5 K in the pseudo critical region, and

(ii)   Scenario 2: A spacing of 0.25 K in the pseudo critical region.

A simple pipe flow example was used to carry out this investigation. A vertical pipe of length (2 m) and diameter (5 mm) was used to perform the simulation with water at supercritical conditions. The boundary conditions for pipe inlet were set at 25 MPa and 652 K and the outlet conditions were set as ambient, representing a LOCA scenario. Adiabatic conditions were specified for the wall and no-slip conditions were used. The mesh for the pipe model is shown in Figure 63.
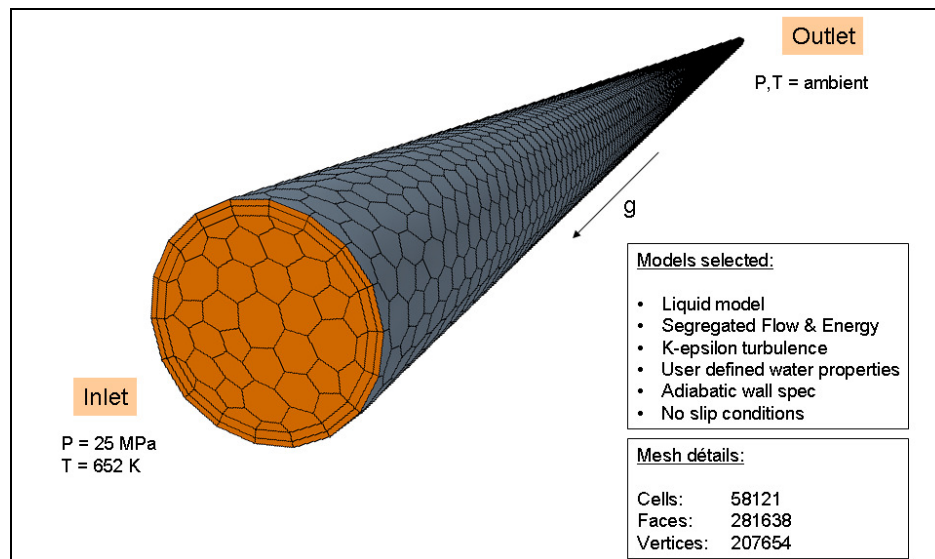
Figure 63: Mesh for the simple pipe flow example

(i) Scenario 1: Temperature grid spacing of 0.5 K in the pseudo critical region

The steady state results for this scenario are shown in Figure 64 to Figure 68. The profiles represent the results obtained along the pipe's central axis. The results indicate that the pseudo critical conditions were encountered in the pipe at around 0.7 m, where the water properties such as density and viscosity change suddenly as seen in Figure 66

and Figure 67. However, these properties do not change smoothly, as highlighted in the results, indicating the possibility of interpolation error in the pseudo critical region.
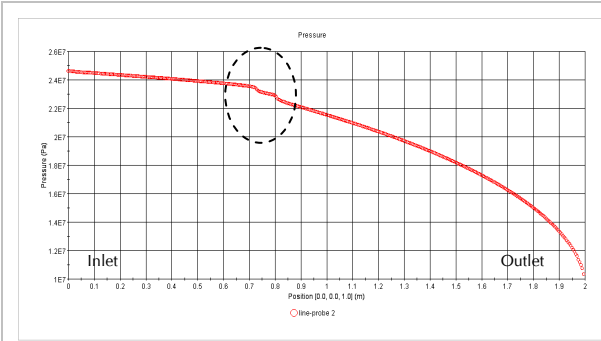
Figure 64: Pressure profile for coarse grid
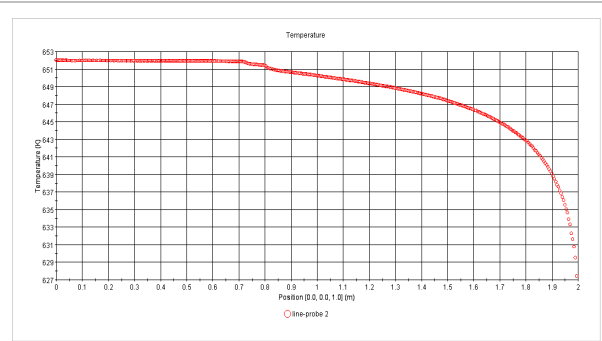
Figure 65: Temperature profile for coarse grid
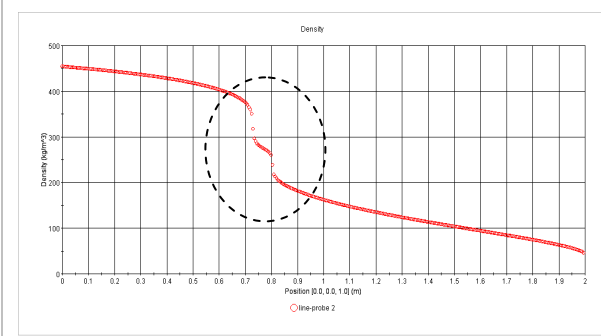
Figure 66: Density profile for coarse grid
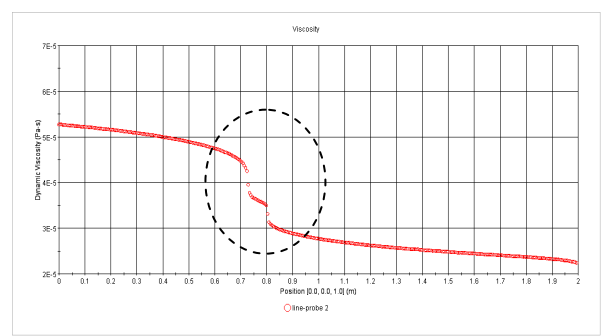
Figure 67: Viscosity profile for coarse grid
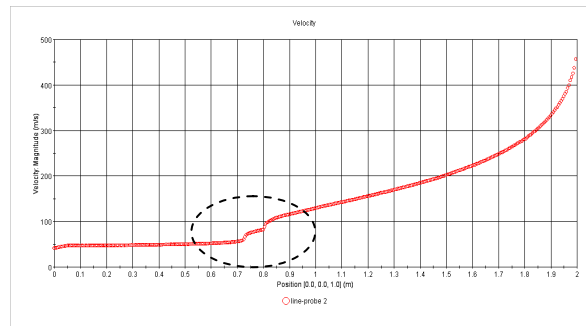
Figure 68: Velocity profile for coarse grid

(ii) Scenario 2: Temperature grid spacing of 0.25 K in the pseudo critical region

This scenario includes a much finer temperature grid. The results for this scenario are shown in Figure 69 to Figure 73, which clearly indicates the smooth transition of water properties in the pseudo critical region. Clearly, a fine temperature grid improves the solution and makes it easily interpretable. Therefore, it is recommended to use a fine grid spacing of 0.25 K or lower along the temperature grid to reduce the margin of error due to linear interpolation.
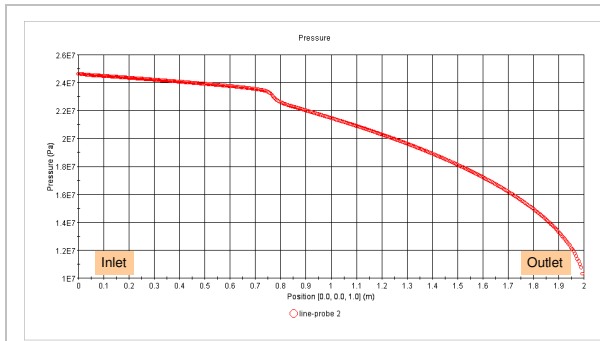
Figure 69: Pressure profile for fine grid
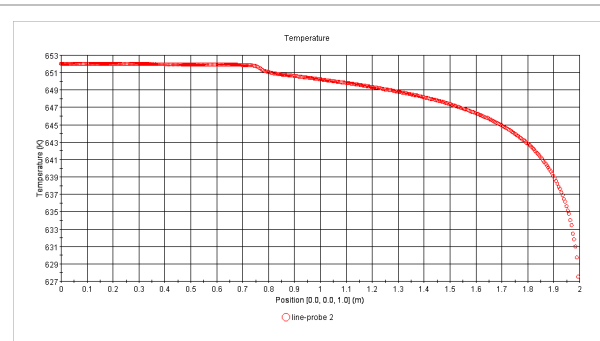
Figure 70: Temperature profile for fine grid
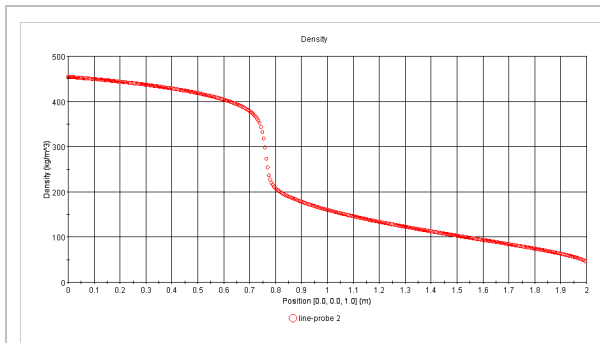
Figure 71: Density profile for fine grid
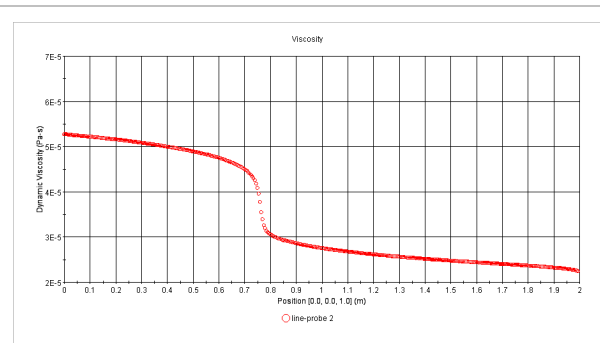
Figure 72: Viscosity profile for fine grid
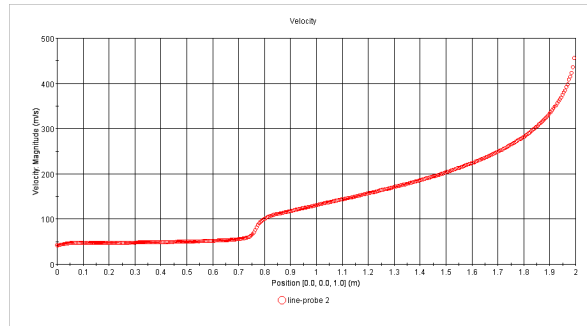
Figure 73: Velocity profile for fine grid

Appendix B

Edwards-Obrien Pipe Blowdown Simulation

To test the application of STAR-CCM+ for transient simulations involving supercritical conditions, a modified version of the Edwards-O'Brien blowdown experiment (Riemke et al., 2003) was simulated. In this test, a straight closed horizontal pipe of 4.096 m length and 0.073 m inner diameter was initially filled with water at 25.0 MPa. One of the pipe ends was then opened abruptly to cause a rapid depressurization, flashing and emptying of the pipe. This test was run with two different initial temperatures (580 K and 700 K) such that the depressurization results in subcooled-liquid in the first scenario and superheated vapor in the second scenario. By performing these simulations, it was verified that STAR-CCM+ is able to simulate a rapid transition between the supercritical and subcritical pressure regions without any water property related issues. The simulation results are discussed as follows.

Scenario 1 (Initial Temperature-580 K):

The results obtained for scenario 1 are presented from Figure 74 to Figure 77. Because experimental data on these modified tests doesn't exist, it is not possible to evaluate how realistic the simulation results are. However, the results seem reasonable because the depressurization time of 0.1 seconds for this scenario appears to be in the same range as the results obtained from RELAP (Riemke et al., 2003) for a similar scenario.

Computational difficulties were encountered during the simulation. It was found that after few iterations, the residuals started to increase rapidly (as shown in Figure 77) causing convergence issues and eventually lead to an execution error. The reason for this behavior could not be identified as transient simulation is beyond the scope of this thesis. From our computational experience, we believe that fine tuning the solver parameters may provide better results, but it needs further investigation and this could be the topic for future work.
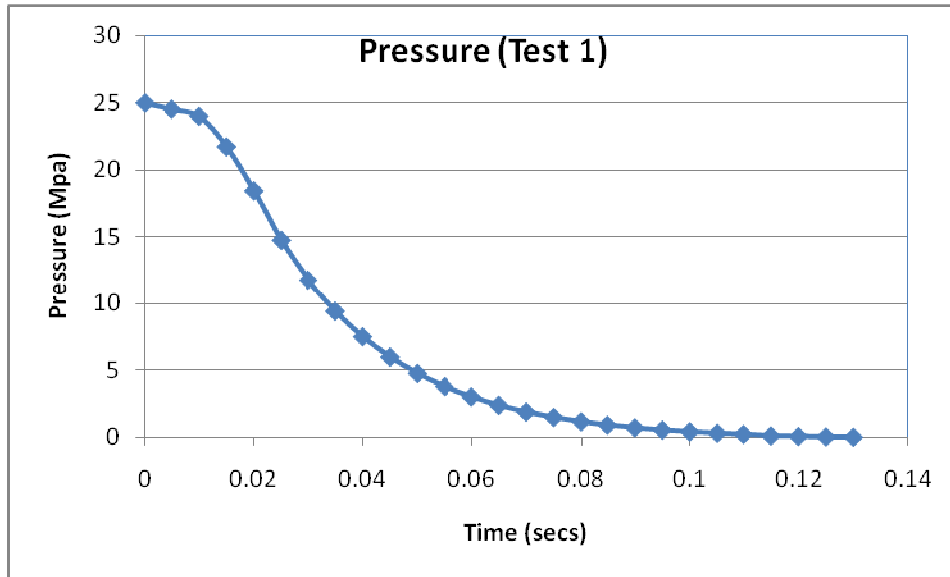
Figure 74. Pressure during a blowdown of Edwards pipe (Test 1)
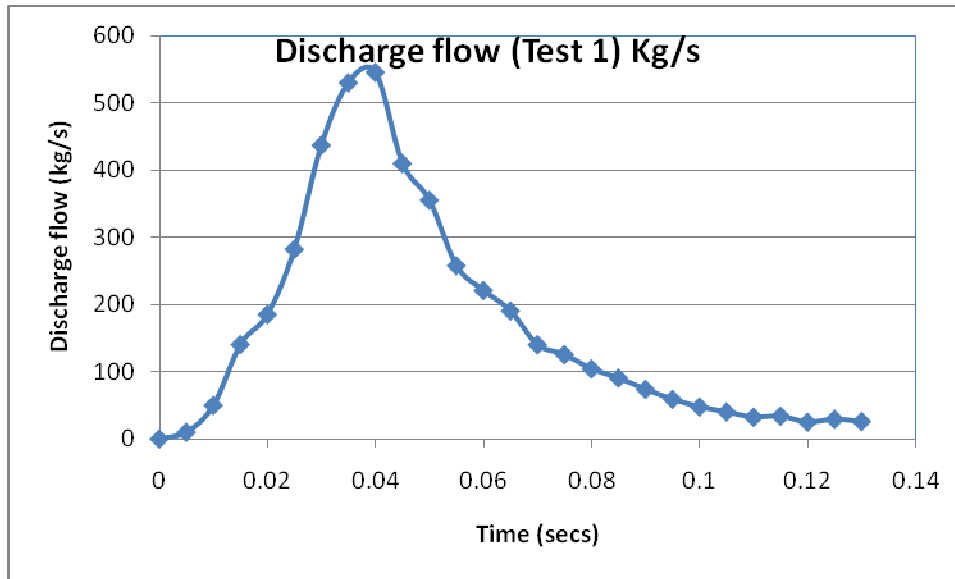
Figure 75. Discharge flow rate during a blowdown of Edwards pipe (Test 1)
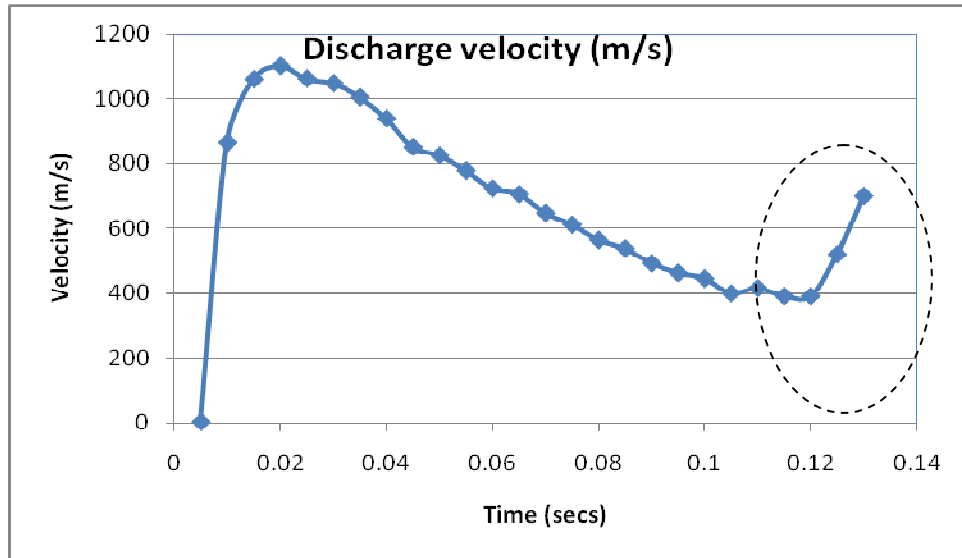
Figure 76. Discharge velocity during a blowdown of Edwards pipe (Test 1)
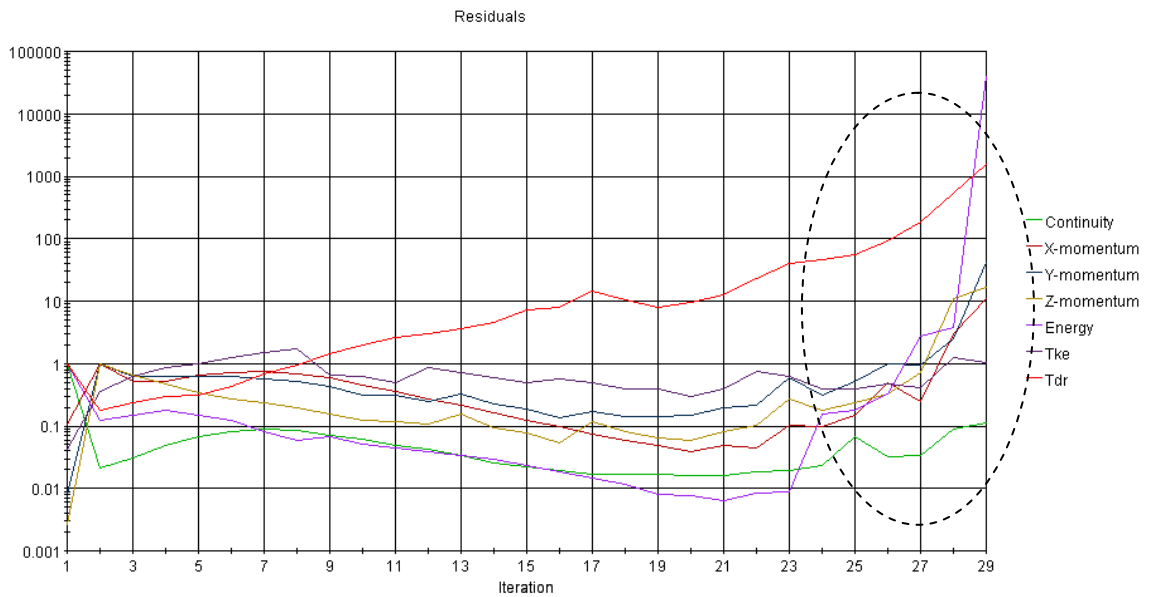
Figure 77. Residuals during the simulation (Test 1)

<u>Scenario 2 (Initial Temperature-700 K)</u>:

The simulation results for scenario 2 are shown in Figure 78 and Figure 79. Although, the pressure profile looks reasonable, the discharge flow rate of 8000 Kg/s does not appear to be in a reasonable range. However, converge issues (divergence of residuals) were not encountered during this simulation. From our computational experience, we strongly believe that, although STAR-CCM+ can be used to perform transient simulations, it needs further investigation for proper application.
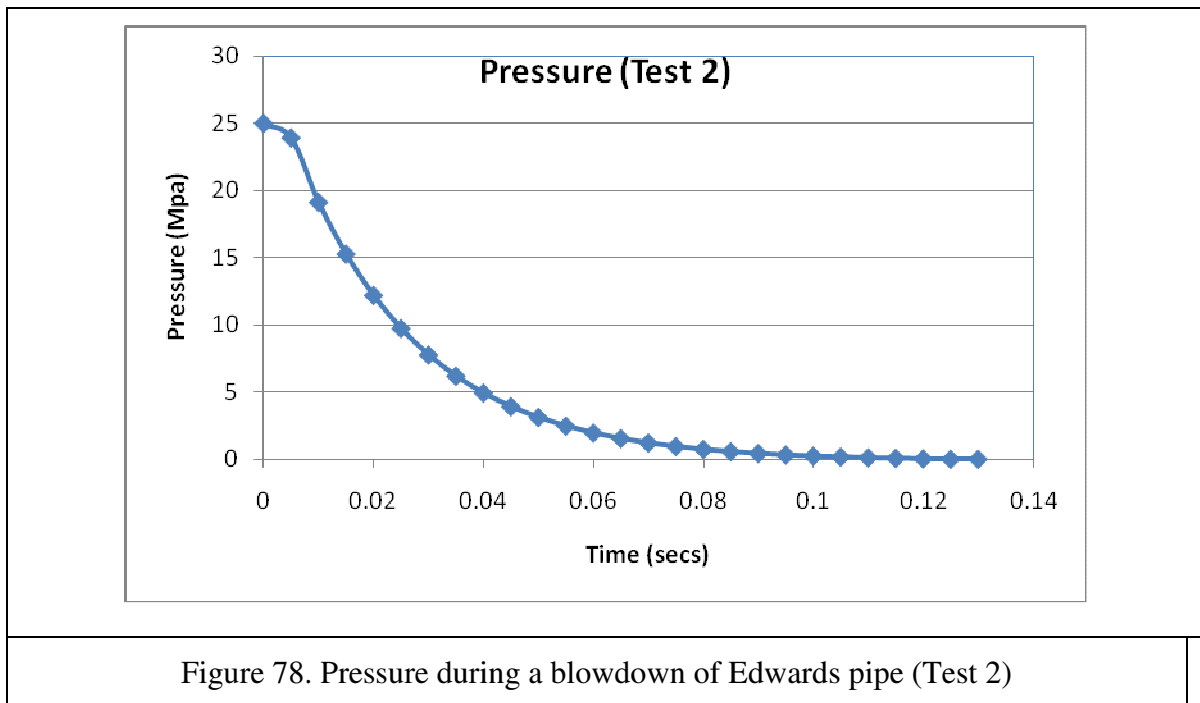
Figure 78. Pressure during a blowdown of Edwards pipe (Test 2)
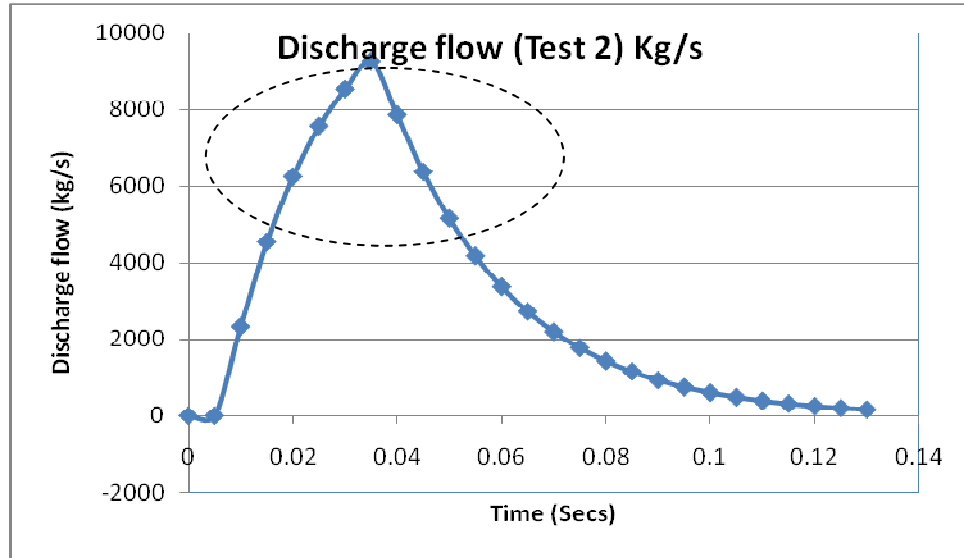
Figure 79. Discharge velocity during a blowdown of Edwards pipe (Test 2)